Fakultät für Medizin

The Influence of Agrin and Extracellular Matrix on Infarct Healing in a Large Animal Model

Victoria Alice Anna Jurisch

Vollständiger Abdruck der von der Fakultät für Medizin der Technischen Universität München zur Erlangung einer

Doktorin der Medizin (Dr.med.)

genehmigten Dissertation.

Vorsitz: Prof. Dr. Susanne Kossatz

Prüfer der Dissertation:

1. apl. Prof. Dr. Christian Kupatt-Jeremias
2. Prof. Dr. Julian Grünewald

Die Dissertation wurde am 20.10.2022 bei der Technischen Universität München eingereicht und durch die Fakultät für Medizin am 18.12.2022 angenommen.

Meinen Eltern in Liebe und Dankbarkeit

Teile dieser Arbeit wurden veröffentlicht in:

Baehr, A., Umansky, K.B., Bassat, E., Jurisch, V., Klett, K., Bozoglu, T., Hornaschewitz, N., Solyanik, O., Kain, D., Ferraro, B., Cohen-Rabi, R., Krane, M., Cyran, C., Soehnlein, O., Laugwitz, KL., Hinkel, R., Kupatt, C., Tzahor, E. (2020). **Agrin Promotes Coordinated Therapeutic Processes Leading to Improved Cardiac Repair in Pigs.** *Circulation*, 142(9), 868-881.

doi:10.1161/circulationaha.119.045116

Table of Contents

1. Abstract

Background: Ischemic heart disease is the leading cause for death and disability worldwide and predominantly manifests as acute myocardial infarction (AMI). Current standard of care is the timely revascularisation of the occluded coronary artery, aiming to reduce infarct size and mortality. However, the heart remodels in response to injury, which can result in progressive cardiac dysfunction and chronic heart failure. Bassat et al. (2017) recently demonstrated, that a single intramyocardial injection of the extracellular matrix protein agrin induces cardiomyocytes to re-enter the cell cycle and preserves cardiac function in a murine ischemia/ reperfusion model. We hypothesize, that agrin acts via a pleiotropic mechanism in the heart and improves cardiac repair in pigs.

Methods: Pigs were subjected to ischemia via balloon occlusion and injected with recombinant human agrin (rhAgrin) or saline at the endpoint of ischemia. This was followed by a three-, seven- or 28-day reperfusion period. *In vivo* functional data was obtained during all interventions and the hearts were harvested post mortem. Cardiac tissue was processed for histological analysis. Ki67, BrdU, Sirius red, TUNEL, haematoxylin and eosin, PECAM-1 and wheat germ agglutinin stainings were performed to assess cardiomyocyte proliferation, fibrosis, cell death, inflammation, angiogenesis, and hypertrophy respectively. Additionally, collagen deposition was analysed via hydroxyproline assay.

Results: Cardiac function improved upon rhAgrin treatment; left ventricular ejection fraction was higher (36.81±2.38% vs. 24.78±1.02%) and left ventricular end diastolic pressure lower (10.26±0.36mmHg vs. 17.72±0.82mmHg) in rhAgrin compared to saline injected pigs. Furthermore, infarct size decreased from 21.03±2.16% to 10.39±1.65% upon rhAgrin treatment. On a cellular level, rhAgrin application promotes cardiomyocytes to re-enter the cell cycle, enhances angiogenesis, and reduces interstitial fibrosis, loss of cardiomyocytes, inflammation, and hypertrophy of the heart. This pleiotropic mechanism of action could already be observed after a three day reperfusion period and was substantiated after 28 days.

Conclusion: A single antegrade injection of rhAgrin ameliorates hallmarks of adverse cardiac remodelling and promotes long term cardiac function in a porcine ischemia/

reperfusion model. rhAgrin application could be a clinically feasible therapy option for patients suffering from AMI and potentially prevent heart failure in the future.

Keywords: agrin, myocardial infarction, heart failure, adverse cardiac remodeling

2. Zusammenfassung

Hintergrund: Ischämische Herzerkrankungen sind der weltweit meist verbreitetste Auslöser für körperliche Einschränkungen und frühzeitiges Versterben, wobei der akute Herzinfarkt die häufigste Modalität der ischämischen Herzerkrankungen darstellt. Therapeutischer Goldstandard ist aktuell die Wiederherstellung der myokardialen Durchblutung mittels perkutaner koronarer Intervention mit dem Ziel, die Infarktgröße und Mortalität zu reduzieren. Dennoch entwickeln viele Patienten im Verlauf eine Herzinsuffizienz, da das Herz Umbauprozessen unterworfen ist. Bassat et al. (2017) legten in einer aktuellen Studie dar, dass das extrazelluläre Matrixprotein Agrin Kardiomyozyten zur Zellteilung anregt und die Herzarbeit nach Herzinfarkt im Mausmodell verbessert. Wir stellen nun die Hypothese auf, dass Agrin über pleiotrope Wirkmechanismen im Herzen agiert und somit die Heilungsprozesse nach Infarktgeschehen im Schweinemodell fördert.

Methoden: Ein Herzinfarkt wurde mittels Ballon-Okklusion im Schweinemodel induziert. Nach Ablauf der Ischämiezeit wurde entweder rekombinantes humanes Agrin (rhAgrin) oder Kochsalzlösung in die Koronararterie injiziert. Anschließend erfolgte eine drei, sieben oder 28-tägige Reperfusionszeit. Während den Intervention wurde die *in vivo* Herzfunktion durch spezifische Herzkathetermessungen bestimmt. Nach Ablauf der Reperfusionszeit wurden die Tiere terminiert, die Herzen post mortem entnommen und histologisch analysiert. Die zelluläre Proliferation-, Gefäßneubildungs- und Zelltodrate, sowie der relative Fibroseanteil, die entzündliche Aktivität und die myokardiale Hypertrophie wurden mittels Ki67, PECAM-1, TUNEL, Sirius red, Hämatoxylin und Eosin und Wheat Germ Agglutinin Färbungen ermittelt. Zusätzlich wurde der Kollagenanteil mittels Hydroxyproline Assay bestimmt.

Ergebnisse: Eine Therapie mit rhAgrin hat zu einer signifikanten Besserung der kardialen Leistung geführt. Die linksventrikuläre Ejektionsfraktion ist nach rhAgrin Injektion im Vergleich zur Kontrollgruppe gestiegen (36.81±2.38% vs. 24.78±1.02%). Zusätzlich ist der linksventrikuläre enddiastolische Druck nach rhAgrin Gabe gefallen (10.26±0.36mmHg vs. 17.72±0.82mmHg). Des weiteren kam es zu einem signifikanten Rückgang der Infarktgröße von 21.03±2.16% auf 10.39±1.65%. Auf zellulärer Ebene konnte ein Anstieg der Kardiomyozytenteilungs- und der Gefäßneubildungsrate nachgewiesen werden. Zusätzlich sind der relative

Fibroseanteil, die Zelluntergangsrate, die entzündliche Aktivität des Myokards und die kardiale Hypertrophie relevant zurückgegangen. Dieser pleiotrope Wirkmechanismus von rhAgrin zeigte sich bereits nach drei Tagen Reperfusionzeit und bestätigte sich erneut nach 28 Tagen.

Fazit: Eine einzelne intrakoronare Injektion von rhAgrin reduziert Kennzeichen kardialer Umbauprozesse nach einem Herzinfarkt und verbessert die Herzarbeit langfristig im Schweinemodell. Dies bietet therapeutische Möglichkeiten für Patienten mit akutem Herzinfarkt und könnte zukünftig den Fortschritt einer kardialen Minderfunktion bis hin zur Herzinsuffizienz verhindern.

3. List of Abbreviations

Abbreviation	Definition
ACE	Angiotensin converting enzyme
AChR	Acetylcholine receptor
ACR	Adverse cardiac remodelling
AMI	Acute myocardial infarction
ANOVA	Analysis of variance
BrdU	5-Bromo-2-deoxyuridine
BSA	Bovine serum albumin
bw	Body weight
CABG	Coronary artery bypass graft
CAD	Coronary artery disease
CD	Cluster of differentiation
CHF	Chronic heart failure
CM	Cardiomyocyte
cTnI	Cardiac Troponin I
CVD	Cardiovascular disease
DAG	Dystrophin-associated glycoproteins
Dag1	α-dystroglycan
DAMP	Danger associated molecular pattern
ddH_2O	Double distilled water
DGC	Dystrophin-glycoprotein complex

DNA	Deoxyribonucleic acid
D1	First diagonal branch of the LAD
ECG	Electrocardiogram
ECM	Extracellular matrix
EGF	Epidermal growth factor
ESC	European Society of Cardiology
FFPE	Formalin fixed and paraffin embedded tissue
HE	Haematoxylin and eosin
HMGB1	High-mobility group box 1 protein
Hsp	Heat shock protein
IHD	Ischemic heart disease
IL	Interleukin
i.a.	Intraarterial
i.m.	Intramuscular
i.v.	Intravenous
LAD	Left anterior descending artery
LDH	Lactate dehydrogenase
LDL	Low density lipoprotein cholesterol
LG	Laminin G homology domain
LOX	Lysyl oxidase
LRP4	Lipoprotein receptor-related protein 4
LV	Left ventricle

LVEDP	Left ventricular end diastolic pressure
LVEDV	Left ventricular end diastolic volume
LVEF	Left ventricular ejection fraction
LVESV	Left ventricular end systolic volume
MMP	Matrix metalloproteinase
MuSK	Muscle-specific kinase
M1	Inflammatory macrophage phenotype
M2	Reparative macrophage phenotype
NSTEMI	Non-ST-elevation myocardial infarction
OD	Optical density
OOC	Organs on chip
PBS	Phosphate buffered saline
PCI	Percutaneous coronary intervention
PECAM-1	Platelet endothelial cell adhesion molecule 1
rhAgrin	Recombinant human agrin
ROS	Reactive oxygen species
rrAgrin	Recombinant rat agrin
RT	Room temperature
SEM	Standard error of mean
SMASH	Semi-automatic muscle analysis using segmentation of histology
SpO2	Oxygen saturation
STEMI	ST-elevation myocardial infarction

SV	Stroke volume
TBS	Tris buffered saline
TGF-ß	Transforming growth factor beta
TIVA	Total intravenous anaesthesia
TLR	Toll-like receptor
TNF α	Tumor necrosis factor α
TTC	Triphenyl tetrazolium chloride
TUNEL	Terminal deoxyribonucleotidyl transferase-mediated dUTP-digoxigenin nick end labeling
VEGFR2	Vascular endothelial growth factor receptor 2
WGA	Wheat germ agglutinin

4. Introduction

4.1. Ischemic Heart Disease and Acute Myocardial Infarction

4.1.1. Definition

Ischemic heart disease (IHD), also known as coronary artery disease (CAD), is defined as the manifestation of atherosclerosis within the coronary arteries, leading to a mismatch of oxygen supply and demand in the cardiac tissue and resulting in myocardial ischemia (Herold, 2021). Significant myocardial ischemia sustained over time results in myocardial cell necrosis, which according to the World Health Organisation is the defining criteria of myocardial infarction (Mendis et al., 2010).

4.1.2. Epidemiology

It is widely recognized that cardiovascular diseases (CVDs) are the leading causes of death and morbidity, accounting for 17.9 million deaths globally in 2019 alone (World Health Organization, 2021). According to the American Heart Association, IHD exclusively accounted for 42.1% of the deaths caused by CVDs in 2018 (Virani et al., 2021). In most cases, IHD manifests as acute myocardial infarction (AMI) with a mortality rate of 20% within one year of the event (Manfroi et al., 2002; Q. Ye et al., 2020). In non-fatal AMI cases, a quarter of the patients develop chronic heart failure (CHF), whereby CHF itself is associated with a significant increase in mortality (Sulo et al., 2016).

The cost of diagnosis and treatment of patients suffering from CVDs, encompassing hospitalization, prescribed pharmacotherapy, interventions, and emergency care, added up to US$863 billion in 2010 and are expected to surpass US$1 trillion globally by 2030. In the United States it is estimated that the financial impact of IHD alone equates to 1–1.5% of the country’s gross domestic product. (Khan et al., 2020)

4.1.3. Aetiology

4.1.3.1. Risk Factors of Ischemic Heart Disease

IHD is the manifestation of atherosclerosis in the coronary arteries (Herold, 2021). Therefore, both entities share the same risk factors, which can be divided into modifiable and non-modifiable risk factors. High age, male gender, ethnicity, and a positive family history are part of the non-modifiable risk factors (Bachmann et al., 2012; Carnethon et al., 2017; Sanchis-Gomar et al., 2016; Volgman et al., 2018). They make up most of the prognostic power in cardiovascular risk models (Pencina et al., 2019). Modifiable risk factors include hypertension, hypercholesteremia and diabetes mellitus (Cavero-Redondo et al., 2017; Neaton & Wentworth, 1992). Additionally, cigarette smoking, lack of physical activity, obesity and a poor diet consisting of saturated and trans fatty acids, high sugar intake and processed meats have been identified as risk factors susceptible to behavioural changes (Assmann et al., 1999; Bechthold et al., 2019; Kromhout et al., 1995; Mons et al., 2015; Q. Yang et al., 2014; Yusuf et al., 2004). Although modifiable risk factors have less prognostic power, it is vital to address them to prevent IHD in the future (Pencina et al., 2019).

4.1.3.2. Risk Factors and Causes of Acute Myocardial Infarction

AMI is most often caused by the dislocation of a ruptured atherosclerotic plaque leading to the occlusion of a major coronary artery (Van de Werf et al., 2008). The risk factors for AMI therefore encompass the ones previously mentioned for IHD and atherosclerosis. Other causes for AMI are rooted in an imbalance of oxygen supply and demand caused by vascular spasm, coronary embolism, coronary artery dissection, hypotension, shock, or an increase in myocardial oxygen demand due to prolonged tachyarrhythmia (Thygesen et al., 2018).

4.1.4. Diagnostic Assessment

The diagnostic assessment of AMI requires at least two criteria to be fulfilled. The first criterion is the detection of the cardiac biomarkers cardiac Troponin I (cTnI) or cardiac Troponin T with a dynamic increase above the 99th percentile (Collet et al., 2020). Secondly, in accordance with the guidelines of the European Society of Cardiology (ESC) at least one of the following presentations is imperative:

- Relevant symptoms of myocardial ischemia, such as angina
- New electrocardiogram (ECG) changes matching ischemic injury
- Pathological Q waves on the ECG
- Loss of viable myocardium or new regional wall motion abnormality in an imaging modality
- Identification of an intracoronary thrombus in angiography. (Collet et al., 2020)

4.1.5. Pathophysiology of Acute Myocardial Infarction

4.1.5.1. Myocardial Ischemia

Ischemia is defined as the “reduction in arterial flow which provides an oxygen supply insufficient to match the oxygen demand” (Jennings et al., 1975). As oxygen supply to the myocardium is diminished, anaerobic glycolysis is initiated to ensure energy supply to the cells (Jennings et al., 1990). This process results in metabolic acidosis and the intracellular accumulation of H^+ (Bond et al., 1991). As the oxygen deficit is sustained, cells undergo necrosis.

4.1.5.2. Ischemia/ Reperfusion Injury

The standard of care for patients with AMI is the timely recanalization of the occluded coronary artery (Collet et al., 2020). However, a sudden reestablishment of blood flow may result in further trauma to the myocardium: a phenomenon called ischemia/ reperfusion injury (Z.-Q. Huang et al., 2019).

This paradox occurs due to the mobilisation of H^+ into the extracellular matrix (ECM) upon perfusion regeneration, initiating a cascade of electrolyte shift involving Na^+, H^+ and Ca^{2+} and culminating in an intracellular Ca^{2+} overload (Bond et al., 1991; Frank et al., 2012). Subsequently, the mitochondrial membrane is permeabilised and cells undergo cell death (Bauer & Murphy, 2020).

Additionally, mitochondria generate reactive oxygen species (ROS) during ischemia (Levraut et al., 2003). When oxygen supply is re-established, ROS accumulate in a burst of oxidant production and initiate an inflammatory response (Frank et al., 2012; Levraut et al., 2003).

4.1.5.3. Impairment of Cardiac Function Beyond Ischemia/ Reperfusion Injury

A pertinent complication of AMI is cardiac dysfunction progressing into heart failure, the reason of which is twofold (Torabi et al., 2014).

First, adult mammal cardiomyocytes (CMs) are predominantly post-mitotic and exhibit a turnover rate of less than 1% per year (Bergmann et al., 2009; Bergmann et al., 2015). Therefore, the potential for regeneration after injury to the myocardium is very limited.

Second, cell necrosis and the inflammatory response initiated during ischemia/ reperfusion injury start off a cascade of events, that leads to the formation of replacement fibrosis in the heart and is called adverse cardiac remodelling (ACR) (Cohn et al., 2000).

4.2. Adverse Cardiac Remodelling

4.2.1. Definition

As defined by a consensus paper from an international forum on cardiac remodelling, ACR encompasses “genome expression, molecular, cellular and interstitial changes, that are manifested clinically as changes in size, shape and function of the heart after cardiac injury” (Cohn et al., 2000). It is a chronic maladaptive process leading to progressive ventricular dilation, fibrosis, and deterioration of the ECM and left ventricular (LV) function (Timmers et al., 2008).

4.2.2. Inflammatory Phase

The first phase of ACR is characterised by an innate immune response triggered by necrotic cell death of the myocardium leading to the degradation of the ECM (Westman et al., 2016).

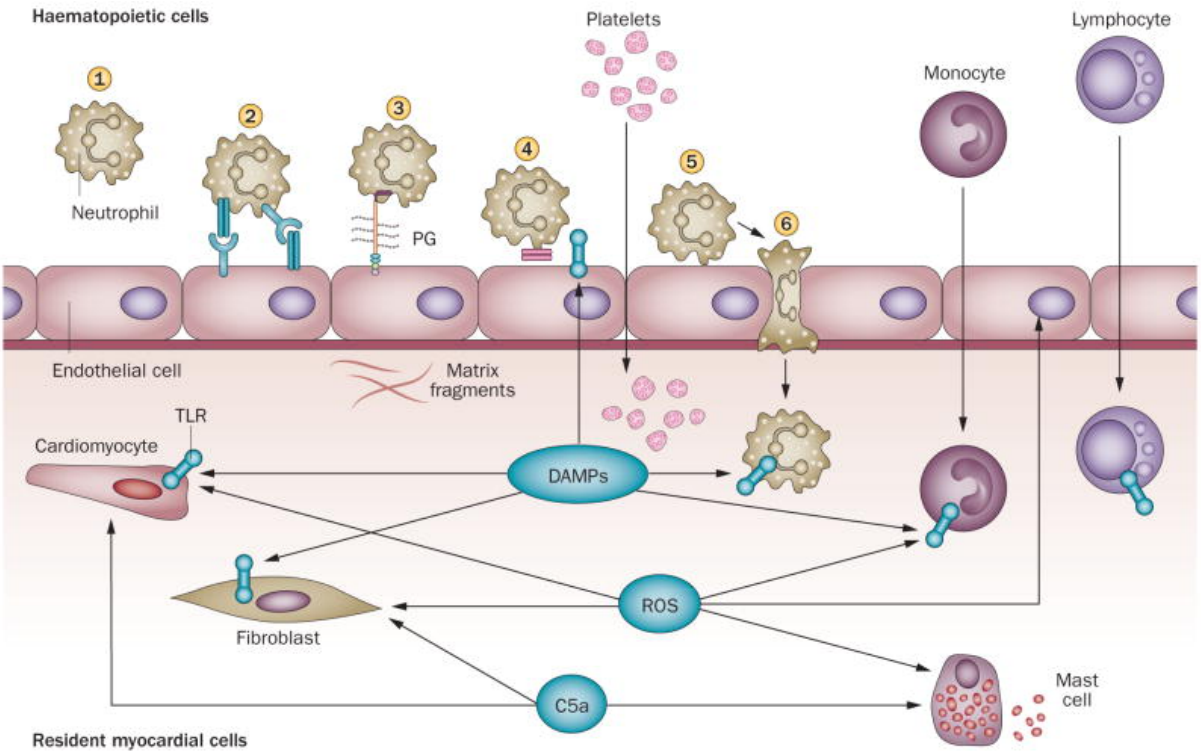

Figure 1: The Inflammatory Phase of ACR (Frangogiannis, 2014)

Following acute myocardial infarction, danger associated molecular patterns are released by necrotic cells within the ischemic myocardium. This triggers an inflammatory response via toll-like receptor

mediated signalling. Neutrophils are recruited and enter the myocardium by means of an adhesion cascade. Here they generate reactive oxygen species (ROS). Complement cascade activation and ROS subsequently potentiates the inflammatory response. (Frangogiannis, 2014)

4.2.2.1. Necrotic Cell Death and Danger Associated Molecular Patterns

In response to cellular damage or stress, danger associated molecular patterns (DAMPs) are released by cells (Iyer et al., 2009; Q. Zhang et al., 2010). Within the DAMP group, heat-shock proteins (Hsp), and high-mobility group box 1 protein (HMGB1) are prominent players in the initiation of a sterile inflammation (Basu et al., 2000; Iyer et al., 2009; Scaffidi et al., 2002). Additionally, the nucleotide ATP acts as a potent DAMP when released into the extracellular compartment (Niles et al., 2021).

4.2.2.2. Toll-like Receptor Mediated Inflammatory Response

Hsp and HMBG1 bind to pattern recognition receptors, such as toll-like receptors (TLRs) (Iyer et al., 2009; Timmers et al., 2008). Ligands binding to TLRs activate the transcription factor NF-kB, resulting in the induction of inflammatory gene expression, such as cytokines and neutrophil specific chemokines (Basu et al., 2000; Davoodi et al., 2012; M. Li et al., 2001). Specifically, Hsp60 induces gene expression of interleukin (IL)-12 and IL-15, which promote the Th1 immune response (W. Chen et al., 1999; Osterloh et al., 2009). HMGB1 mediates the production of IL-8 via binding to TLRs, hence evoking a proinflammatory response in cells of the innate immune system (Yu et al., 2006). Additionally, Hsp60 and HMGB1 both stimulate the synthesis of tumor necrosis factor α (TNF-α) (Ohashi et al., 2000; Yu et al., 2006).

4.2.2.3. ATP Mediated Activation of the Nlrp3 Inflammasome

The nucleotide ATP is released into the ECM by necrotic, apoptotic, and inflammatory cells (Chekeni et al., 2010; Denning et al., 2019; Elliott et al., 2009; Eltzschig et al., 2006; Eltzschig et al., 2003; Niles et al., 2021). High ATP concentrations directly recruit phagocytes and guide chemotaxis of inflammatory cells (Chekeni et al., 2010; Y. Chen et al., 2006; Elliott et al., 2009). Additionally, ATP mediates the caspase-1 dependant maturation of IL-1 α, IL-1 ß and IL-18 by Nlrp3 inflammasome activation (Agostini et al., 2004; Iyer et al., 2009; Kuida et al., 1995; Mariathasan et al., 2006; Sutterwala et al., 2006).

4.2.2.4. Adrenergic Cytokine Activation

Besides DAMP mediated activation of cytokines and chemokines, catecholamines released post AMI potentiate the proinflammatory stimulus by increasing IL-6 and IL-1 ß expression in cardiac fibroblasts (Barth et al., 2000; Bürger et al., 2001; Deten et al., 2002).

4.2.2.5. Recruitment of Inflammatory Cells to the Myocardium

The maturation and activation of these cytokines, most prominently IL-1, IL-6 and TNF-α, initiates the recruitment of neutrophils to the injured myocardium and the activation of their phagocytic activity via Hsp60 signaling (Bujak et al., 2008; Deten et al., 2002; Nian et al., 2004; Osterloh et al., 2009; Westman et al., 2016). Additionally, hypoxemia induces IL-6 expression and disrupts the endothelial cell barrier, further enhancing the migration of inflammatory cells (Ali et al., 1999; Ogawa et al., 1990). Within minutes neutrophiles release ROS, additionally amplifying the inflammatory response via diverse signalling pathways, such as the expression of chemokines and cytokines (Ciz et al., 2012; Westman et al., 2016).

4.2.2.6. Degradation of the Extracellular Matrix

Matrix metalloproteinases (MMPs) are a family of endopeptidases that degrade all elements of the myocardial ECM, thereby influencing the myocardial structural integrity (Cleutjens, Kandala, et al., 1995; Yarbrough et al., 2003). In the heart, neutrophils are the dominant cellular source of MMPs and express MMP9 in the ischemic myocardium in response to TNF-α and IL-1 ß mediated activation (Romanic et al., 2002; Siwik et al., 2000). This promotes the resorption of necrotic tissue following AMI and initiates ECM turnover (Deten et al., 2002; Siwik et al., 2000). Elevated plasma MMP9 levels positively correlate with ECM degradation and increased LV diastolic dimension in the human heart (Sundström et al., 2004). Vice versa, the inhibition of MMPs in preclinical ischemia/ reperfusion models displayed a significant reduction in infarct size and attenuated CHF progression (Ducharme et al., 2000; Lindsey et al., 2002; Peterson et al., 2001; Rohde et al., 1999; Romanic et al., 2002).

4.2.3. Proliferation Phase

The proliferative phase of ACR is dominated by a downregulation of the inflammatory response followed by an extensive ECM turnover and collagen deposition (Talman & Ruskoaho, 2016).

4.2.3.1. Resolution of the Inflammatory Phase

During AMI, hypoxia induces apoptosis in CMs (F. Han et al., 2019). At the same time, aged neutrophils undergo apoptosis (Whyte et al., 1993). Additionally, neutrophiles guide macrophages from an inflammatory (M1) towards a reparative (M2) phenotype, in which they clear off cellular debris and apoptotic CMs (Horckmans et al., 2017; Jia et al., 2022). The ingestion of these apoptotic cells by M2 macrophages stimulates the secretion of transforming growth factor-ß (TGF-ß) and the anti-inflammatory cytokine IL-10 (Frangogiannis et al., 2000; Huynh et al., 2002; M. Jung et al., 2017). TGF-ß suppresses pro-inflammatory mediators, for example TNF α, leading to a reduction of neutrophils, lymphocytes and macrophages (Huynh et al., 2002).

4.2.3.2. Extracellular Matrix Turnover and Collagen Deposition

Furthermore, TGF-ß and IL-10 regulate the ECM composition. They both promote fibroblast migration to the infarcted myocardium, where they transdifferentiate to activated myofibroblasts (Desmoulière et al., 1993; Dobaczewski, Bujak, et al., 2010; M. Jung et al., 2017). Following activation, TGF-ß induces ECM synthesis of collagen type I and III in cardiac myofibroblasts: the primary source of collagens (Cleutjens, Verluyten, et al., 1995; Dobaczewski, Bujak, et al., 2010). Additionally, TGF-ß enables matrix-preserving processes by repressing MMP gene expression and inducing tissue inhibitor of metalloprotease expression in fibroblasts (Leivonen et al., 2013; Verrecchia et al., 2001; W. Yuan & Varga, 2001). These processes aim to replace tissue lost with a fibrous scar, prevent wall thinning and LV rupture (Hammoud et al., 2011; Ma et al., 2013). However, prominent TGF-ß signalling has also been detected in the border zone adjacent to the infarct, where collagen deposition promotes remote cardiac remodelling and diastolic dysfunction of the heart (Bujak et al., 2007).

ACR is also modulated by neurohumoral agents, such as angiotensin II. Angiotensin II expression is significantly upregulated in the remote myocardium post AMI; it stimulates collagen synthesis and inhibits expression of MMPs in cardiac fibroblasts. (K. Chen et al., 2004; Lindpaintner et al., 1993)

4.2.3.3. Induction of Cardiac Hypertrophy

Cardiac hypertrophy is the main driver of CHF. CM hypertrophy is mediated by the release of TGF-ß and endothelin-1 via Angiotensin II binding to AT1 receptors on cardiac fibroblasts (Gray et al., 1998; Schultz Jel et al., 2002).

4.2.4. Maturation Phase

The maturation phase of ACR is defined by further ECM modifications resulting in the formation of a fibrotic scar based on a mature collagen matrix (Talman & Ruskoaho, 2016).

It is initiated by the switch from type III to type I collagen (Cleutjens, Verluyten, et al., 1995). Cardiac fibroblasts express lysyl oxidase (LOX) by TGF-ß activation and hypoxia dependant pathways as early as three days post AMI (González-Santamaría et al., 2015). LOX are a family of enzymes mediating cross-linking of mature collagen; this increases collagen tensile strength and results in enhanced myocardial stiffness (Badenhorst et al., 2003; González-Santamaría et al., 2015; Norton et al., 1997). They are expressed in the infarcted and the adjacent border zone of the myocardium (González-Santamaría et al., 2015). Rodent models have demonstrated that LOX inhibition after AMI reduces cardiac dysfunction, ventricular remodelling, and scar formation (González-Santamaría et al., 2015; M. Lu et al., 2019).

4.2.5. Structural and Functional Changes of the Heart

Cellular and ECM changes during ACR are at the core of heart failure progression following AMI and lead to structural and functional changes of the infarcted and remote myocardium. This includes LV dilation, increased sphericity of the heart and global cardiac dysfunction. (Cohn et al., 2000)

4.2.5.1. Early Systolic Dysfunction

During ischemia, the myocardium undergoes contraction-rigor as energy supplies are depleted by insufficient use of anaerobic glycolysis (Frank et al., 2012). Subsequently, with impaired contractility the infarcted region becomes dys- or akinetic, resulting in systolic dysfunction of the heart (Witkowski et al., 1994).

4.2.5.2. Infarct Expansion

Early cellular and extracellular matrix changes during the inflammatory phase lead to an expansion of the infarct (Hochman & Bulkley, 1982). As first observed by Hutchins and Bulkley in 1978, infarct expansion describes an “acute dilatation and thinning of the area of infarction not explained by additional myocardial necrosis” (Hutchins & Bulkley, 1978). This has since been attributed to a side-to-side slippage of CMs leading to LV cavity dilation (Olivetti et al., 1990; Weisman et al., 1988).

4.2.5.3. Progression Into Global Heart Failure

Adding to infarct expansion, CMs undergo hypertrophy during ACR which amplifies LV cavity dilation and systolic dysfunction of the heart (J. M. Pfeffer et al., 1991). As a result, LV end-diastolic volume (LVEDV) and LV end-systolic volume (LVESV) increase (McKay et al., 1986). An increase in LVEDV and LVESV generates wall stress, initiates volume overload hypertrophy in the remote myocardium and results in a rise of LV end diastolic pressure (LVEDP) (McKay et al., 1986). Studies have shown, that an elevated LVEDP is a hallmark of a diastolic dysfunction of the heart (Zile et al., 2001). At this point endocardial perimeter length increases both in the infarcted and remote myocardium leading to a change of LV dimension from an ellipsoidal to a spherical shape as demonstrated in figure 2 below (Cohn et al., 2000; McKay et al., 1986).

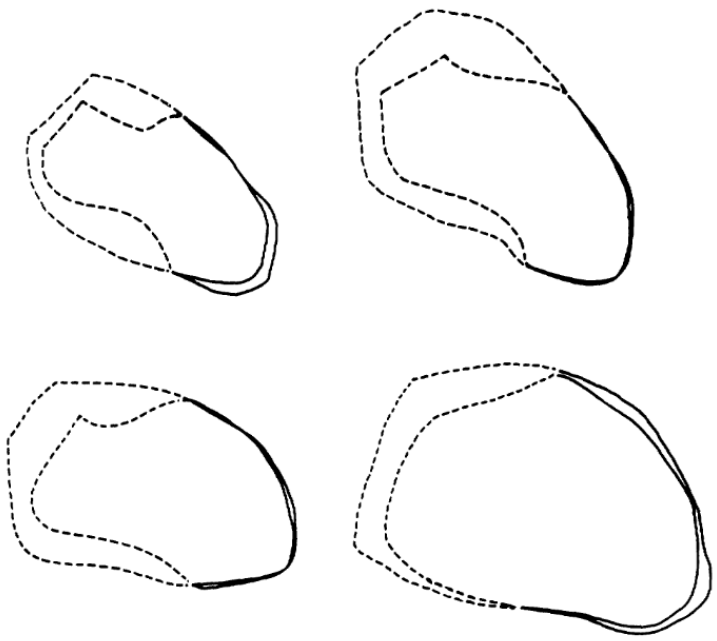

Figure 2: Structural Remodeling of the Left Ventricle (McKay et al., 1986)

Cardiac outlines in diastole and systole from two patients on day 0 (left) and day 14 (right) after admission for acute myocardial infarction in right anterior oblique view. Solid lines represent akinetic/ dyskinetic (infarcted) regions of the myocardium. Dotted lines represent non-infarcted regions of the myocardium. In both patients, left ventricular volume increased, and the infarcted and non-infarcted perimeters elongated. (McKay et al., 1986)

As global cardiac remodelling progresses a fibrous scar is formed (González-Santamaría et al., 2015). This accentuates myocardial stiffness, diminishes diastolic distensibility and provokes diastolic dysfunction of the heart (González-Santamaría et al., 2015).

Consequently, the progression of ACR leads to systolic and diastolic heart function impairment due to dilation of the heart and formation of a fibrous scar. Over time this pathogenesis culminates in the development of global heart failure. (McKay et al., 1986)

4.3. Chronic Heart Failure

4.3.1. Definition

CHF is defined as “a clinical syndrome with current or prior symptoms and/ or signs caused by a structural and/ or functional cardiac abnormality and corroborated by either elevated natriuretic peptide levels and/ or objective evidence of cardiogenic pulmonary or systemic congestion by diagnostic modalities, such as imaging or hemodynamic measurement at rest or with provocation” (Bozkurt et al., 2021).

4.3.2. Epidemiology

In 2017, 64.3 million people were living with heart failure globally (S. L. James et al., 2018). In developed countries it is estimated that 1-2% of the adult population are affected by CHF (Groenewegen et al., 2020; McDonagh et al., 2021). In the USA, the annual medical cost per patient amount to about US$24,000, a majority of which is allocated to hospitalisation costs (Urbich et al., 2020). The high prevalence, as well as the noteworthy associated costs make CHF a significant burden on society.

4.3.3. Aetiology

There is a large variety of causes for CHF. In developed countries CAD and hypertension are predominantly associated with the development of CHF (S. L. James et al., 2018; McDonagh et al., 2021). Globally, 26.4% of CHF is attributed to CAD (S. L. James et al., 2018). Other causes include pre-existing heart conditions, such as valve diseases, arrhythmias, or congenital heart disease, as well as certain drugs (e.g., anthracyclines, trastuzumab), autoimmune diseases or storage disorders (e.g., haemochromatosis) (McDonagh et al., 2021).

4.3.4. Signs and Symptoms

Typical symptoms of CHF encompass breathlessness, orthopnea, paroxysmal nocturnal dyspnea, fatigue, ankle swelling, reduced exercise tolerance or inability to exercise. Additionally, evident clinical signs can entail elevated jugular venous pressure, third heart sound, cardiomegaly, hepatojugular reflux, peripheral edema, tachycardia and/or -pnea and Cheyne Stokes respiration in advanced CHF. (Bozkurt et al., 2021)

4.3.5. Classification of Heart Failure

There are different approaches in classifying heart failure. One commonly used by physicians has been postulated by the New York Heart Association and classifies CHF into four groups according to the severity of symptoms experienced by the patient during physical activity and at rest (Rogers et al., 2017). Another approach classifies CHF according to left ventricular ejection fraction (LVEF) with the advantage of assigning patients to different groups with distinct therapy strategies (Bozkurt et al., 2021). The classification according to LVEF is stated in the table 1 below.

Table 1: Classification of CHF According to LVEF (Bozkurt et al., 2021)

Group	Description	LVEF
HFrEF	Heart failure with reduced ejection fraction	≤ 40%

HFmrEF	Heart failure with mildly reduced ejection fraction	41-49%
HFpEF	Heart failure with preserved ejection fraction	≥ 50%
HFimpEF	Heart failure with improved ejection fraction	Baseline ≤ 40%, a 10-point increase from baseline and second measurement > 40%

4.3.6. Prognosis

As a chronic disease, CHF is not only associated with an impaired quality of life, but also results in a significantly reduced life expectancy (Drozd et al., 2021; Juenger et al., 2002).

The quality of life reduction is mainly caused by a pronounced loss in physical functioning (Juenger et al., 2002). This generates a mental health impairment, which in advanced CHF stages is comparable to patients suffering from major depression (Juenger et al., 2002).

According to an observational study of the ESC Heart Failure Long-Term Registry, the one-year mortality rate of patients suffering from CHF is 6.4%; nearly half of the deaths are attributed to cardiovascular aetiologies (Crespo-Leiro et al., 2016). Research has outlined that patients who develop late CHF post AMI have a tenfold increased risk for cardiac death compared to other patients surviving AMI (Lewis et al., 2003). Furthermore, the ESC reports a 9.9% one-year hospitalisation rate in patients suffering from CHF (Crespo-Leiro et al., 2016).

4.4. Current Therapy Standards

The current therapy standards outlined are in accordance with the international guidelines of the ESC.

4.4.1. Resolving Myocardial Infarction

4.4.1.1. Acute Patient Management

The initial AMI pharmacotherapy relieves symptoms and prevents further progression of the myocardial ischemia. It is based upon analgesia, oxygen supply, anxiolysis and platelet inhibition.

To relieve pain and reduce breathlessness, intravenous (i.v.) opioids (e.g., morphine) are applied (Borja Ibanez et al., 2017). This is a priority, as it not only provides comfort to the patient, but also reduces sympathetic activation and, therefore, workload on the ischemic heart (Feldberg & Wei, 1986; Borja Ibanez et al., 2017). Next, in hypoxic patients with an oxygen saturation (SpO2) < 90%, the use of oxygen is indicated (Borja Ibanez et al., 2017). Additionally, a mild tranquilizer, such as diazepam, may be used in patients experiencing anxiety (Borja Ibanez et al., 2017). To prevent further progression of the ischemia, a therapy with platelet inhibitors can be initiated (Collet et al., 2020; Borja Ibanez et al., 2017). Aspirin in loading dose (150-300 mg per os) is the gold standard in all patients. In ST-elevation myocardial infarction (STEMI) patients, therapy should be expanded to include a P2Y12 receptor inhibitor, hence initiating a dual platelet therapy in loading dose (Collet et al., 2020; Borja Ibanez et al., 2017). Studies have shown that prasugrel and ticagrelor are superior in both pharmacodynamics and -kinetics, such as rapid onset time, potency, and clinical outcome, and should therefore be preferred over the use of clopidogrel (Wallentin et al., 2009; Wiviott et al., 2007).

4.4.1.2. Reperfusion Therapy

Reperfusion strategies for AMI involve three methods: percutaneous coronary intervention (PCI), fibrinolysis and coronary artery bypass graft (CABG).

During acute AMI presentation, primary PCI is the gold standard. This applies to STEMI patients with an onset of symptoms ≤120min, or non-ST-elevation myocardial infarction (NSTEMI) patients with symptom onset ≤24h (Collet et al., 2020; Borja

Ibanez et al., 2017). As an access route, both the femoral and the radial artery can be utilized. Once the coronary anatomy is demonstrated using intraarterial (i.a.) injected contrast captured on a c-arch x-ray, the flow in the occluded coronary artery is re-established using balloon angioplasty and/ or coronary stenting (Borja Ibanez et al., 2017). To date, standard of care is the use of drug-eluting stents; they are superior regarding safety and efficacy compared to bare-metal stents (Hao et al., 2010; Sabaté et al., 2014).

If primary PCI is not an option, fibrinolysis is indicated in STEMI patients with symptom onset ≤12h and no contraindications, such as previous intracranial haemorrhages or strokes, recent trauma or gastro-intestinal haemorrhage, aortic dissection or a known coagulopathy (Agewall et al., 2017; Borja Ibanez et al., 2017).

An emergency CABG should be considered in patients presenting with cardiogenic shock or a coronary anatomy unsuitable for effective PCI (Borja Ibanez et al., 2017).

4.4.1.3. Periinterventional Anticoagulation

All patients receiving primary PCI require a periinterventional anticoagulation. The standard of care is the use of unfractionated heparin. Other options entail the low-molecular weight heparin enoxaparin and the recombinant hirudin bivalirudin. The anticoagulation should be discontinued after PCI. (Collet et al., 2020; Borja Ibanez et al., 2017)

4.4.2. Long-term Management

The long-term management of patients post AMI aims to prevent recurring ischemic events, reduce ACR and halt progression into CHF. It includes sufficient adjustment of cardiovascular risk factors, a continual antithrombotic therapy, and the reduction of ACR.

4.4.2.1. Adjustment of Cardiovascular Risk Factors

Adjusting cardiovascular risk factors is of paramount importance, as it impedes the progression of atherosclerosis within the coronary arteries. This includes lifestyle management, as well as management of dyslipidaemia, hypertension, and diabetes mellitus.

Lifestyle management entails the adjustment of risk factors susceptible to behavioural change: smoking, diet, and physical activity (Kromhout et al., 1995; Mons et al., 2015; Yusuf et al., 2004). As Chen et al. (2012) demonstrated, each reduction of five cigarettes per day decreases the mortality risk by 72% post-PCI, proving the cessation of smoking to be critical in the prevention of further cardiac events (T. Chen et al., 2012).

According to the ESC, dyslipidaemia should be addressed with goal low density lipoprotein cholesterol (LDL) levels <55mg/dl or a ≥50% reduction, if the baseline LDL is within 70-135 mg/dl (Collet et al., 2020). The standard pharmacotherapy to reduce LDL is the use of statins, however an add-on therapy with ezetimibe and/or PCSK9 inhibitors is recommended, if the goal LDL cannot be achieved using monotherapy (Collet et al., 2020). Recent studies suggest that especially a high LDL to high density lipoprotein cholesterol ratio amounts to an increased risk of major adverse cardiac events and stent thrombosis following PCI and stent implantation (Zhong et al., 2019).

Hypertension can be controlled by lifestyle changes, such as reduced salt intake, weight loss and physical activity and the initiation of antihypertensive pharmacotherapy with a goal systolic blood pressure <140 mmHg (Borja Ibanez et al., 2017).

For most diabetic patients suffering from CAD, a target HbA1c <7% is recommended (Knuuti et al., 2019). However, this target can vary and depends on patients age, comorbidities, and duration of diabetes mellitus (Collet et al., 2020).

4.4.2.2. Antithrombotic Therapy

An antithrombotic therapy is standard of care in preventing in-stent thrombosis and restenosis of previously occluded coronary arteries. This entails a lifelong therapy with Aspirin, as well as the additional intake of P2Y12 inhibitors for twelve months following primary PCI with stent implantation. (Collet et al., 2020; Borja Ibanez et al., 2017)

4.4.2.3. Preventing Adverse Cardiac Remodelling

In patients with heart failure and/ or a compromised LV systolic function following AMI, a therapy using angiotensin converting enzyme (ACE) inhibitors and beta blockers should be initiated to prevent ACR (Borja Ibanez et al., 2017).

It is well established that long-term administration of ACE inhibitors reduces morbidity and mortality following AMI and slows down the progression of CHF (Flather et al., 2000; M. A. Pfeffer et al., 1992; The Acute Infarction Ramipril Efficacy Study, 1993). This has been attributed to the potent anti-inflammatory effect of ACE inhibitors, as they prevent the splenic release of neutrophils and monocytes (Gao et al., 2017; Ma et al., 2019). Additionally, pharmacotherapy using ACE-inhibitors suppresses the angiotensin II mediated CM hypertrophy, resulting in a reduction of LV mass (Paoletti et al., 2007).

The beneficial effect on mortality reduction using long-term beta blocker therapy after AMI has been demonstrated even before reperfusion therapy became standard of care (Freemantle et al., 1999; Yusuf et al., 1980). It has since been revealed that this involves a reduction in infarct size and a preserved LVEF after AMI (B. Ibanez et al., 2013).

4.4.3. Controlling Chronic Heart Failure

Therapy of CHF involves pharmacotherapy, as well as device therapy in more advanced stages.

Pharmacotherapy is the foundation of CHF therapy. It entails the inhibition of the renin angiotensin aldosterone system, utilizing ACE inhibitors, angiotensin receptor-neprilysin inhibitors, mineralocorticoid receptor antagonists and angiotensin receptor blockers (McDonagh et al., 2021). Additionally, beta blockers and sodium-glucose co-transporter 2 inhibitors have proven effective in impeding the progression of CHF and reducing the associated high mortality rate (Doughty et al., 1997; McDonagh et al., 2021; Zannad et al., 2020). To reduce signs of congestion the use of diuretics is recommended (McDonagh et al., 2021).

In advanced stages of symptomatic CHF with reduced LVEF ≤ 35% and an ischemic aetiology, the addition of an implantable cardioverter-defibrillator to the pre-existing pharmacotherapy is indicated (McDonagh et al., 2021).

4.5. Agrin

4.5.1. Biochemical Structure

The protein agrin is a 200kDa matrix proteoglycan, which can be broken down into distinct domains (Chakraborty et al., 2021; Glass et al., 1996). The C-terminus contains three regions homologous to the G-domain of laminin, as well as four domains like the ones found in the epidermal growth factor (EGF) (Burgess et al., 2002; Raats et al., 1998; Tsim et al., 1992). The laminin G homology domain (LG) 1 and 2, and the EGF-like repeats mediate agrin binding to α-dystroglycan (Dag1) (Hopf & Hoch, 1996). LG3 is essential for agrin binding to the lipoprotein receptor-related protein 4 (LRP4), which is attached to the postsynaptic membrane and mediates muscle-specific kinase (MuSK) activation (Kim et al., 2008; Scotton et al., 2006). The N-terminus holds nine folistatin-like domains, similar to Kazal-type protease inhibitor domains; it facilitates agrin binding to laminin in the synaptic basal lamina (Mascarenhas et al., 2003; Tsim et al., 1992).

4.5.2. Function

4.5.2.1. Agrin in the Nervous System

Agrin was first discovered due to its ability to cluster acetylcholine receptors (AChR) at the postsynaptic membrane during the formation of neuromuscular junctions (Hopf & Hoch, 1996; Tsim et al., 1992). This has since been proven to be the result of an increased MuSK phosphorylation via agrin binding to LRP4 (Glass et al., 1996; Kim et al., 2008). Phosphorylated MuSK induces downstream signalling, which enhances clustering of LRP4, MuSK and AChR and thereby results in synapse-specific gene expression (Burden et al., 2013; Yumoto et al., 2012). This process is vital for synapse formation and postsynaptic differentiation (Yumoto et al., 2012).

4.5.2.2. Agrin in the Heart

Dag1 expressed by CMs serves as an agrin receptor, mediating CM proliferation via a Yap-related signalling mechanism (Bassat et al., 2017).

The extracellular protein Dag1, along with five transmembrane proteins (ß-dystropglycan, adhalin and other dystrophin-associated glycoproteins (DAG)) and four

cytoplasmatic proteins (syntrophin triplet and dystrophin) make up the dystrophin-glycoprotein complex (DGC) (Ibraghimov-Beskrovnaya et al., 1992; D. Jung et al., 1995; Roberds et al., 1993; B. Yang et al., 1994). The DGC facilitates a linkage between the actin-based cytoskeleton and the ECM in muscle cells (Ervasti & Campbell, 1993; D. Jung et al., 1995). This linkage is comprised of Dag1 binding to the LG of ECM proteins, such as laminin, agrin and perlecan (Blake et al., 2002; Bowe et al., 1994; Gee et al., 1994; Ibraghimov-Beskrovnaya et al., 1992; Peng et al., 1998; Sunada et al., 1994). Furthermore, Dag1 binds ß-dystroglycan, which in turn interacts with dystrophin linked to actin (Fealey et al., 2018; D. Jung et al., 1995).

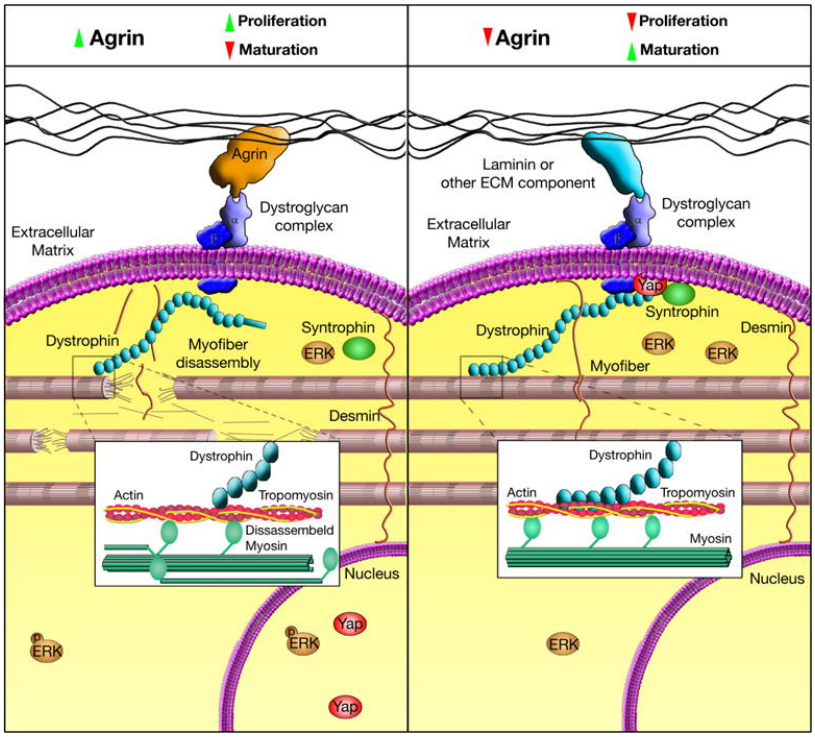

Figure 3: Agrin-DGC-Yap Signaling Axis in the Heart (Bassat et al., 2017)

In neonatal mice, agrin disrupts dystrophin-glycoprotein (DGC) complex maturation and leads to partial sarcomere disassembly. This induces downstream signaling, which results in the translocation of Yap into the nucleus where it facilitates cardiomyocyte (CM) cell-cycle re-entry. On day seven postpartum, agrin levels decrease and extracellular matrix/ DGC interaction stabilizes the sarcomere. CMs differentiate and mature. (Bassat et al., 2017).

In the heart, the agrin-Dag1 interplay induces changes in the conformation of the DGC, which results in a partial sarcomere disassembly, diminished matrix rigidity and a subsequent activation of downstream signalling including Yap and ERK within the Hippo pathway (Bassat et al., 2017; Chakraborty et al., 2017). The Hippo pathway is a conserved signalling pathway which regulates cardiac growth and size by

suppressing CM proliferation and controlling apoptosis (Heallen et al., 2011; Meng et al., 2021). Loss of matrix rigidity, as well as the induction of Yap have previously been linked to an increase in CM proliferation and cardiac regeneration (von Gise et al., 2012; Xin et al., 2013; Yahalom-Ronen et al., 2015).

4.5.2.3. Agrin in the Tumorous Microenvironment

Recently, a proangiogenic role has been attributed to agrin. Njah et. al (2019) demonstrated that agrin secreted by hepatocellular carcinoma cells enhances angiogenesis by stabilising the vascular endothelial growth factor receptor 2 (VEGFR2) of endothelial cells (Chakraborty et al., 2020; Njah et al., 2019).

4.5.3. Therapeutic Potential

Prior research has illustrated that agrin promotes cardiac regeneration in mice after AMI by enhancing CM proliferation. After a single intramyocardial injection of recombinant rat agrin (rrAgrin), it is sustained in the murine heart for up to three days and causes a peak in CM proliferation after seven days. However, a prolonged regenerative effect of agrin up to five weeks after the injury could be observed; this included a reduction in scar size, improved cardiac function quantified by an upheld LVEF and a maintenance of wall thickness with subsequent protection from dilated cardiomyopathy. This suggests a pleiotropic mechanism of action in cardiac repair and poses agrin's therapeutic potential in the restoration of damaged hearts. (Bassat et al., 2017)

5. Aim of Study

AMI is one of the leading causes for death and disability worldwide. Following AMI, necrotic and apoptotic cell death trigger an inflammatory cascade, which culminates in ACR; this involves a compensatory process, in which tissue loss is replaced by an akinetic fibrous scar due to the limited regenerative capacity of the heart (Bergmann et al., 2015; Talman & Ruskoaho, 2016). As the heart remodels, the ECM is actively turned over and the remote myocardium undergoes fibrosis, hypertrophy, and LV cavity dilation (Cohn et al., 2000). This results in further deterioration of the heart and global heart failure (Cohn et al., 2000). Therefore, the standard of care for AMI is the timely reperfusion of the occluded coronary artery via angioplasty to reduce cell loss and impede the progression into ACR (Collet et al., 2020; Borja Ibanez et al., 2017).

Prior studies have shown that a single dose of agrin promotes heart regeneration in mice by stimulating CM cell cycle re-entry, reducing scar formation, and sustaining LVEF and systolic cardiac function (Bassat et al., 2017). This study aims to substantiate these findings in a preclinical porcine ischemia/ reperfusion model by assessing *in vivo* cardiac function, scar formation and CM proliferation. Porcine heart models relate close to the human heart and diminish the gap between animal studies and their clinical application.

Additionally, a pleitropic mechanism of action for agrin's role in heart regeneration post AMI has been suggested by Bassat et al. (2017). As a second goal, the porcine ischemia/ reperfusion model aims to explore agrin's role in angiogenetic, apoptotic, inflammatory, and hypertrophic processes during ACR.

We hypothesize that a single antegrade injection of recombinant human agrin (rhAgrin) into the coronary artery is a novel therapeutic target in the prevention of ACR and CHF following AMI and can readily be introduced into current therapy standards.

6. Materials

6.1. Drugs and i.v. Infusions

Drug/ i.v. Infusion	Manufacturer	Reference number
Adrenaline	InfectoPharm Arzneimittel u. Consilium GmbH, Heppenheim, Germany	EAN: 4150095170068
Amiodarone	Ratiopharm GmbH, Ulm, Germany	EAN: 4150035581688
Atropine sulfate	B. Braun Melsungen AG, Meldungen, Germany	EAN: 4150006480378
Azaperone	Elanco GmbH, Cuxhaven, Germany	Manufacturer article number: 797-548
Cefuroxim 750mg	Dr. Friedrich Eberth Arzneimittel GmbH, Ursensollen, Germany	Zul.-Nr. 94997.00.00
Fentanyl	Eurovet Animal Health BV, AE Bladel, Netherlands	Zul.-Nr. 401495.00.00
Heparine	B. Braun Melsungen AG, Meldungen, Germany	EAN: 4150157826988
Ketamine	CP-Pharma Handelsgesellschaft mbH, Burgdorf, Germany	Manufacturer article number: 1200
Magnesiumsulfate 50%	Inresa Arzneimittel GmbH, Freiburg, Germany	Zul.-Nr. 6914444.00.00
Midazolame 15mg	Hexal AG, Holzkirchen, Germany	PZN: 00886423

Propofol 20mg/ml	B. Braun Melsungen AG, Melsungen, Germany	PZN: 00194346
Ringer-Lactate	B. Braun Melsungen AG, Melsungen, Germany	EAN: 4030539053006

6.2. Catheters and Surgical Consumables

Catheter / Surgical Consumable	**Manufacturer**	**Reference number**
Angioset	B. Braun Melsungen AG, Melsungen, Germany	5010660
Guide catheter (judkins R)	Cordis, Hialeah, Florida, USA	670-083-00
Manometer	Merit Medical GmbH, Eschborn, Germany	IN8152 Version B
Over the wire balloon catheter 3.50 x 20mm (TREK)	Abbott Vascular, Santa Clara, CA, USA	1012409-20
Pigtail Catheter	Cordis, Hialeah, Florida, USA	534-650S
Pressure volume catheter	Transonic Scisense Inc., London, Ontario, Canada	FDH-5018B-E245B
Sheath 8F	Cardinal Health, Norderstedt, Germany	504608X
Ultravist-370	Bayer AG, Leverkusen, Germany	85922882

6.3. Injections

Injection	Manufacturer	Reference number
BrdU	Sigma Aldrich Co., St. Louis, USA	B5002
KCl	B. Braun Melsungen AG, Melsungen, Germany	EAN: 4030539078276
rhAgrin	R&D systems, Minneapolis, Minnesota, USA	6624-AG
NaCl (Saline)	B. Braun Melsungen AG, Melsungen, Germany	EAN: 4030539005159

6.4. Chemicals and Reagents

Chemical / Reagent	Manufacturer	Reference number
Acetone	Carl Roth GmbH & Co. KG, Karlsruhe, Germany	T906.1
Aqueous mounting medium	Abcam, Cambridge, United Kingdom	Ab 128982
Borate buffer (20X)	Thermo Scientific, Rockford, USA	28341
Bovine serum albumin	Sigma Aldrich Chemie GmbH, Steinheim, Germany	A9647-50G
Calcium chloride dihydrate, minimum 99%	Sigma Aldrich Chemie GmbH, Steinheim, Germany	C7902-500G
Direct Red 80	Sigma Aldrich Co., St. Louis, USA	365548
Entellan	Merck KGaA, Darmstadt, Germany	HX56880760

Eosin G-solution 0.5%	Carl Roth GmbH & Co. KG, Karlsruhe, Germany	X883.1
Ethanol 96%	Carl Roth GmbH & Co. KG, Karlsruhe, Germany	T171.3
Ethanol absolute	Merck KGaA, Darmstadt, Germany	8.18760.2500
Formaldehyde 37%	Carl Roth GmbH & Co. KG, Karlsruhe, Germany	4979.2
HCl (10N)	Carl Roth GmbH & Co. KG, Karlsruhe, Germany	0226.1
Heat inactivated horse serum	Gibco Life Technologies Limited, Aukland, NZ	26050-088
Hoechst 33342 staining dye solution	Abcam, Munich, Germany	Ab228551
Hydrochloric acid 25%	Riesel-de Haen, Seelze, Germany	70780
Hämalaunlösung sauer nach Meyer	Carl Roth GmbH & Co. KG, Karlsruhe, Germany	T865.2
Methylene blue	Sigma Aldrich, St. Louis, USA	
Paraformaldehyde	Sigma Aldrich Co., Steinheim, Germany	P-6148
Phosphate buffered saline tablets	Gibco life technologies limited, Paisley, UK	18912-014
Picric acid solution 1.3% in H_2O (saturated)	Sigma Aldrich Co., Steinheim, Germany	P6744-1GA
Roti®-Plast Paraffin	Carl Roth GmbH & Co. KG, Karlsruhe, Germany	6642.2

Sodium citrate monobasic anhydrous	Sigma Aldrich Chemie GmbH, Steinheim, Germany	2427346
Sodium hydroxide platelets	MERCK, Darmstadt, Germany	1.06462.1000
Tris buffered saline	Sigma, St Louis, USA	T-6664
Triton X 100	Carl Roth GmbH & Co. KG, Karlsruhe, Germany	3051.2
Tween 20	Sigma Aldrich Chemie GmbH, Steinheim, Germany	P9416
Vectashield® Mounting Medium with DAPI	Vector Laboratories Inc., Burlingame, USA	H-1200
Wheat germ agglutinin, Alexa Fluor® 488	Invitrogen, Eugene, Oregon, USA	W11261
Wheat germ agglutinin, Alexa Fluor® 594	Invitrogen, Eugene, Oregon, USA	W11262
Xylol	Sigma Aldrich Chemie GmbH, Steinheim, Germany	534056
Xylene	Carl Roth GmbH & Co. KG, Karlsruhe, Germany	9713.3
2-Propanol	Otto Fischar GmbH & Co. KG, Saarbrücken, Germany	PZN 02679450
2,3,5 triphenyl tetrazolium chloride	Carl Roth GmbH & Co. KG, Karlsruhe, Germany	KK13.1

6.5. Antibodies

Antibody Target	Properties	Manufacturer	Reference number
BrdU	*Clonality:* polyclonal IgG *Host species:* rabbit *Target:* synthetic BrdU	Bio Rad, Hercules, California, USA	AHP2405
Donkey IgG	*Clonality:* polyclonal IgG *Host species:* donkey *Target species:* rabbit *Alexa Fluor ®:* 488	Invitrogen, Waltham, Massachusetts, USA	A-21206
Ki67	*Clonality:* polyclonal IgG *Host species:* rabbit *Target species:* human, mouse, rat, pig	Lifespan Biosciences, Seattle, Washington, USA	LS-B13463
Mouse IgG	*Clonality:* polyclonal IgG *Host species:* goat *Target species:* mouse *Alexa Fluor®:* 594	Invitrogen, Waltham, Massachusetts, USA	A-11032
PECAM-1	*Clonality*: monoclonal IgG *Host species:* mouse *Target species:* mouse, rat, human	Santa Cruz Biotechnology, Dallas, Texas, USA	sc-376764
Rabbit IgG	*Clonality:* polyclonal IgG *Host species:* goat *Target species:* rabbit Alexa Fluor®: 568	Invitrogen, Waltham, Massachusetts, USA	A-11011
Rabbit IgG	*Clonality:* polyclonal IgG *Host species:* donkey *Target species:* rabbit Alexa Fluor®: 488	Invitrogen, Waltham, Massachusetts, USA	A-21206

Troponin I	*Clonality:* polyclonal IgG *Host species:* rabbit *Target species:* mouse, rat, human, pig	Abcam, Cambridge, United Kingdom	ab47003

6.6. Kits

Kit	Manufacturer	Reference number
Hydroxyproline assay kit (colorimetric)	Abcam, Munich, Germany	Ab222941
In situ cell death detection kit, TMR red	Roche Diagnostics GmbH, Mannheim, Germany	12156792910

6.7. Histology Consumables

Histology Consumable	Manufacturer	Reference number
Deckgläser für die Mikroskopie	Gerhard Menzel B.V. & Co. KG, Braunschweig, Germany	
Feather microtome blade carbon steel C35	Pfm medical ag, Köln, Germany	02.075.00.003
Menzel-Gläser Polysine slides	Gerhard Menzel B.V. & Co. KG, Braunschweig, Germany	J2800AMNZ
O.C.T. Compound	Sakura Finetek Europe B.V., Alphen aan den Rijn, NL	4583
Solidofix®-Kältespray	Carl Roth GmbH & Co. KG, Karlsruhe, Germany	T200.1
Type F Immersion Liquid	Leica Microsystems CMS GmbH, Wetzlar, Germany	11 513859

Type G Immersion Liquid	Leica Microsystems CMS GmbH, Wetzlar, Germany	11 513910

6.8. Laboratory Devices

Laboratory Device	Manufacturer	Reference number
Mortar with Pestle Agate	VWR, Leuven, Belgium	410-1008
Plate, 96 well with lid, flat bottom	Thermo Scientific, Roskilde, Denmark	442404

6.9. Technical Devices

Technical Device	Model	Manufacturer
Bright light microcope	Olympus BX41	Olympus, Tokyo, Japan
C arch x-ray	Ziehm Vision RFD	Ziehm Imaging GmbH, Nuremberg, Germany
Centrifuge	Micro Star 17	VWR, Leuven, Belgium
Confocal microscope	Leica TCS SP8 X	Leica Microsystems CMS GmbH, Mannheim, Germany
Fluorescent microscope	Leica DMI 6000 B	Leica Microsystems GmbH, Wetzlar, Germany
Fluorescent and bright light microscope	Leica DMi8 Thunder	Leica Microsystems GmbH, Wetzlar, Germany
Gewebeeinbettautomat	Typ Karussel STP-120	MICROM International GmbH, Walldorf, Germany
Incubator	Heratherm IGS100	Thermo Fisher Scientific, Waltham, USA

Kryotom	Microm HM 560	Thermo Fisher Scientific, Waltham, USA
Kryotom	Leica CM 1850	Leica Biosystems Nussloch GmbH, Nussloch, Germany
Mikrotom	RM 2245	Leica Biosystems Nussloch GmbH, Nussloch, Germany
Mikrotom	HM 335S-2	MICROM International GmbH, Walldorf, Germany
Plate reader	Infinite M200 PRO	TECAN, Männedorf, Switzerland
Ultrasonic probe homogeniser	Art-Miccra D8	MICCRA GmbH, Heitersheim, Germany
Waterbath	HI 1210	Leica Biosystems Nussloch GmbH, Nussloch, Germany
Waterbath	Typ 1052	Gesellschaft für Labortechnik mbH, Burgwedel, Germany
Ultra low temperature freezer		VWR, Darmstadt, Germany

6.10. Software

Software	Version	Provider
Excel	16.55 (21111400)	Microsoft®, Redmond, Washington, USA
ImageJ	Java 1.8.0_172	Java, Sun Microsystems, Santa Clara, USA
Leica Application Suite X (LAS X)	3.7.5.24914	Leica Microsystems CMS GmbH, Mannheim, Germany

MATLAB	R2019a	MathWorks, Natick, Massachusetts, USA
Prism	9.3.0 (345)	GraphPad Software, LLC, San Diego, California
Transonic PV Loop System	ADV500	Transonic, Ithaca, NY, USA

7. Methods

7.1. Study Design

The study design is an experimental study.

7.2. Ethics Approval

Every experiment and intervention performed on pigs was approved by the district government of upper Bavaria, registered under the number ROB-55.2-2532.Vet_02-18-72, and executed accordingly. The animals were kept and cared for according to the *German and National Institutes of Health* animal legislation guidelines, the “Animal Welfare Act” and the “Animal Welfare Laboratory Animal Regulations”. Animal housing and interventions took place in the “Zentrum für Präklinische Forschung” (Klinikum rechts der Isar of the Technical University of Munich).

7.3. Acute Ischemia/ Reperfusion Pig Model

7.3.1. Laboratory Animals

Wildtype pigs from either sex were purchased from the “Lehr- und Versuchsgut der tierärztlichen Fakultät der LMU München“. They were divided into four groups at random: a three-day, seven-day, 28-day group, and sham animals. Three sham animals were chosen, which did not undergo any kind of intervention. All other animals underwent two interventions; the first took place at an age of 3 months and a weight of approximately 25kg.

7.3.2. Primary Intervention

The setup for the primary intervention was identical among all animals receiving treatment.

7.3.2.1. Anesthesia

Initially, the animals received sedation via intramuscular (i.m.) injection of 2 mg/kg body weight (bw) azaperone, 20 mg/kg bw ketamin and 0.02 mg/kg bw atropinsulfate. This was followed by the placement of an i.v. drip into the vena auricularis caudalis and i.v. injection of 5 mg midazolam, 2.5 µg/kg bw fentanyl and 1 mg/kg bw propofol, as required. The pigs were then intubated using a cuffed intratracheal tube and ventilated with a bag until they were brought into theater, placed on the operating table, and connected to the ventilation machine. During the intervention, anesthesia was upheld using a propofol perfusor running at a rate of 10 mg/kg bw/h. Analgesia was achieved using a fentanyl perfusor running at 3 µg/ kg bw/h. To maintain appropriate circulation and blood pressure, an adrenalin perfusor and 500 ml Ringer with 5.0 g magnesiumsulfate and 150 mg amiodarone were running continuously. Vital signs were being monitored via ECG, pulsoxymetry and invasive arterial blood pressure measurements. At the end of the procedure the animals received 10 mg/ kg bw cefuroxime as an antibiotic infection prophylaxis. (Bähr et al., 2021)

7.3.2.2. Catheterization and In Vivo Measurements

An incision was placed approximate to the sternocleidomastoid muscle. The external carotid artery was mobilized, ligated cranially, and a 9F port was introduced into the vessel. Prior to vessel ligation, the pigs were anticoagulated using 10 000 IE heparin. A pigtail catheter was lead through the port into the artery and advanced forward into the LV. The correct placement of the catheter was confirmed using a mobile c-arch x-ray. To determine LVEF, contrast (Ultravist-370) was injected rapidly into the LV while a series of x-ray images (‘loops’) were taken. The pigtail catheter was removed and replaced by a scisense pressure-volume catheter; the correct placement in the LV was confirmed via x-ray imaging. A pressure-volume curve of the LV was recorded, and the was catheter removed. (Bähr et al., 2021)

7.3.2.3. Left Ventricular Ejection Fraction Analysis

The LVEF is a measure of global heart function and defined by the relative stroke volume (SV) of the heart in relation to the LVEDV. It can be calculated as such:

$$LVEF = SV/LVEDV \times 100\%$$

The c arch x-ray loops were analyzed and the largest expansion of the LV, the LVEDV, and the smallest expansion of the LV, the LVESV, were isolated. Using ImageJ

software, the respective LV sizes were calculated. The SV can also be described as the change in ventricular volume from diastole to systole, hence SV = LVEDV – LVESV. Consequently, LVEF was calculated using the formula below:

$$LVEF = (LVEDV-LVESV)/LVEDV \times 100\%$$

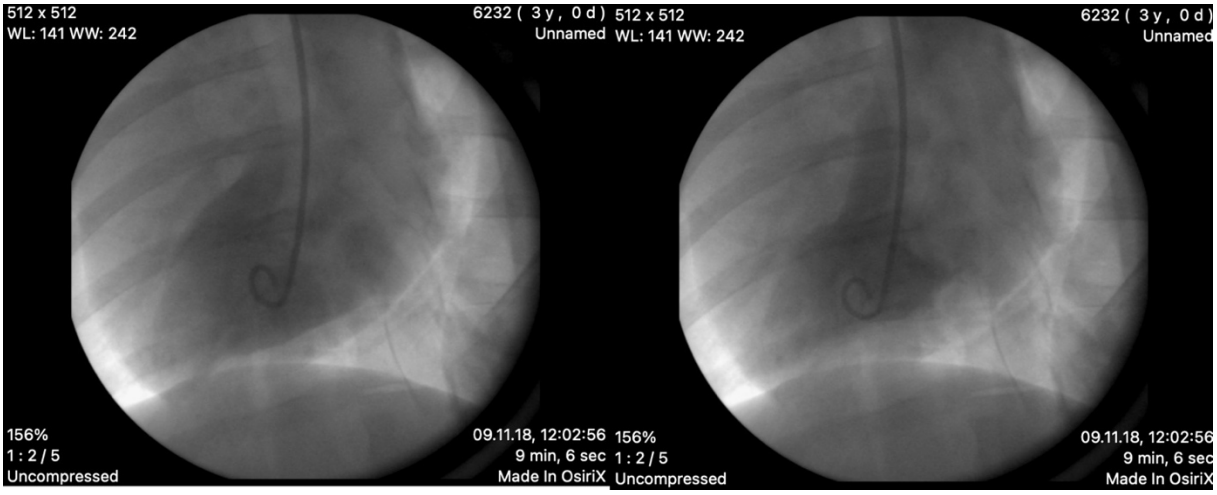

Figure 4: Cardiac C-Arch X-Ray Images

Porcine cardiac images of the left ventricle (LV) were obtained during primary and secondary intervention using contrast injected via a pigtail catheter and captured with a mobile c-arch x-ray. On the left, the LV is displayed in diastole. On the right, the LV is displayed in systole. The pigtail catheter is visible on both images within the LV.

7.3.2.4. Acute Ischemia, rhAgrin Application and Reperfusion

A guide catheter (Judgkins R) was fed through the port and placed into the left anterior descending artery (LAD). An over the wire balloon catheter was advanced atop the guide catheter and a 3.5 x 20 mm balloon placed distally of the bifurcation of the first diagonal LAD branch (D1), as indicated by the white arrow in figure 5 below. The correct placement of the balloon was ensured using x-ray imaging. The balloon was inflated with four to six bar to completely occlude the LAD distal D1 and induce acute ischemia. This was immediately confirmed and reconfirmed after 30 minutes using x-ray imaging. At the time of acute ischemia induction 150 mg amiodarone was injected to support cardiac function. After 57 minutes of ischemia time either 33 µg/kg bw rhAgrin diluted in 5 ml saline, or 5 ml pure saline were injected slowly over three minutes; rhAgrin consists of the C-terminal half of human agrin (Ala1260-Pro2045) with an N-terminal 6-His tag. The balloon was deflated after exactly 1 h ischemia time

and reperfusion confirmed using x-ray imaging. Afterwards, all instruments were removed from the animal and the punctured artery and skin were sutured close.

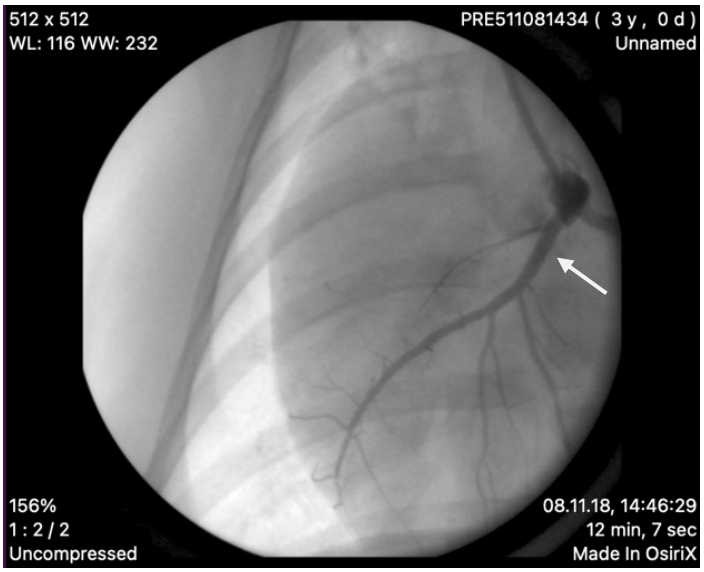

Figure 5: Left Anterior Descending Artery on C-Arch X-Ray

C-arch x-ray imaging of a porcine heart displaying the contrasted left anterior descending artery (LAD). The white arrow indicates the appropriate location for coronary occlusion distal of the first diagonal branch of the LAD. On image the artery is not occluded, and perfusion is fully established.

7.3.3. Animal Groups

Animals undergoing intervention were split into three groups according to the post-ischemia reperfusion time between primary and secondary intervention. Animals of each sex were allocated to the groups at random. After primary intervention, three-day animals were kept for 72h until the second intervention and termination, seven-day animals for 7 days and 28-day animals for 28. Moreover, the 28-day animals receiving agrin were further split into two groups, one of which only receiving one dose of agrin during the primary intervention, the other receiving an additional dose of rhAgrin (33 µg/kg bw) i.v. 72h post acute ischemia. The exact group distribution can be found in table 2 below.

Table 2: Animal Groups

Post-Ischemia Reperfusion Time	Injection Received	Animals (=n)
Three days	Saline	3
	rhAgrin	4
Seven days	Saline	2
	rhAgrin	3
28 days	Saline	8
	1x rhAgrin	6
	2x rhAgrin	5

7.3.4. Application of BrdU

5-bromo-2-deoxyuridine (BrdU) is a synthetic pyrimidine analog used as a marker for cell proliferation; it is incorporated into the deoxyribonucleic acid (DNA) of proliferating cells during the S-phase of mitosis (Riccardi et al., 1988). All animals from the seven-day group received 20 mg/kg bw BrdU every other day after the primary intervention as an i.v. injection.

7.3.5. Secondary Intervention

The setup for the secondary intervention was identical among all animals receiving an intervention. The time point for secondary intervention was chosen according to group allocation after three, seven or 28 days. The anesthesia protocol matches the one for primary intervention, described in chapter 7.3.2.1., except for the omission of the antibiotic prophylaxis. Catheterization and *in vivo* measurements correspond to the ones performed during primary intervention as well.

7.4. Infarct Staining, Tissue Sample Collection and Processing

7.4.1. Infarct Staining and Tissue Sample Collection

Following the collection of *in vivo* data on day three, seven or 28, a median sternotomy with opening of the pericardium was performed. The LAD distal D1 was ligated at the previous occlusion site and injected with 2% methylene blue solution. Methylene blue serves as a visual aid to determine the cardiac tissue still being perfused after occlusion of the LAD, hence the non-infarcted or remote area of the myocardium. The pigs were terminated using a direct injection of saturated KCl into the myocardium and the subsequent removal of the heart. This was followed by an injection of 150mg triphenyl tetrazolium chloride (TTC) dissolved in 10ml 0.9% NaCl into the LAD. TTC is a redox indicator and reacts with the lactate dehydrogenase (LDH) in viable heart tissue to stain it deep red. In the absence of a functioning LDH, the tissue assumes a pale color. TTC therefore served as an aid to distinguish between infarct and border zone.

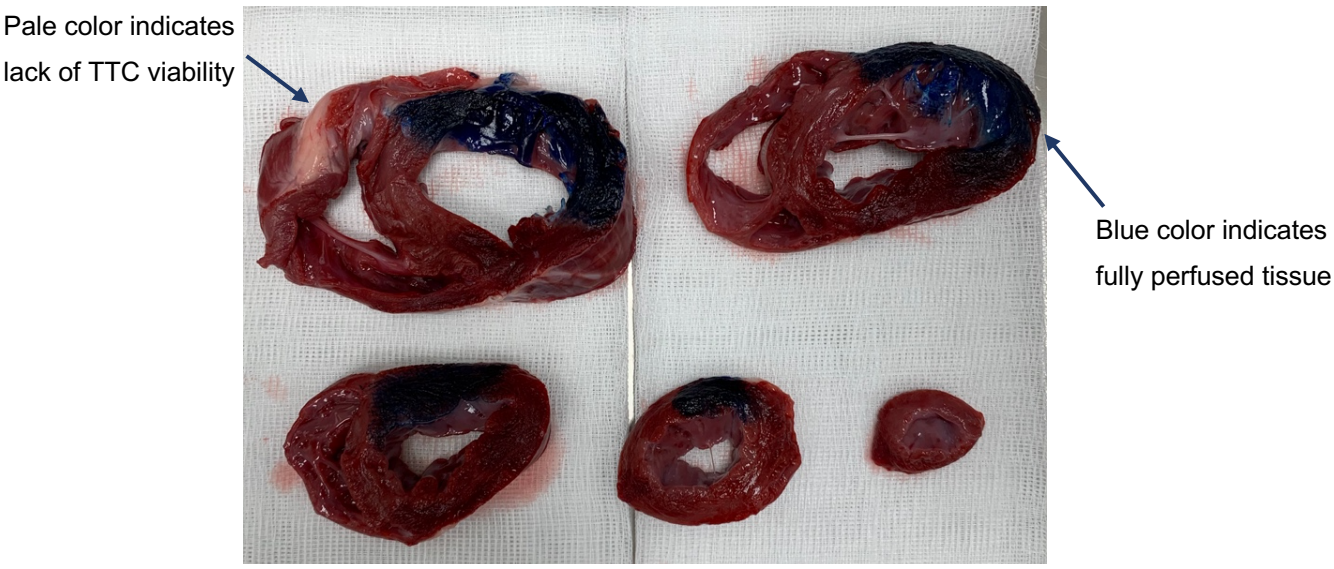

Figure 6: Tissue Viability Staining on Porcine Heart Slices Post-mortem

After termination of the pig, the porcine heart was explanted. Cardiac tissue viability was assessed using methylene blue and triphenyl tetrazolium chloride (TTC) staining. Methylene blue injected into the occluded left anterior descending artery serves as a visual aid for fully perfused tissue during occlusion and therefore marks the remote area of the myocardium blue. A lack of TTC viability marks infarcted areas of the heart pale or white in color, due to the absence of functioning LDH. The heart is then cut into five slices. Slice one is approximate to the base (top left) and slice five is the apex of the heart (bottom right).

The hearts were then cut vertical to their axis into five slices of 1 cm thickness each, slice one being approximate to the base and slice five forming the apex of the heart. Images were taken of the heart to determine infarct size using ImageJ software. The LV in slices one to four was then further divided into eight samples, the LV in slice five into four samples of equal size. This totals 36 transmural LV tissue samples per pig. According to methylene blue stain and TTC viability, the samples were categorized into infarct, remote and border zone. Each sample was then divided into two pieces; one was placed on dry ice and the other into 4% formaldehyde solution for further processing.

7.4.2. Tissue Sample Processing

7.4.2.1. Cryopreservation

Samples on dry ice were transferred and stored in a -80°C freezer.

7.4.2.2. Paraffin-embedding

Samples in 4% formaldehyde were embedded in paraffin by hand according to the paraffin embedding protocol in table 3 below. The formalin fixed and paraffin embedded tissue (FFPE) samples were then mounted onto histology cassettes and stored at room temperature (RT).

Table 3: Paraffin Embedding Protocol

Method	Time (h)	Temperature
1. Fixation:		
7% Formaldehyde	12	RT
2. Washing in running tap water	3	RT
3. Dehydration:		RT
50% Isopropanol	2	
75% Isopropanol	3	
90% Isopropanol	6	
100% Isopropanol	4	
100% Isopropanol	4	

4.	Infiltration:		
	Paraffin	8	60°C

7.5. Histology Staining

7.5.1. Conventional Histopathology

Conventional histopathology stains were performed to assess the level of inflammation and the extent of the fibrotic scarring in the myocardium by means of a haematoxylin and eosin (HE) and Sirius red stain. For this purpose, seven FFPE samples comprising of two samples for infarct and remote zone and three samples for border zone were chosen from each animal in the relevant groups. Only samples from the second and third heart slice were hereby chosen. The samples were cut at 4 µm using a microtome, transferred to slides, dried on a 36°C hotplate overnight and subsequently stained according to the protocols described in tables 4 and 6. The slides were then mounted using Entellan® mounting medium and a coverslip and stored at RT.

7.5.1.1. Haematoxylin and Eosin

HE is a routine stain in pathology and serves as a topographical overview. As one of the principal tissue stains in histology, HE can be used to visualize tissue inflammation and cell infiltration.

Tissue samples from each animal in the three-day group were chosen and processed as described above. They were stained according to the HE staining protocol in table 4. Five independent and representative images for each sample were obtained using bright light microscopy at 200- and 100-fold magnification. Conforming to Lin et al. (2015), the extent of cellular tissue infiltration was semi-quantitatively analyzed in a blinded manner using a 1-3 scoring system, as demonstrated in table 5 below (Lin et al., 2015).

Table 4: Haematoxylin and Eosin Staining Protocol

Method	Time (min)	Temperature
1. Deparaffinization:		RT
100% Xylol I	10	
100% Xylol II	10	
2. Rehydration:		RT
100% Isopropanol	4	
100% Isopropanol	4	
96% Isopropanol	4	
96% Isopropanol	4	
70% Isopropanol	4	
ddH_2O	Rinse	
3. 100% Hämalaun nach Mayer	10	RT
4. Running tap water	5	RT
5. 1% HCl in 70% Isopropanol	2 x 1 sec	RT
6. Running tap water	5	RT
7. 0.1% Eosin	4	RT
8. ddH_2O	Rinse	RT
9. Dehydration:		RT
70% Isopropanol	Rinse	
96% Isopropanol	1	
96% Isopropanol	1	
100% Isopropanol	4	
100% Isopropanol	4	
10. 100% Xylol II	4	RT
11. 100% Xylol I	4	RT
12. Mounting with Entellan®		RT

Table 5: Scoring System for the Extent of Cellular Tissue Infiltration (Lin et al., 2015)

Score	Extent of cellular infiltration
1	Mild infiltration
2	Moderate infiltration, inflammatory cells scattered throughout the tissue but background stromal connective tissue still intact
3	Severe infiltration, inflammatory cells infiltrate the tissue densely

7.5.1.2. Sirius Red

Sirius red is a strong anionic dye with a sulphonic acid group, that reacts with basic groups in collagen molecules to stain collagen fibers red, while the cytoplasm remains yellow in color (Junqueira et al., 1979). As collagen is a main player in ACR and the formation of a fibrotic scar after AMI, Sirius red staining was used to quantify the extent of fibrosis present in the LV (Y. Sun et al., 2000).

Tissue samples from each animal in the three- and 28-day group were chosen and processed as described above. The samples were stained according to the Sirius red staining protocol in table 6 below. Five independent images of each sample were taken at 200-fold magnification using bright light microscopy and the relative fibrosis quantity was analyzed using ImageJ software in a blinded manner.

Table 6: Sirius Red Staining Protocol

Method	Time (min)	Temperature
1. Preparation of 0.1% Sirius red solution: 0.1% Direct Red 80 in 1.3% picric acid solution in ddH_2O with consequent maturing for one week		RT
2. Deparaffinization:		RT
100% Xylol I	10	
100% Xylol II	10	
100% Xylol III	10	

3.	Rehydration:		RT
	100% Isopropanol	2	
	90% Isopropanol	2	
	70% Isopropanol	2	
	ddH_2O	5	
	ddH_2O	10	
4.	0.1% Sirius red solution	60	RT
5.	ddH_2O	2 x rinse	RT
6.	Dehydration:		RT
	90% Isopropanol	2	
	100% Isopropanol	2	
7.	100% Xylol III	10	RT
8.	100% Xylol II	10	RT
9.	100% Xylol I	10	RT
10.	Mounting with Entellan®		RT

7.5.2. Immunofluorescence

Immunofluorescent histology stains were performed to assess angiogenesis, cell proliferation, CM cell cycle reentry, CM hypertrophy, and cell death. Both cryopreserved and FFPE tissue samples from the three-, seven-, 28-day group and sham animals were utilized, whereby only samples from the second and third heart slice were chosen for further processing. For each animal out of the three-, seven- and 28-day groups a total of six samples, two from each area (infarct, remote and border zone), were chosen. For the sham animals two LV samples each were analyzed.

7.5.2.1. PECAM-1 WGA

Platelet endothelial cell adhesion molecule 1 (PECAM-1), also known as cluster of differentiation (CD) 31 is a molecule expressed on the surface of a variety of cells within the vascular system, such as platelets, monocytes, and neutrophils (Lertkiatmongkol et al., 2016). Additionally, it is a key component of the endothelial

intercellular junctions and can therefore be used as a marker to visualize the presence of endothelial cells and consequently angiogenesis (H. Wei et al., 2005; Winkler et al., 2018). Following myocardial infarction, angiogenesis serves as a repair mechanism to preserve microvascular circulation and enable a functional recovery (Fan et al., 2015).

Wheat germ agglutinin (WGA) is a lectin binding to glycoconjugates, which are abundantly present in cellular membranes (Chazotte, 2011). As a co stain it visualizes the outlines of cells present.

Cryopreserved tissue samples from every animal in the three-day and 28-day group were chosen according to the previous description, sectioned at 5 µm using a cryotome and subsequently stained according to the PECAM-1 WGA staining protocol in table 7 below. With a fluorescent and confocal microscope five independent representative images were taken at 200-fold magnification from each sample in a blinded manner. PECAM-1 signals were counted twice using ImageJ and statistical analysis was performed via GraphPad Prism software.

Table 7: PECAM-1 WGA Staining Protocol

Method	Time (min)	Temperature
1. Thaw sections	15	RT
2. Fixation of sections with precooled acetone	15	4 °C
3. Cycle tissue sections with Liquid Blocker (DAKO pen)		RT
4. Preparation of blocking buffer: 2% BSA, 0.1% Triton X-100 and 1% normal goat serum in 1X PBS-T (0.1% Tween20 in 1X PBS)		
5. Incubation with blocking buffer	30	RT
6. Incubation with primary antibody diluted in blocking buffer (ratio 1:50)	Overnight	4 °C
7. Washing in 1x PBS-T	3 x 10	RT
8. Preparation of fluorescent labeling solution: 2% BSA, 0.2% Triton X-100, secondary antibody (ratio		

	1:50), 0.1% 1mM CaCl2 and WGA (ratio 1:10) in 1X PBS-T		
9.	Incubation with fluorescent labeling solution	120	RT
10.	Washing in 1x PBS-T	3 x 10	RT
11.	Mounting with Vectashield antifade mounting medium with DAPI®		RT
12.	Storing protected from light		4 °C

Table 8: Antibodies and Fluorescent Agents Used in PECAM-1 WGA Staining Protocol

Antibody	Target	Clonality	Fluorescent tag	Host	Dilution
Primary antibody	Anti-PECAM-1	Monoclonal IgG		Mouse	1:50
Secondary antibody	Anti-mouse	Polyclonal IgG	Alexa Fluor® 594	Goat	1:50
Wheat germ agglutinin (WGA)			Alexa Fluor® 488		1:10

7.5.2.2. Ki67 Cardiac Troponin I

Ki67 is a nuclear protein linked to cell proliferation and mitosis, which is abundantly present during S, G2 and M phases and undergoes a continuous degradation process in G1 and G0 phases. Cells in quiescence, that recently underwent mitosis, still express moderately high levels of Ki67, whereas cells that have remained in a state of quiescence for longer do not express Ki67 above levels of detection; thereby, Ki67 is a sensitive marker to detect active and recently active cell proliferation. (Miller et al., 2018)

cTnI is an integral part of the cardiac muscle cell and serves to identify CMs.

Cryopreserved tissue samples were chosen from the three-day and sham animal groups as previously described and cut at 5 µm using a cryotome. After establishing a working protocol to sensitively detect Ki67 and cTnI (as stated in table 9), the samples were then stained accordingly. Sections were imaged at 630-fold

magnification using a fluorescent and confocal microscope in a blinded manner and five representative independent images were taken each. All CMs, as well as Ki67 positive CMs were counted twice. A CM was determined Ki67 positive if ≥50% of the nucleus and the entire circumference of the nucleus expressed a Ki67 signal. A statistical analysis of the relative amount of Ki67 positive cells was performed using GraphPad Prism.

Table 9: Ki67 cTnI Staining Protocol

Method	Time (min)	Temperature
1. Thawing sections	15	RT
2. Fixation of sections with precooled acetone	15	4 °C
3. Cycle tissue sections with Liquid Blocker (DAKO pen)		RT
4. Preparation of blocking buffer: 0.2% Triton X-100 and 2% BSA in 1X PBS-T (0.1% Tween20 in 1X PBS)		
5. Incubation in blocking buffer	30	RT
6. Incubation of primary Ki67 antibody diluted in blocking buffer (ratio 1:100)	Overnight	4 °C
7. Washing in 1X PBS-T	3 x 10	RT
8. Incubation with secondary Ki67 antibody diluted in blocking buffer (ratio 1:200)	120	RT
9. Washing in 1X PBS-T	3 x 10	RT
10. Incubation with primary cTnI antibody diluted in blocking buffer (ratio 1:100)	Overnight	4 °C
11. Washing in 1X PBS-T	3 x 10	RT
12. Incubation with secondary cTnI antibody diluted in blocking buffer (ratio 1:200)	120	RT

13. Washing in 1X PBS-T	3 x 10	RT
14. Mounting with Vectashield antifade mounting medium with DAPI®		RT
15. Storing protected from light		4 °C

Table 10: Antibodies Used in Ki67 cTnI Staining Protocol

Antibody	Target	Clonality	Fluorescent tag	Host	Dilution
Primary Ki67 antibody	Anti-MKI67	Polyclonal IgG		Rabbit	1:100
Secondary Ki67 antibody	Anti-rabbit	Polyclonal IgG	Alexa Fluor® 568	Goat	1:200
Primary cTnI antibody	Anti-cTnI	Polyclonal IgG		Rabbit	1:100
Secondary cTnI antibody	Anti-rabbit	Polyclonal IgG	Alexa Fluor® 488	Donkey	1:200

7.5.2.3. BrdU

In the mammal heart, CM proliferation regresses shortly after embryonic and fetal development (Bergmann et al., 2015). Cardiac growth in an adult heart is predominantly achieved via cellular hypertrophy, rather than proliferation, with a CM turnover rate of only 0.3-1% per year (Bergmann et al., 2009; Waring et al., 2014). However, studies have displayed that the stimulation of endogenous CM proliferation is not only possible, but also has the ability to restore systolic cardiac function (Gabisonia et al., 2019).

To visualize CM proliferation rate during the point of infarction until the termination of the animals, an anti-BrdU stain on animals in the seven-day group was utilized. BrdU, being a synthetic nucleoside that had previously been applied to the animals, is integrated in newly formed DNA during mitosis. FFPE samples were chosen as described above and sectioned at 4 µm using a microtome. First, a working method

for heat induced epitope retrieval for antigen retrieval in FFPE preserved samples was established; the protocol is described in table 11, subpoint 1 to 5 below. Following that, the sections were stained according to the protocol described in table 11, subpoint 6 to 20. Five independent images were taken at 630-fold magnification from each sample using fluorescent and confocal microscopy. The BrdU expressing signals were counted twice in a blinded manner. A statistical analysis was then performed using GraphPad Prism.

Table 11: BrdU Staining Protocol

Method	Time (min)	Temperature
1. Deparaffinization:		RT
100% Xylol I	15	
100% Xylol II	15	
100% Xylol : 100% EtOH (1:1)	5	
2. Rehydration:		RT
100% EtOH	5	
95% EtOH	5	
80% EtOH	5	
50% EtOH	5	
3. Washing in 1X PBS	3 x 5	RT
4. Preparation of 1X citrate buffer, pH 6.0: Dilution of 10X citrate buffer		RT
5. Antigen Retrieval:		
Rinse in ddH_2O	1	RT
Cover slides with 1X citrate buffer		
Cook slides in the pressure cooker	10	120°C
Cool slides in ice water	10	0°C
Wash slides in ddH_2O	2 x 5	RT
Wash slides in 1X PBS-T (0.1% Tween20 in 1X PBS)	5	RT
6. Preparation of 0.1M borate buffer: Dilution of 20X borate buffer		RT

7.	Denaturation of DNA: Incubate in 2N HCl:PBS (1:6) Neutralize with 0.1M borate buffer	 30 10	 37°C RT
8.	Washing in 1X PBS	3 x 5	RT
9.	Preparation of blocking buffer: 20% heat inactivated horse serum and 0.5% Triton X-100 in 1X PBS		
10.	Blocking: Incubation with 120 µl blocking buffer per slide	60	RT
11.	Preparation of incubation buffer: 2% normal horse serum and 0.5% Triton X-100 in 1X PBS		
12.	Preparation of primary antibody solution: Primary antibody diluted 1:100 in incubation buffer		
13.	Incubation with 120 µl primary antibody solution per slide	Overnight	RT
14.	Washing in 1X PBS	3 x 5	RT
15.	Washing in 1X TBS	5	RT
16.	Preparation of secondary antibody solution: Secondary antibody diluted 1:200 in incubation buffer		
17.	Incubation with 120 µl secondary antibody solution per slide	90	RT
18.	Washing in 1X PBS	3 x 5	RT
19.	Mount slides with Vectashield antifade mounting medium with DAPI®		
20.	Store slides protected from light		4°C

Table 12: Antibodies Used in BrdU Staining Protocol

Antibody	Target	Clonality and antibody class	Fluorescent tag	Host	Dilution
Primary antibody	Anti-BrdU	Polyclonal IgG		Rabbit	1:100
Secondary antibody	Anti-rabbit	IgG	Alexa Fuor® 568	Goat	1:200

7.5.2.4. WGA DAPI

ACR includes not only fibrosis, but also cellular hypertrophy; both mechanisms leading to a thickening of the ventricular wall and impairment of global cardiac function (Cong et al., 2017). To analyze CM hypertrophy, cryopreserved samples of the three-day group have been chosen as stated above. The samples were cut at 5 µm and stained according to the WGA DAPI staining protocol in table 13. Five independent images were obtained at 630 and 200-fold magnification in a blinded manner using fluorescent and confocal microscopy. The maximum and minimum ferret diameter, as well as the average fiber size were calculated via the semi-automatic muscle analysis using segmentation of histology (SMASH) toolbox within the MathLab software. Statistical analysis was performed using GraphPad Prism.

Table 13: WGA DAPI Staining Protocol

Method	Time (min)	Temperature
1. Thawing sections	15	RT
2. Fixation in precooled acetone	15	4°C
3. Cycle organ sections with a liquid blocker (DAKO pen)		RT
4. Preparation of blocking buffer: 2% BSA in 1X PBS-T (0.1% Tween20 in 1X PBS)		
5. Incubation with blocking buffer	30	RT

6.	Preparation of fluorescent labeling solution: 0.2% Triton X-100, 0.1% WGA, 0.1% 1mM $CaCl_2$, Hoechst 33342 (ratio 1:500) in blocking buffer		
7.	Incubation with fluorescent labeling solution	60	RT
8.	Washing with 1X PBS-T	3 x 10	RT
9.	Mount slides with aqueous mounting medium		
10.	Storage protected from light		4°C

7.5.2.5. TUNEL Cardiac Troponin I

Terminal deoxyribonucleotidyl transferase-mediated dUTP-digoxigenin nick end labeling (TUNEL) assay is a method to trace cell death via detection of 3'-hydroxyl termini in DNA fragments (Crowley et al., 2016). The assay does not distinguish among the different causes for cell death, such as apoptosis or necrosis (Grasl-Kraupp et al., 1995). In combination with a cTnI co-stain as a sensitive marker for CMs, it can be used to visualize CM death following AMI.

After establishing the TUNEL cTnI co-staining protocol, cryopreserved border zone samples from the three-day animal group were cut at 5 µm using a cryotome and stained according to the protocols depicted in table 14 and 15. Following that, five independent images were taken at 630-fold magnification from each sample in a blinded manner using fluorescent and confocal microscopy. All CMs, as well as TUNEL expressing CMs were counted twice. A CM was determined TUNEL positive if ≥ 50% of the nucleus and the entire circumference of the nucleus expressed the signal. A statistical analysis of the relative amount of TUNEL positive CM was performed using GraphPad Prism.

Table 14: In Situ Cell Death Detection Kit, TMR Red® Protocol

Method	Time (min)	Temperature
1. Thawing sections	15	RT
2. Cycle tissue sections with Liquid Blocker (DAKO pen)		RT

3.	Preparation of fixation solution: 4% paraformaldehyde in 1X PBS, pH 7.4		
4.	Fixation of tissue sections with fixation solution	20	RT
5.	Washing with 1X PBS	3 x 10	RT
6.	Preparation of permeabilization solution: 0.1% Triton X-100 and 0.1% sodium citrate in ddH_2O		
7.	Incubation in permeabilization solution on ice	2	4°C
8.	Preparation of TUNEL reaction mixture: Add 50 µl of enzyme solution to 450 µl label solution and mix well to equilibrate components		
9.	Washing with 1X PBS	3 X 5	RT
10.	Incubation with 50 µl of TUNEL reaction mixture per tissue section	60	37 °C
11.	Washing with 1X PBS	3 x 5	RT

Table 15: cTnI Co-staining Protocol

Method	Time (min)	Temperature
12. Washing in 1X PBS	3 x 5	RT
13. Preparation of blocking buffer 0.2% Triton X-100 and 2% BSA in 1X PBS		
14. Incubation with blocking buffer	30	RT
15. Incubation with primary antibody diluted in blocking buffer (ratio 1:100)	Over night	4°C
16. Washing in 1X PBS	3 x 10	RT

17. Incubation with secondary antibody diluted in blocking buffer (ratio 1:200)	120	RT
18. Washing with 1X PBS	3 x 10	RT
19. Mounting with Vectashield antifade mounting medium with DAPI®		
20. Storing protected from light		4°C

Table 16: Antibodies Used in cTnI Staining Protocol

Antibody	Target	Clonality and antibody class	Fluorescent tag	Host	Dilution
Primary antibody	Anti-cTnI	Polyclonal IgG		Rabbit	1:100
Secondary antibody	Anti-rabbit	Polyclonal IgG	Alexa Fluor® 488	Donkey	1:200

7.6. Hydroxyproline Assay

The amino acid hydroxyproline is commonly found in collagen. As collagen is an integral part of ECM accumulation in cardiac fibrosis, the quantification of hydroxyproline present in LV tissue samples via hydroxyproline assay serves as a marker for the presence and extent of myocardial fibrosis (Schipke et al., 2017). For this assay, six cryopreserved samples were chosen: two remote, border and infarct zone samples for each animal from the three-day group. Firstly, a new method to mechanically powder cryopreserved tissue utilizing liquid nitrogen, mortar and pestle was established. 40 to 80 mg of each sample were powdered and stored on dry ice. This was followed by the execution of the hydroxyproline assay kit, according to the manufacturers protocol, as stated in table 17. Each sample and the standard were hereby loaded as duplicates. Absorbance was then measured thrice at 560 nm optical density (OD) with a microplate reader and statistical analysis performed using GraphPad Prism.

Table 17: Hydroxyproline Assay Kit (Colorimetric) Protocol

Method	Time (min)	Temperature
1. Standard preparation: i. Prepare 200 µl of 0.1 µg/µl standard by diluting 20 µl of the provided standard (1 mg/ml solution) in 180 µl of ddH_2O. ii. Then dilute the standard using ddH_2O to receive 0.1 µg/µl, 0.08 µg/µl, 0.06 µg/µl, 0.04 µg/µl and 0.02 µg/µl. Use ddH_2O for a 0.00 µg/µl concentration. iii. Transfer the standard into a 96 well plate in duplicates.		RT
2. Add 100 µl of ddH_2O for every 10mg of powdered tissue and thoroughly homogenize with an ultrasonic probe homogenizer.		RT
3. Transfer 100 µl of sample homogenate to a pressure-tight, screw-capped polypropylene vile.		RT
4. Add 100 µl of 10N concentrated NaOH to each tissue sample homogenate. Heat the samples up to 120°C using a pressure cooker and incubate for one hour.	60	120°C
5. Following alkaline hydrolysis, place vile on ice.	5	4°C
6. Add 100 µl of 10N concentrated HCl to neutralize residual NaOH. Vortex vile.		RT
7. Centrifuge vile at 10,000 x g to pellet any insoluble debris that may remain following hydrolysis.	5	RT
8. Collect supernatant and transfer to a new tube. Keep on ice.		4°C
9. Add 50 µl of each sample in duplicates to a 96-well plate.		4°C

10. Evaporate the sample hydrolysate and standard curve wells to dryness. A crystalline residue will be left in the well.		65°C
11. Preparation of oxidation reagent mix: Add 6 µl of Chloramine T concentrate to 94 µl of oxidation buffer for each sample.		RT
12. Add 100 µl of oxidation reagent mix to each well and incubate the plate at RT for 20 min.	20	RT
13. Add 50 µl of developer to each reaction well and incubate the plate at 37°C for 5 min.	5	37°C
14. Add 50 µl of DMAB concentrate solution to each reaction well and mix contents thoroughly.		RT
15. Seal the plate with the provided microplate sealer film and incubate at 65°C for 45 min.	45	65°C
16. Measure absorbance at OD 560 nm on a microplate reader.		RT

7.7. Statistical Analysis

Statistical analysis was performed using Microsoft® Excel (Version 16.55 (21111400)). GraphPad Prism (Version 9.30 (345)) was used for further statistical analysis, as well as the generation of statistical figures and graphs. For each experiment, the remote, border and infarct zone of saline and rhAgrin injected pigs were compared. First, the Shapiro Wilk normality test was performed to analyze normality according to the gaussian distribution. Then, the appropriate statistical test was chosen for each experiment. For normally distributed data in two unpaired groups, the statistical significance was interpreted using an unpaired two-tailed t test with Welch's correction for unequal variances. If samples in two unpaired groups were not normally distributed, the non-parametric Mann-Whitney-U test was used. For the 28

day group, a one-way analysis of variance (ANOVA) test was executed. Finally, as the HE stain was analyzed semi quantitatively, only descriptive data was collected. For all statistical test performed, a p-value <0.05 was identified as statistically significant. Further annotations of statistical significance are explained in table 18 below.

Table 18: Notation of Statistical Significance

P-value	Implication	Notation
≥ 0.05	Not significant	ns
< 0.05	Significant	*
< 0.01	Very significant	**
< 0.001	Highly significant	***
< 0.0001	Extremely significant	****

8. Results

8.1. Agrin's Regenerative Potential in a Large Animal Model

8.1.1. Measurement of Cardiac Function *In Vivo*

In vivo cardiac function was assessed on the day of AMI and after a three- and 28-day reperfusion period in animals from the 28-day group.

LVEF serves as a measure for systolic cardiac function. As early as three days after AMI, a relevant reduction in LVEF in saline and rhAgrin treated animals can be noticed compared to the baseline at day 0. However, compared to the saline injected control LVEF is significantly upheld upon single and dual dose rhAgrin treatment. After 28 days, a further reduction in LVEF to 24.78 ± 1.02% can be objectified in saline injected animals, whereas LVEF is preserved in single dose rhAgrin treated animals at 36.81 ± 2.38%. This represents a 48.55% gain of systolic function upon a single injection of rhAgrin. There is a trend towards further cardio protection after dual dose rhAgrin injection, with an upheld LVEF at 41.66 ± 1.79% and a gain of 68.12% compared to the saline injected control. *Republished from (Baehr et al., 2020)*

LVEDP is a distinguishing prognostic parameter in diastolic dysfunction and heart failure (Zile et al., 2001). Three days after AMI, a significant increase in LVEDP can be objectified in saline injected animals, whereas LVEDP is maintained just above baseline in rhAgrin treated animals, with no relevant difference between a single or dual dose injection. This trend is exacerbated after 28 days as LVEDP rises even further to 17.72 ± 0.82 mmHg in saline injected animals and remains unchanged at 10.26 ± 0.36mmHg and 10.13 ± 0.92mmHg in single and dual dose rhAgrin treated animals respectively. *Republished from (Baehr et al., 2020)*

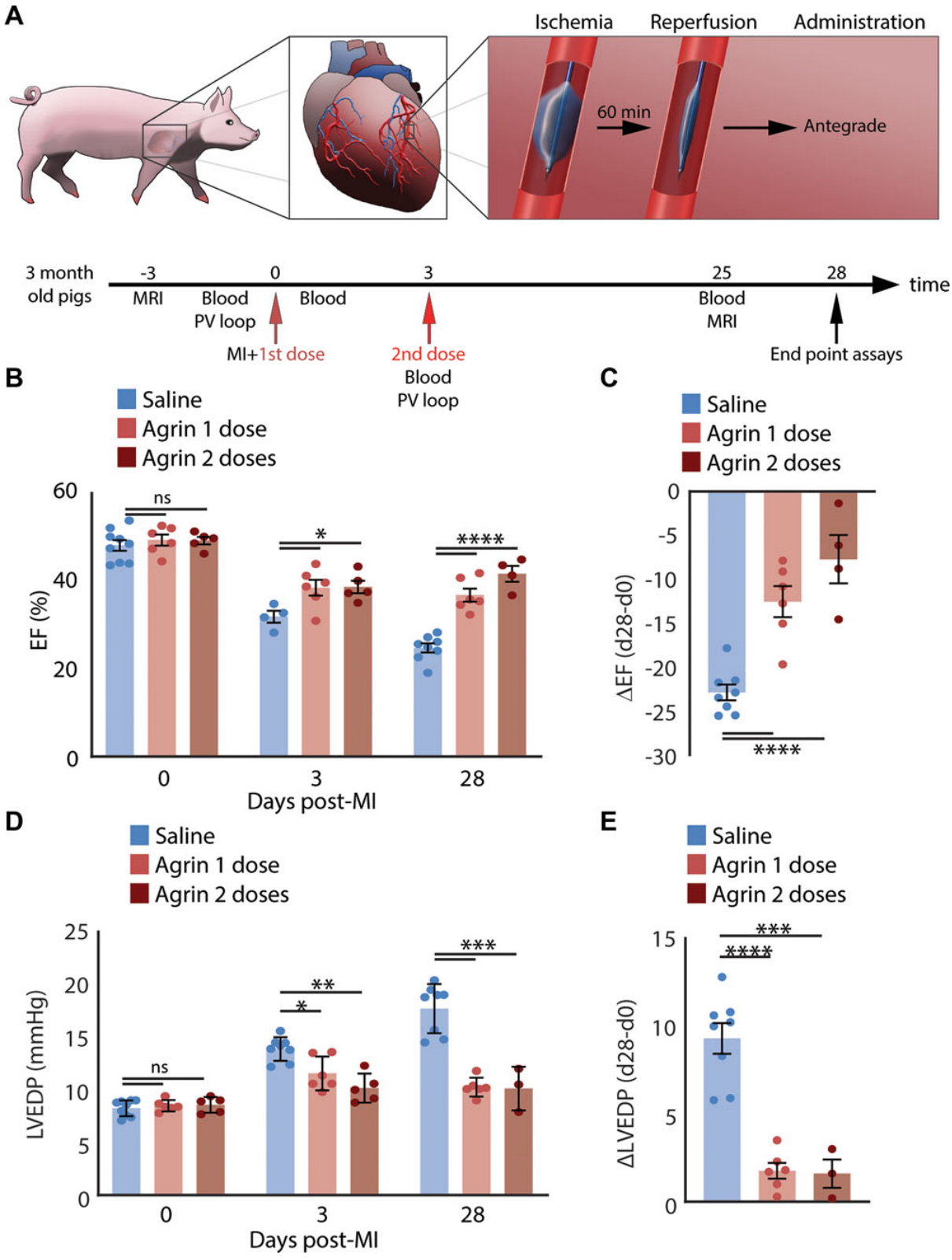

Figure 7: Cardiac Function in Saline and rhAgrin Treated Pigs (Baehr et al., 2020)

A, Scheme describing the experimental plan. Animals were treated with 1 or 2 doses of rhAgrin at days 0 and 3 after AMI and followed until day 28. Saline was used as a control. **B** and **C**, Bar graphs depicting the LVEF measurements derived from c-arch x-ray imaging. **B**, Bar graph depicting LVEF values at baseline and 3 and 28 days after AMI. **C**, Bar graph describing LVEF reduction in different treatments

at end point. **D** and **E**, Bar graphs showing the change in LVEDP, measured by pressure-volume loop catheter. **D**, Bar graph depicting LVEDP values at baseline and 3 and 28 days after AMI. **E**, Bar graph demonstrating LVEDP changes in different treatments at experimental end point. AMI indicates acute myocardial infarction; rhAgrin, recombinant human agrin; LVEF, left ventricular ejection fraction; LVEDP, left ventricular end diastolic pressure. **P*<0.05, ***P*<0.01, ****P*<0.001, *****P*<0.0001. (Baehr et al., 2020)

***A**, **B**, **C**, **D** and **E** republished from (Baehr et al., 2020).*

8.1.2. Cardiomyocyte Proliferation

CM proliferation and cell-cycle re-entry was measured by Ki67 cTnI staining in the three-day group and BrdU-incorporation in the seven-day group.

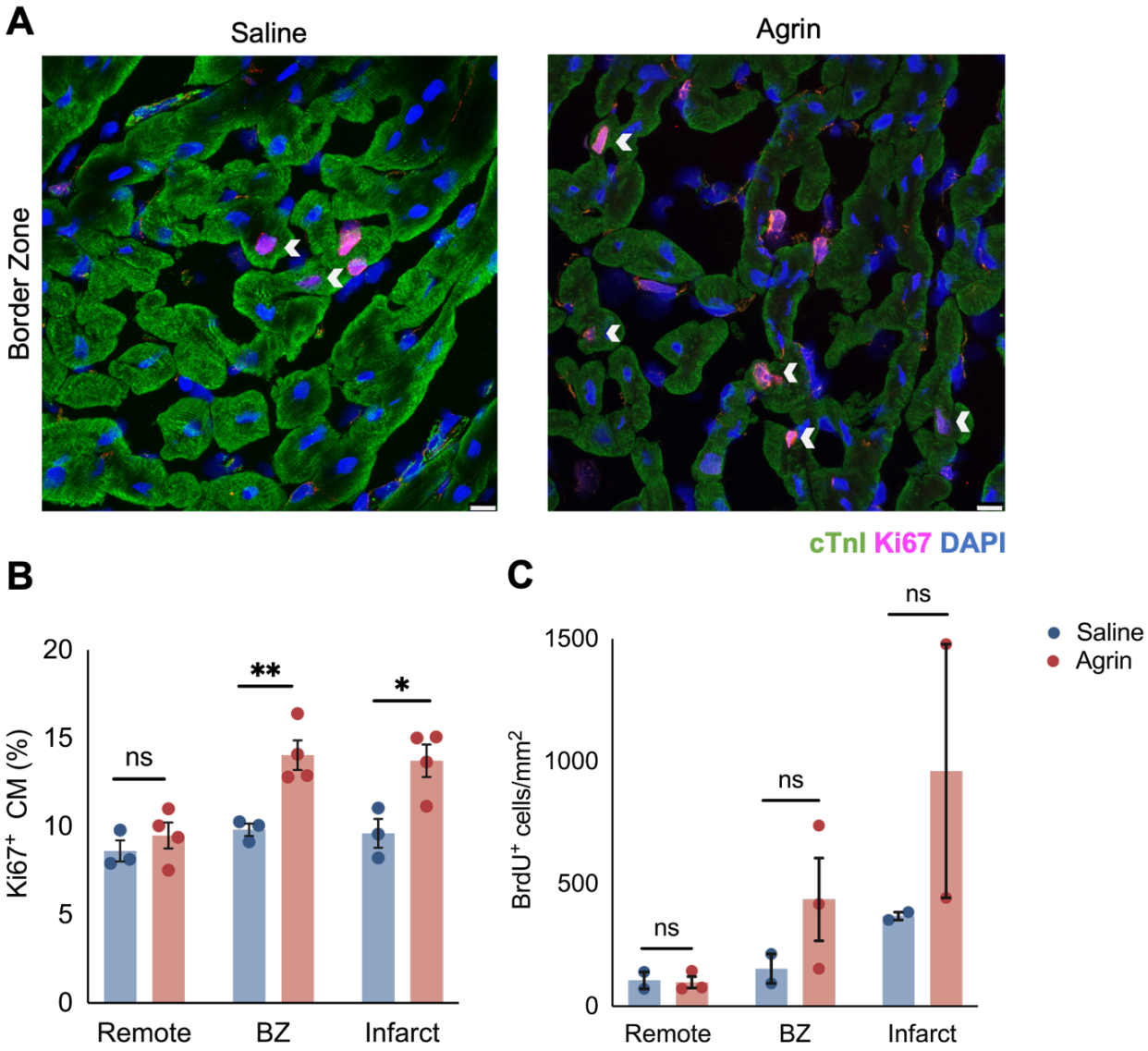

Figure 8: Cardiomyocyte Proliferation in Saline and rhAgrin Treated Pigs (Baehr et al., 2020)

Pigs underwent AMI, and reperfusion was sustained for three or seven days. The hearts were harvested on day three or seven, and histological analysis was performed. Three-day group: saline, n=3; rhAgrin, n=4. Seven-day group: saline, n=2; rhAgrin, n=3. **A** and **B**, CM proliferation/ cell cycle reentry was assessed by Ki67 immunofluorescent staining in the three-day group. A co-staining protocol using immunofluorescent cTnI was applied as a CM specific marker. **A**, Representative images at 630-fold magnification of Ki67 cTnI co-stained sections from the border zone of saline and rhAgrin treated animals. White arrows indicating $Ki67^+$ CMs. White scale bar in bottom right corner represents 10 µm. **B**, Bar graph depicting mean ± SEM of $Ki67^+$ CMs (%) in the remote, border and infarct zone of saline and rhAgrin treated animals. **C**, Pigs from the seven-day group were administered BrdU every other day for a week after AMI. CM proliferation/ cell cycle reentry was measured by immunofluorescent staining of BrdU incorporation. Bar graph depicting mean ± SEM of $BrdU^+$ cells in the remote, border and infarct zone of saline and rhAgrin treated animals. AMI indicates acute myocardial infarction; CMs, cardiomyocytes; cTnI, cardiac troponin I; SEM, standard error of mean; BrdU, bromodeoxyuridine; BZ, border zone; ns, nonsignificant. **P*<0.05, ***P*<0.01, ****P*<0.001, *****P*<0.0001. (Baehr et al., 2020)

***A** and **B** republished from (Baehr et al., 2020).*

Ki67 is a nuclear protein linked to mitosis and can be utilized to demonstrate cell proliferation. In adult sham animals, the baseline cell-cycle activity was measured at 1.09 ± 0.40% $Ki67^+$ CMs. Both saline and rhAgrin injected animals revealed an increased proliferative activity. Across the heart, proliferation was enhanced from remote areas to the infarct zone in both groups. However, a significant upregulation of cell cycle re-entry in rhAgrin compared to saline injected animals could be observed. This was most prominent in the border zone, with a rise of $Ki67^+$ CMs from 9.82 ± 0.35% to 14.04 ± 0.84% (P = 0.0099). Additionally, a 42.77% gain in proliferative activity was apparent in the infarct zone (saline, 9.61 ± 0.81%; rhAgrin, 13.72 ± 0.92%). *Republished from (Baehr et al., 2020)*

Animals in the seven-day group were administered BrdU every other day following AMI. BrdU is a base analog and is incorporated into the DNA of proliferating cells, thereby serving as a marker for accumulative cell-cycle re-entry over time. An increase in $BrdU^+$ signal density upon rhAgrin treatment compared to the saline injected control was measured. This accounts for a 183.94% gain of proliferative activity in the border zone (saline, 153.72 ± 59.97/mm^2; rhAgrin, 436.48 ± 169.14/mm^2) and a 160.60% gain in the infarct zone (saline, 368.61 ± 16.14/mm2; rhAgrin, 960.63 ± 518.06/mm^2). However, both sets of data were statistically non-significant.

8.1.3. Infarct Size and Fibrosis of the Heart

8.1.3.1. Infarct Size

Infarct size was assessed using TTC viability staining and normalized in relation to the LV area.

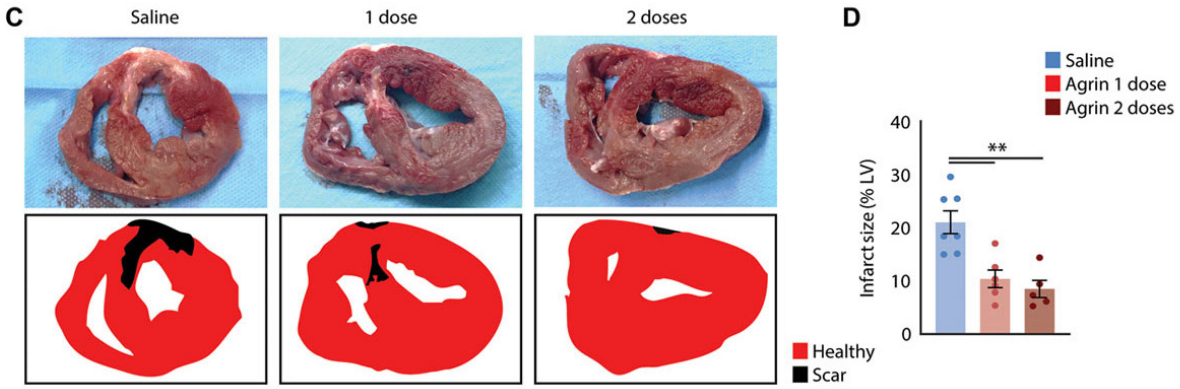

Figure 9: Infarct Size of Saline and rhAgrin Treated Pig Hearts (Baehr et al., 2020)

Pigs underwent AMI, and reperfusion was sustained for 28 days. The hearts were harvested on day 28, and histological analysis was performed. Saline, n=8; rhAgrin 1 dose, n=6; rhAgrin 2 doses, n=5. **C** and **D**, Scar assessment after saline or rhAgrin treatment at 28 days after AMI. **C**, Upper panel: representative images of heart section after TTC staining (white represents scar tissue, red represents viable myocardium); lower panel: same images with a graphic mask depicting healthy tissue (red) and scar (black). **D**, Bar graph describing the scar tissue in percent of the left ventricular wall, derived from TTC image analysis. AMI indicates acute myocardial infarction; TTC, triphenyltetrazolium chloride. **P*<0.05, ***P*<0.01, ****P*<0.001, *****P*<0.0001. (Baehr et al., 2020)

***C** and **D** republished from (Baehr et al., 2020).*

28 days post AMI, a significant reduction in infarct size from 21.03 ± 2.16% to 10.39 ± 1.65% in single dose rhAgrin treated animals compared to the saline injected control was objectified. A further decrease in infarct size to 8.51 ± 1.62% was measured upon dual rhAgrin injection. *Republished from (Baehr et al., 2020)*

8.1.3.2. Fibrosis

The relative amount of fibrosis in the heart of three- and 28-day animals was assessed by quantitative analysis of the collagen density in Sirius red stained heart sections using ImageJ software. Additionally, the amount of collagen present in samples from the three-day group was appraised by the amount of hydroxyproline detected.

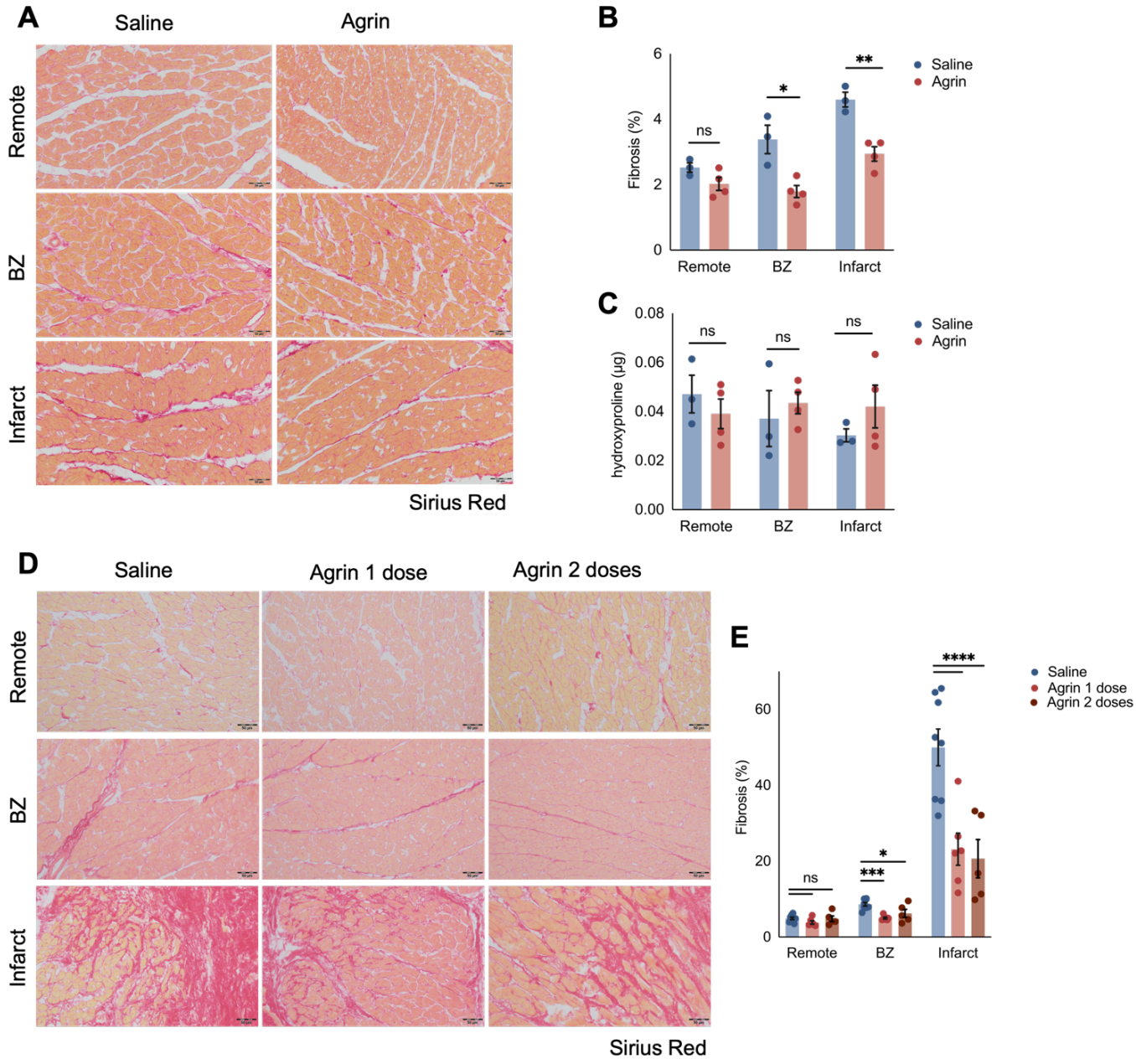

Figure 10: Fibrosis in Saline and rhAgrin Treated Pigs (Baehr et al., 2020)

Pigs underwent AMI, and reperfusion was sustained for three or 28 days. The hearts were harvested on day three or 28, and histological analysis was performed. Three-day group: saline, n=3; rhAgrin, n=4. 28-day group: saline, n=8; rhAgrin 1 dose, n=6; rhAgrin 2 doses, n=5. **A** and **B**, Interstitial fibrosis was assessed by Sirius Red staining for animals in the three-day group. **A**, Representative images at 200-fold magnification of Sirius Red stained sections from the remote, border and infarct zone of saline and rhAgrin treated animals. Black scale bar in bottom right corner represents 50 µm**. B**, Bar graph depicting mean ± SEM of the percentage of collagen measured in heart sections of the remote, border and infarct zone of saline and rhAgrin treated animals. **C**, Bar graph depicting mean ± SEM of hydroxyproline (µg) measured in samples from the remote, border and infarct zone of saline and rhAgrin treated animals in the three-day group. **D** and **E**, Interstitial fibrosis was assessed by Sirius red staining for animals in the 28-day group. **D**, Representative images at 200-fold magnification of Sirius red stained sections from the remote, border and infarct zone of saline, single and dual dose rhAgrin treated animals. Black scale bar in bottom right corner represents 50 µm**. E**, Bar graph depicting mean ± SEM

of the percentage of collagen measured in heart sections of the remote, border and infarct zone of saline, single and dual dose rhAgrin treated animals. AMI indicates acute myocardial infarction; SEM, standard error of mean; BZ, border zone; ns, nonsignificant. *P<0.05, **P<0.01, ***P<0.001, ****P<0.0001. (Baehr et al., 2020)

***A**, **B**, **D** (Infarct) and **E** (Infarct) republished from (Baehr et al., 2020).*

Collagen density measured by Sirius red staining is reduced in rhAgrin treated animals of the 28-day and three-day group compared to the saline injected control in the infarct and border zone of the heart. *Republished from (Baehr et al., 2020)*

This was most pronounced in the infarct zone of 28-day animals, where a 53.65% loss of relative interstitial fibrosis from 49.97 ± 4.84% to 23.16 ± 4.22% (P < 0.0001) was measured in single dose rhAgrin treated animals. After a second dose of rhAgrin, a trend towards further reduction to 20.66 ± 5.04% interstitial fibrosis was observed. Within the border zone, a significant reduction of collagen density from 8.64 ± 0.48% in saline injected to 5.01 ± 0.26% and 6.25 ± 1.06% in single and dual dose rhAgrin injected animals respectively was quantified (single dose, P = 0.0009; dual dose, P = 0.0289). *Republished from (Baehr et al., 2020)*

Like in the 28-day group, collagen density was reduced in the border and infarct zone of rhAgrin treated animals as early as three days post AMI. This accounts for a 36.09% (saline, 4.60 ± 0.23%; rhAgrin, 2.94 ± 0.22%) reduction of interstitial fibrosis in the infarct zone and a 47.04% (saline, 3.38 ± 0.43%; rhAgrin, 1.79 ± 0.18%) reduction in the border zone. *Republished from (Baehr et al., 2020)*

No significant difference in the amount of hydroxyproline present between rhAgrin treated and control animals was objectified. Interestingly, a downwards trend of hydroxyproline content from the remote to the infarct zone in saline injected animals can be observed. Hydroxyproline content in rhAgrin treated animals remains approximately consistent across all areas of the heart.

8.2. Investigating Agrin's Pleiotropic Mechanism of Action

8.2.1. Cell Death

A TUNEL assay was applied to quantify cell death within the border zone of hearts from the three-day animal group. To differentiate between CM and other cells, such as invading inflammatory cells, the CM-specific marker cTnI was introduced in a second approach. This is represented in figure 11 below.

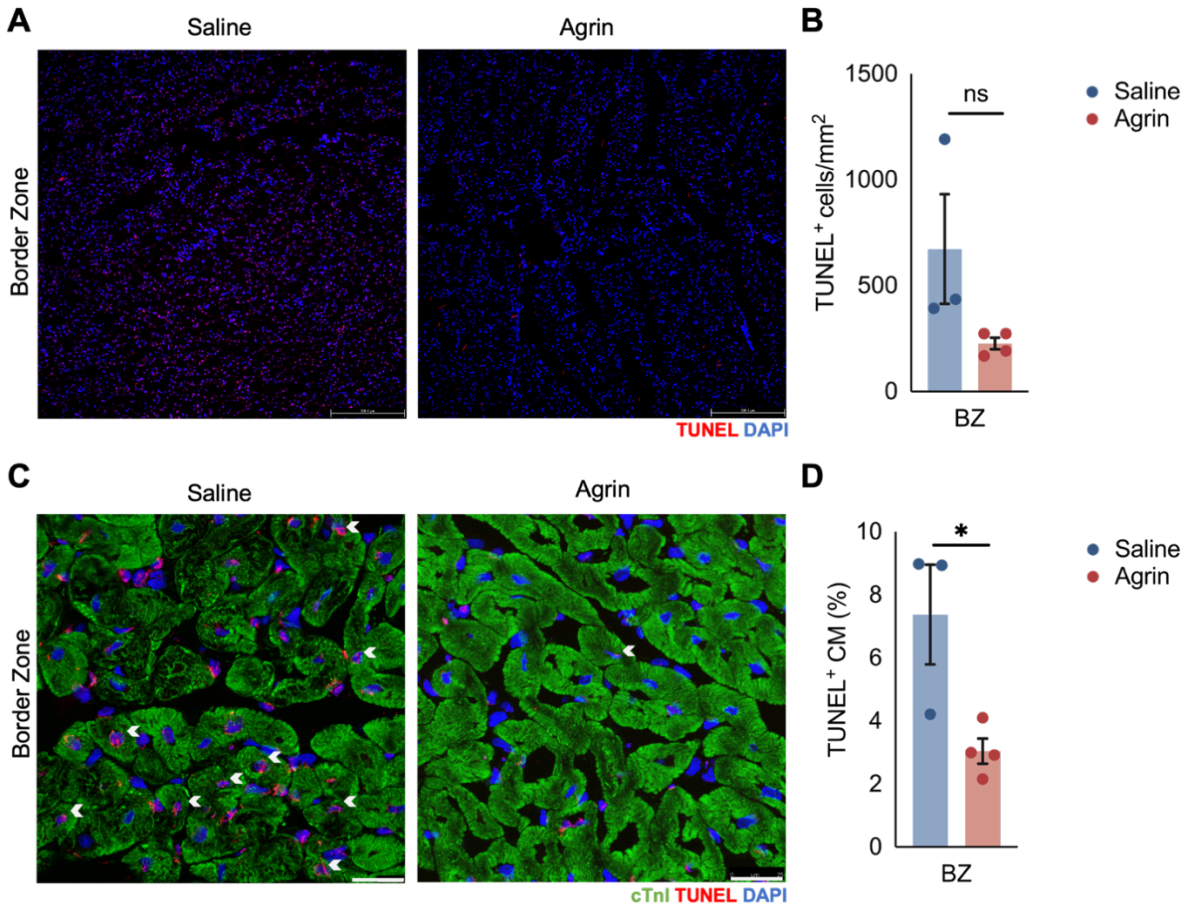

Figure 11: Cell Death in Saline and rhAgrin Treated Animals (Baehr et al., 2020)

Pigs underwent AMI, and reperfusion was sustained for three days. The hearts were harvested on day three, and histological analysis was performed. Saline, n=3; rhAgrin, n=4. **A** and **B**, Cell death was assessed by TUNEL immunofluorescent staining in the three-day group. **A**, Representative images at 100-fold magnification of TUNEL stained sections from the border zone of saline and rhAgrin treated animals. White scale bar in bottom right corner represents 301.9 µm. **B**, Bar graph depicting mean ± SEM of TUNEL$^+$ cells in the border zone of saline and rhAgrin treated animals. **C** and **D**, Cell death was assessed by TUNEL immunofluorescent staining in the three-day group. A co-staining protocol using immunofluorescent cTnI was applied as a CM specific marker. **C**, Representative images at 630-fold magnification of TUNEL cTnI co-stained sections from the border zone of saline and rhAgrin treated animals. White arrows indicate TUNEL$^+$ CMs. White scale bar in bottom right corner represents 25 µm.

D, Bar graph depicting mean ± SEM of TUNEL$^+$ CMs (%) in the border zone of saline and rhAgrin treated animals. AMI indicates acute myocardial infarction; TUNEL, terminal deoxyribonucleotidyl transferase-mediated dUTP-digoxigenin nick end labeling; CMs, cardiomyocytes; cTnI, cardiac troponin I; SEM, standard error of mean; BZ, border zone; ns, nonsignificant. *P<0.05, **P<0.01, ***P<0.001, ****P<0.0001. (Baehr et al., 2020)

***B**, **C** and **D** republished from (Baehr et al., 2020).*

TUNEL assay gives evidence for a reduction in the cell death density in rhAgrin treated animals compared to the saline control. TUNEL$^+$ signals were downregulated from 672.42 ± 259.55 /mm^2 to 226.16 ± 27.35 /mm^2, resulting in a 66.37% reduction of cell death upon rhAgrin administration. *Republished from (Baehr et al., 2020)*

This trend was confirmed in the analysis of CM death specifically. The relative amount of TUNEL$^+$ expressing CMs in rhAgrin treated animals was significantly reduced from 7.38 ± 1.58% in control animals to 3.05 ± 0.40% upon rhAgrin treatment (P = 0.0286). This amounts for a 58.67% reduction in CM death on account of rhAgrin treatment. *Republished from (Baehr et al., 2020)*

8.2.2. Inflammation

HE staining was utilised to detect cell infiltration and the level of inflammation in the heart of animals within the three-day group. Analysis was performed applying a semi-quantitative scoring system from one to three (1, mild infiltration; 2, moderate infiltration, inflammatory cells scattered throughout the tissue but background stromal connective tissue still intact; 3, severe infiltration, inflammatory cells infiltrate the tissue densely) (Lin et al., 2015). Representative images accounting for the different levels of infiltration are depicted in figure 12 A below.

Cell infiltration and inflammation is severely enhanced in both saline and rhAgrin injected animals in the infarct compared to the remote area of the heart (saline, 1.40 ± 0.10 to 2.29 ± 0.14; rhAgrin, 1.30 ± 0.10 to 1.85 ± 0.14).

The level of inflammation is reduced in rhAgrin treated animals compared to saline injected control animals across the entire heart. This depletion in inflammatory cell infiltration upon rhAgrin treatment is most pronounced in the infarct zone.

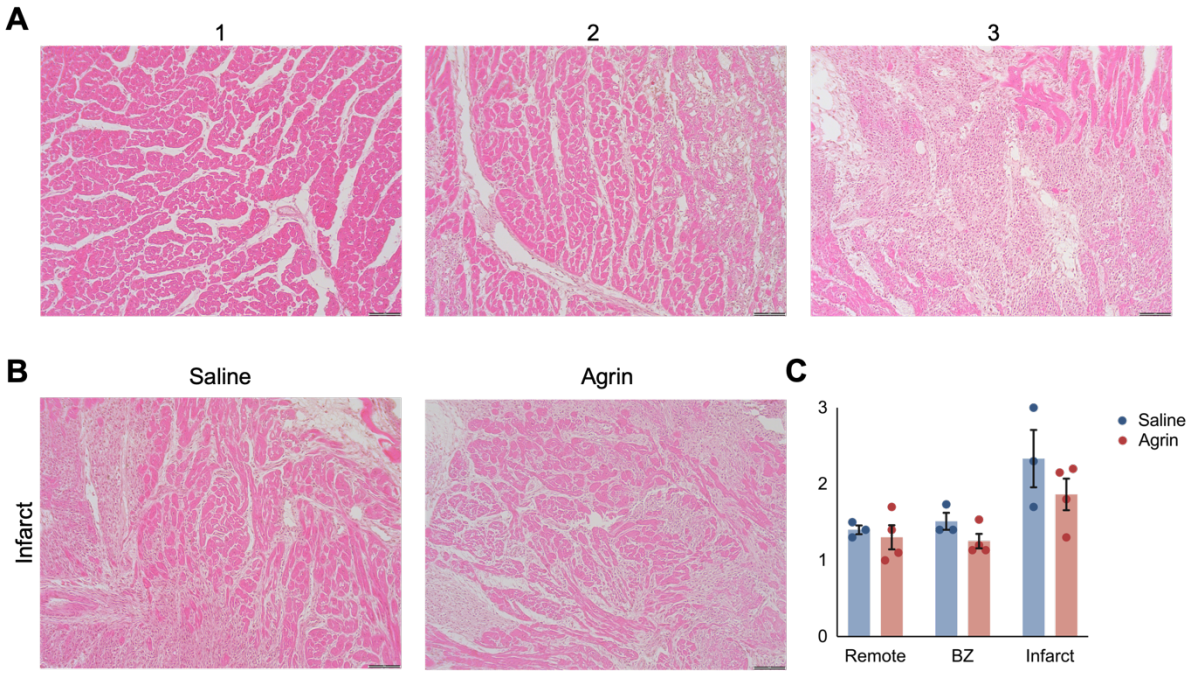

Figure 12: Level of Cell Infiltration in Saline and rhAgrin Treated Pigs

Pigs underwent AMI, and reperfusion was sustained for three days. The hearts were harvested on day three, and histological analysis was performed. Saline, n=3; rhAgrin, n=4. **A**, **B** and **C**, Inflammation was assessed semi-quantitatively by density of cell infiltration using HE staining in the three-day group. **A**, Representative HE stained heart sections at 100-fold magnification depicting three different levels of cell infiltration and inflammation. Black scalebar in the bottom right corner represents 100 µm. **B**, Representative images at 100-fold magnification of HE stained sections from the infarct zone of saline and rhAgrin treated animals. Black scalebar in the bottom right corner represents 100 µm. **B**, Bar graph depicting mean ± SEM of level of cell infiltration in the remote, border and infarct zone of saline and rhAgrin treated animals. AMI indicates acute myocardial infarction; HE, Hematoxylin and eosin; SEM, standard error of mean; BZ, border zone.

8.2.3. Capillary Network

The capillary network of saline, single and dual dose rhAgrin treated animals from the three-day and 28-day group was assessed using a PECAM-1 WGA co-staining protocol. PECAM-1 is a potent marker for endothelial cells.

The density of PECAM-1^{+} signals was reduced in the border and infarct zone compared to the remote area of the heart in both, saline and rhAgrin injected animals of the three- and 28-day group. *Republished from (Baehr et al., 2020)*

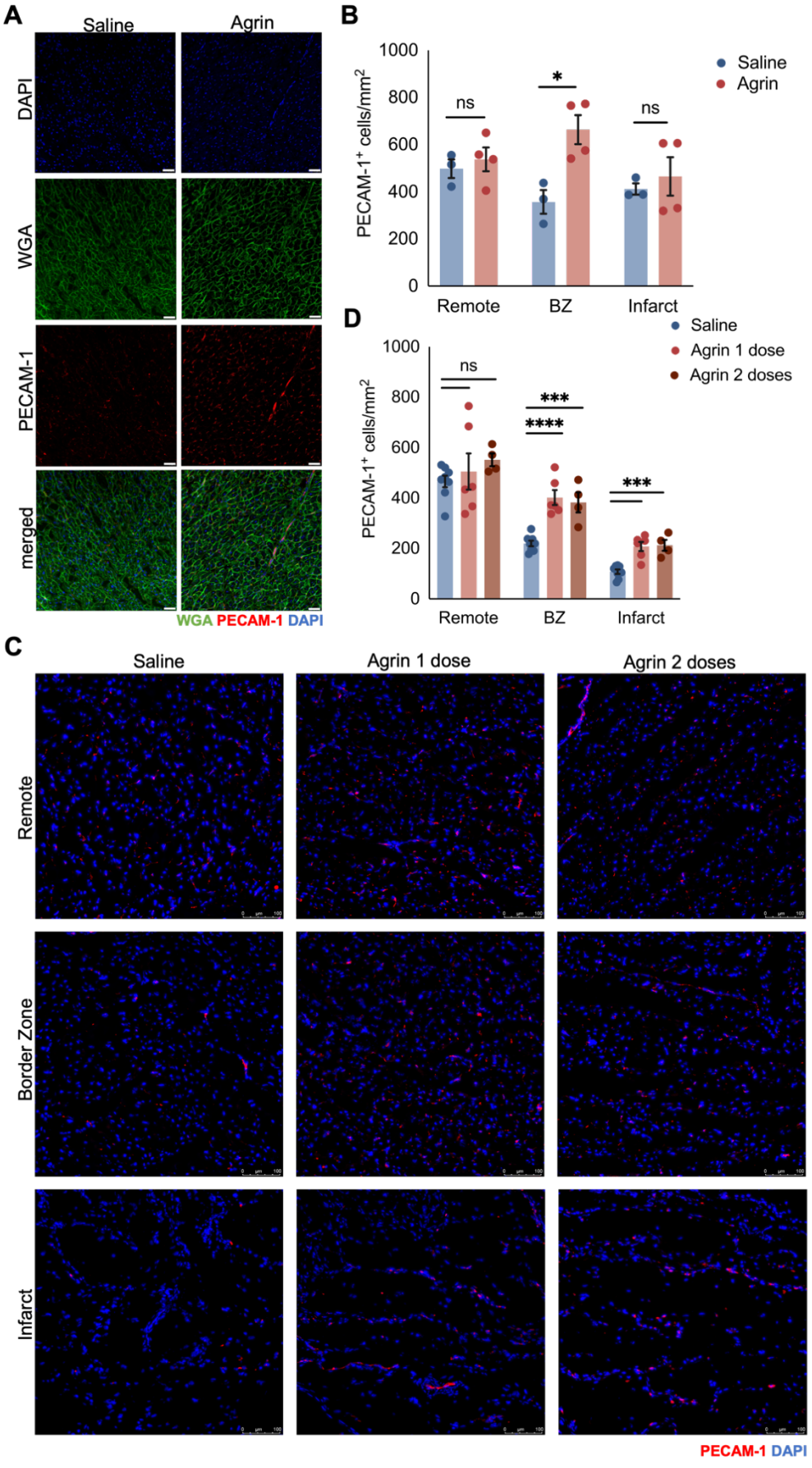

Figure 13: Capillary Network in Saline and rhAgrin Treated Pigs (Baehr et al., 2020)

Pigs underwent AMI, and reperfusion was sustained for three or 28 days. The hearts were harvested on day three or 28, and histological analysis was performed. Three-day group: saline, n=3; rhAgrin, n=4. 28-day group: saline, n=8; rhAgrin 1 dose, n=6; rhAgrin 2 doses, n=5. **A** and **B**, Capillary network was assessed by PECAM-1 WGA co-staining for animals in the three-day group. **A**, Representative images at 200-fold magnification of PECAM-1 WGA co-stained sections from the border zone of saline and rhAgrin treated animals. White scale bar in bottom right corner represents 50 µm**. B**, Bar graph depicting mean ± SEM of PECAM-1$^+$ signals per mm^2 measured in heart sections of the remote, border and infarct zone of saline and rhAgrin treated animals. **C** and **D**, Capillary network was assessed by PECAM-1 staining for animals in the 28-day group. **C**, Representative images at 200-fold magnification of PECAM-1 stained sections from the remote, border and infarct zone of saline, single and dual dose rhAgrin treated animals. White scale bar in bottom right corner represents 100 µm**. D**, Bar graph depicting mean ± SEM of PECAM-1$^+$ signals per mm^2 measured in heart sections of the remote, border and infarct zone of saline, single and dual dose rhAgrin treated animals. AMI indicates acute myocardial infarction; PECAM-1, platelet endothelial cell adhesion molecule 1; WGA, wheat germ agglutinin; SEM, standard error of mean; BZ, border zone; ns, nonsignificant. *P<0.05, **P<0.01, ***P<0.001, ****P<0.0001. (Baehr et al., 2020)

***A** (merged), **B** and **D** republished from (Baehr et al., 2020).*

Within the three-day group, rhAgrin injected animals expressed a denser capillary network across the whole heart compared to the control. This was most evident in the border zone adjacent to the infarct, where an increase from 356.98 ± 50.59 to 663.15 ± 61.15 PECAM-1$^+$ signals /mm^2 was registered upon rhAgrin treatment (P = 0.0119). This accounts for an 85.77% gain in endothelial cells. *Republished from (Baehr et al., 2020)*

The elevation of capillary network density upon rhAgrin treatment was confirmed in the 28-day group across the whole heart. A 45.53 % gain in PECAM-1$^+$ signals from 218.86 ± 11.25 /mm^2 to 401.83 ± 29.60 /mm^2 after a single dose of rhAgrin compared to the control was observed in the border zone of the heart (P < 0.0001). No further increase in PECAM-1$^+$ signals was displayed in dual rhAgrin treated animals (382.85 ± 39.99 /mm^2). Within the infarct zone, higher numbers of PECAM-1$^+$ signals were quantified in single and dual dose rhAgrin treated animals (single dose, 207.41 ± 18.04 /mm^2; dual dose, 211.84 ± 21.80 /mm^2) compared to the saline-injected control (107.35 ± 9.00 /mm^2); both increments are statistically significant (single dose rhAgrin, P = 0.0003; dual dose rhAgrin, P = 0.0006). Again, no further rise in PECAM-1$^+$ signals was observed in dual compared to single dose rhAgrin treated animals. *Republished from (Baehr et al., 2020)*

8.2.4. Cardiomyocyte Size

To quantify CM size and assess cardiac hypertrophy, a WGA staining protocol was applied to animals from the three-day group. CMs were identified, due to the central position of their DAPI stained nuclei and size was analysed via SMASH toolbox within the MathLab software.

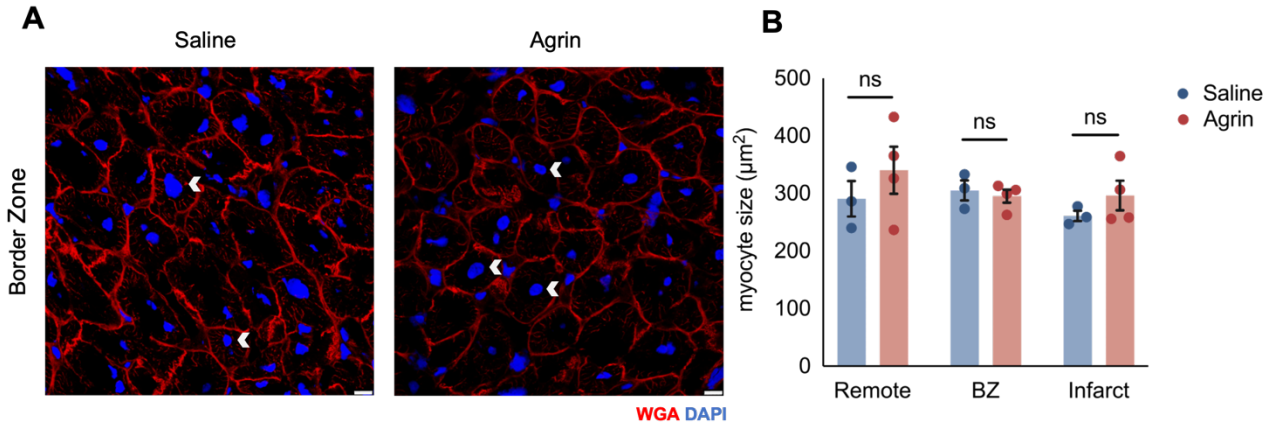

Figure 14: Cardiomyocyte Size in Saline and rhAgrin Treated Pigs

Pigs underwent AMI, and reperfusion was sustained for three days. The hearts were harvested on day three, and histological analysis was performed. Saline, n=3; rhAgrin, n=4. **A** and **B**, CM size was assessed by WGA immunofluorescent staining in the three-day group. **A**, Representative images at 630-fold magnification of WGA stained sections from the border zone of saline and rhAgrin treated animals. White arrows indicating the exemplary central position of the nucleus in CMs. White scale bar in bottom right corner represents 10 µm. **B**, Bar graph depicting mean ± SEM of CM size in the remote, border and infarct zone of saline and rhAgrin treated animals. AMI indicates acute myocardial infarction; CMs, cardiomyocytes; WGA, wheat germ agglutinin; BZ, border zone; ns, nonsignificant. **P*<0.05, ***P*<0.01, ****P*<0.001, *****P*<0.0001.

CMs are enlarged in the remote compared to the infarct zone of the heart of both saline and rhAgrin treated animals (saline, 261.10 ± 8.96 µm to 290.85 ± 30.78 µm; rhAgrin 296.37 ± 25.63 µm to 340.31 ± 40.98 µm). However no significant difference in CM size of rhAgrin treated animals compared to saline injected control animals could be observed across the heart.

9. Discussion

9.1. Investigative Results

9.1.1. rhAgrin Treatment Improves Heart Regeneration and Long-term Cardiac Function after AMI in Pigs

A recent study unveiled agrin's crucial role in the regenerative capacity of neonatal mouse hearts and demonstrated that rrAgrin application following AMI induces CM proliferation and cardiac repair in an ischemia/ reperfusion mouse model (Bassat et al., 2017). Now, this investigation provides new insights to substantiate the cardioprotective role of rhAgrin application following AMI in a large animal model and serves as a translational approach to bridge the gap between preclinical mouse models and clinical application.

9.1.1.1. Prevention of Global Cardiac Dysfunction

LVEF, commonly used to appraise systolic cardiac function, was improved upon rhAgrin treatment as early as three days after AMI. This trend was accentuated after 28 days, as LVEF was upheld in rhAgrin treated animals, but distinctly decreased in the saline injected control. LVEF recovery after AMI is pertinent, as it is associated with a reduction in long-term cardiovascular mortality (Otero-García et al., 2021).

Additionally, LVEDP data collected suggests a regression of diastolic dysfunction in rhAgrin treated pigs. LVEDP is significantly reduced upon rhAgrin treatment compared to the saline injected control and nearly returns to baseline measures after 28 days. Recent studies have demonstrated that HFpEF is the dominant type of CHF following AMI, putting the appraisal and treatment of diastolic dysfunction to the forefront of future investigations (Kamon et al., 2021).

Both measures of cardiac function do not remarkably change with a second dose of rhAgrin on day three. This suggests, that agrin's cardioprotective potential enfolds early after AMI.

Taken together, this study demonstrates a global improvement of cardiac function upon rhAgrin treatment.

9.1.1.2. Enhanced Cardiomyocyte Cell Cycle Re-entry

There have previously been successes in reactivating the proliferative potential of CMs in the adult murine heart, leading to improved cardiac repair (Bassat et al., 2017; D'Uva et al., 2015; Eulalio et al., 2012; Morikawa et al., 2017; K. Wei et al., 2015). This study now demonstrates a likewise capacity of cell-cycle re-entry in the porcine heart.

CM proliferation, as assessed by $Ki67^{+}$ CMs and BrdU incorporation, was enhanced in both the infarct and border zone of the myocardium upon rhAgrin treatment. Proliferative activity is increased due to an agrin mediated activation of Yap1 with subsequent suppression of the Hippo pathway (Bassat et al., 2017; von Gise et al., 2012). Increased CM proliferation following AMI has previously been linked to improved cardiac function, which is in line with *in vivo* functional data demonstrated in this study (Bassat et al., 2017; D'Uva et al., 2015; Eulalio et al., 2012; K. Wei et al., 2015). Still, the proliferative stimulus should not be prolonged indefinitely, as it can result in uncontrolled CM proliferation and lethal arrhythmias (Gabisonia et al., 2019). Bassat et al. (2017) provided evidence for the transient retention of rrAgrin within the murine heart for no more than three days (Bassat et al., 2017). However, these findings need to be substantiated in the porcine or human heart prior to clinical application.

Interestingly, both the saline and rhAgrin treated porcine hearts displayed a vast increase in CM proliferative activity across the entire heart compared to the sham control. This is consistent with an investigation performed on rats, which demonstrated a re-entry of CM into the cell cycle after induction of AMI (Y. Li et al., 2013).

9.1.1.3. Reduction of Scar Formation and Fibrosis within the Heart

Scar formation and fibrosis following AMI is an ambiguous process, with both favourable and detrimental effects on cardiac function and patient outcome.

On one hand, within the infarct zone replacement fibrosis is imperative to preserve LV structural integrity, avoid ventricular rupture and initially maintain cardiac output

(Barandon et al., 2003; Cohn et al., 2000; Gao et al., 2010; Gao et al., 2005). On the other hand, ACR results in reactive fibrosis of the remote myocardium, leading to increased tissue stiffness, potentially lethal arrhythmias, and heart failure (Arunachalam et al., 2018; González-Santamaría et al., 2015; Gordon et al., 2018; Ripplinger et al., 2009; Roberts et al., 1975; Tschabrunn et al., 2016).

In this study, a relevant reduction of interstitial fibrosis was demonstrated as early as three days post AMI in the infarct and border zone upon rhAgrin treatment. Less fibrosis in both infarct and border zone might reflect the attenuation of both, replacement and reactive fibrosis. This was further accentuated after 28 days, resulting in a macroscopically reduced infarct size. Like the *in vivo* functional data, no significant additive effect was observed upon dual rhAgrin injection on day three. Taken together with the relevant reduction of interstitial fibrosis on day three already, this suggests an early initiation of agrin's reparative processes.

A reduction in cardiac fibrosis is strongly associated with improved diastolic function due to lower myocardial stiffness (Moreo et al., 2009; Piccoli et al., 2017; Santos-Gallego et al., 2021). In this study, this is reflected in a reduction of LVEDP, as demonstrated previously. Interestingly, LOX gene expression, the enzyme responsible for maturation of the collagen matrix and therefore enhancing myocardial stiffness, peaks early (at day three) post AMI (González-Santamaría et al., 2015). An interplay of agrin and LOX is currently unknown but might be a relevant target for future investigations.

9.1.2. rhAgrin's Pleiotropic Mechanism of Action Ameliorates Hallmarks of ACR Following AMI in Pigs

Agrin's cardioprotective potential has previously been attributed to promoting CM proliferation and diminishing scar formation (Bassat et al., 2017). This research now demonstrates a pleiotropic mechanism of action, which additionally involves cell survival, immune modulation, and proangiogenic pathways. Just recently, a remarkably similar mechanism of action has been revealed in a murine cerebral ischemia/ reperfusion model upon intrathecal injection of agrin (S. Li et al., 2020).

9.1.2.1. Reduction of Cardiomyocyte Loss Within the Heart

Following AMI, necrotic and apoptotic cell death results in the loss of CMs and inflammatory cells (F. Han et al., 2019; T. N. James, 1998; Whyte et al., 1993). TUNEL staining can be utilised to detect fragmented DNA, which is characteristic for both mechanisms of cell loss and therefore nonspecific for detection of apoptosis (Grasl-Kraupp et al., 1995; Mizuta et al., 2013). In this study, histological analysis demonstrated a significant reduction in $TUNEL^+$ CMs within the border zone upon rhAgrin application. This might be the result of agrin inhibiting the Hippo pathway via Yap- and ERK-mediated signalling in the heart; a repression of the Hippo pathway has previously been linked to improved CM survival and cardiac function (Bassat et al., 2017; J. Huang et al., 2005; Triastuti et al., 2019).

9.1.2.2. Impeding Inflammation

The initial inflammatory response following AMI is imperative for adequate wound healing, as it allows for the clearing of cellular debris and apoptotic cells from the infarct zone (Horckmans et al., 2017; Jia et al., 2022; X. Wang et al., 2018). Suppression of the sterile inflammation following AMI can therefore lead to adverse effects and worsening of cardiac function (Timmers et al., 2007; X. Wang et al., 2018). Nonetheless, a prolonged inflammatory response leads to the degradation of the ECM, progressive ACR and the development of heart failure (Dobaczewski, Xia, et al., 2010; S. Liu et al., 2020; Sundström et al., 2004; Tripathi et al., 2020).

A relevant reduction of inflammatory cell infiltration in the infarct zone was demonstrated in this study. However, HE staining only serves as a topographic overview and cells could not be further classified. For this purpose, Baehr et al. (2020) analysed the density of $CD14^+$ and $CD68^+$ signals across the heart and revealed a reduction in both $CD14^+$ and $CD68^+$ signals in the border and infarct zone upon rhAgrin treatment (Baehr et al., 2020). $CD14^+$ is a well-known marker for monocytes and has recently been identified as a TLR coreceptor, modulating the inflammatory response (Baumann et al., 2010; Nielsen et al., 2020; Weber et al., 2012). A downregulation of $CD14^+$ monocytes proves beneficial to long term patient outcome; the presence of $CD14^+$ monocytes is positively correlated with ischemic cardiovascular events and the suppression of TLR mediated inflammatory pathways reduces ACR and cardiac

hypertrophy (Berg et al., 2012; X. Yuan et al., 2014). $CD68^+$ expression is commonly used as a marker for M1 macrophages (Nakagawa et al., 2021; Wijesundera et al., 2014). The loss of these inflammatory macrophages could be explained by an enhanced polarisation towards a reparative (M2) type upon rhAgrin treatment. Studies revealed that a reduction of M1 macrophages in favour of M2 improved wound healing and cardiac function, which is in line with *in vivo* functional data obtained in this study (M. Jung et al., 2017; D. Liu et al., 2019; W. Lu et al., 2019; Ma et al., 2013). However, follow up studies are needed to determine the presence and density of M2 macrophages and substantiate this hypothesis.

9.1.2.3. Increased Density of the Capillary Network

Capillary density and microvascular integrity are compromised due to ischemia/ reperfusion injury following AMI (Campbell et al., 2013; Hollander et al., 2016). The extent of this vascular injury positively correlates with the extent of subsequent ACR (Gerber et al., 2000). Increasing angiogenesis has therefore proven beneficial towards cardiac function post AMI in animal models (Hinkel et al., 2013; Kupatt et al., 2005; J. Sun et al., 2020).

This study demonstrates an enhanced capillary network, as represented by PECAM-1^+ signal density, upon rhAgrin treatment in both infarct and border zone after a three and 28-day reperfusion period.

Proliferation of the capillary network after a 28 day reperfusion period might be attributed to a reduction of M1 macrophages, as demonstrated previously. M1 macrophages release proinflammatory exosomes and miRNAs, such as miRNA-155, which exert anti-angiogenic properties and exacerbate cardiac dysfunction (S. Liu et al., 2020). Additionally, M2 macrophages mediate a potent pro-angiogenic response via fibroblast growth factor signalling (Jetten et al., 2014; W. Lu et al., 2019). This supports the notion, that rhAgrin application might induce macrophage polarisation from a proinflammatory (M1) to a reparative (M2) phenotype.

Recent studies also demonstrated agrin's potent pro-angiogenic potential in the tumorous environment; agrin stabilises VEGFR2 and induces migration and adhesion of endothelial cells via LRP4-MuSK pathways (Chakraborty et al., 2020; Njah et al., 2019). Activation of VEGFR2 promotes angiogenesis and physiological cardiac growth

(Kivelä et al., 2019). It's involvement in promoting angiogenesis in the heart upon rhAgrin treatment should be the target of future investigations.

Nonetheless, angiogenesis is a relatively slow process; basal coronary flow is only re-established on day seven post AMI in a rat model (Nelissen-Vrancken et al., 1996). Therefore, an increase in capillary density on day three is most likely due to a salvage of pre-existing capillaries upon rhAgrin treatment, presumably via Yap1 mediated inhibition of the Hippo pathway (Bassat et al., 2017). Yap1 activation has recently been linked to a relevant reduction in cardiac microvascular endothelial cell apoptosis (Q. Zhang et al., 2021).

Overall, rhAgrin application promotes the capillary network by protecting against endothelial cell loss and enhancing angiogenesis.

9.1.2.4. Hypertrophic Growth

Compensatory cardiac hypertrophy following AMI is a hallmark of ACR and associated with adverse events, such as development of CHF and enhanced mortality (Behar et al., 1992; Rubin et al., 1983)

After a three-day reperfusion period no significant difference in CM size was observed upon rhAgrin treatment. This is in line with agrin's signalling pathway; Yap1 activation has been demonstrated to induce heart growth via CM proliferation but does not seem to influence hypertrophic growth (von Gise et al., 2012). On the contrary, Baehr et al. (2020) demonstrated a relevant reduction of AMI induced CM hypertrophy after a 28 day reperfusion period (Baehr et al., 2020). This might be the result of a reduced stimulus for hypertrophic growth due to a reduction in infarct size and interstitial fibrosis, an enhancement of CM proliferation and angiogenesis, and the depletion of the inflammatory reaction upon rhAgrin treatment.

9.2. Clinical Implications

CADs are the primary cause for death and disability globally, accounting for 20% of annual deaths in Europe alone (Townsend et al., 2016). Even in non-fatal cases of AMI, more than a quarter of patients develop heart failure, which itself is associated with a substantial rise in mortality (Sulo et al., 2016). Infarct size and LV ACR have been identified as major determinants of long-term patient outcome following AMI (Timmers et al., 2008). Revascularization strategies therefore aim to reduce infarct size, preserve cardiac function, and diminish mortality (Le May et al., 2012; Olimulder et al., 2012).

This study now demonstrates, that a single antegrade injection of rhAgrin into the revascularized coronary artery ameliorates hallmarks of ACR, such as fibrosis, cell death and inflammation, and promotes CM proliferation to sustain global cardiac function in the long run.

Additionally, findings from this study suggest an evolutionary conserved mechanism of action in mammals; agrin's regenerative potential in mice has now been substantiated in a porcine model with remarkably similar outcomes. Additionally, Bassat et al. (2017) demonstrated a likewise capacity of inducing CM proliferation in human induced pluripotent stem cell derived CMs, posing agrin's translational potential for clinical application. (Bassat et al., 2017)

Antegrade rhAgrin injection, as compared to retrograde or intramyocardial injection, proves most efficient in delivering the agent into targeted ischemic regions of the heart (Baehr et al., 2020). This provides translationality, as an antegrade injection into the coronary artery can easily be incorporated into current procedural standards during PCI.

Furthermore, experimental data gives the impression, that rhAgrin's mechanism of action enfolds early within the heart; cellular events were observed as early as three days post AMI and no relevant additive effect could be demonstrated upon dual injection on day three. This makes an agrin based therapy more feasible in a clinical setting, as no additional intervention is required beyond revascularisation for its effect to enfold properly.

All in all, a single antegrade injection of rhAgrin can easily and readily be incorporated into current procedural standards during PCI and has the potential to ameliorate ACR

and progression into heart failure by means of a conserved, pleiotropic mechanisms of action.

9.3. Methods and Limitations

9.3.1. Advantages and Disadvantages of the Porcine Ischemia/ Reperfusion Model

The pig is an appropriate model to mimic heart disease, as the porcine cardiac anatomy, function and response to injury are remarkably similar to that of men (Crick et al., 1998; Lelovas et al., 2014; Mehran et al., 1991; Sahni et al., 2008). Still, cardiovascular diseases are a challenge regarding animal models, as diverse pathological entities and the contribution of comorbidities need to be considered.

The mean age of patients presenting with AMI varies between 55.9 and 62.9 years (Sharif Nia et al., 2018). However, this study was performed on young pigs, as adult pigs are very difficult to handle due to their vast size and weight. This is particularly relevant as age impacts cardiovascular response to injury. The neonatal pig heart has a regenerative capacity after AMI which preserves cardiac function and is attributed to CM proliferation (L. Ye et al., 2018; Zhu et al., 2018). Within the first week of life regenerative capacity of the porcine heart declines as CMs become post mitotic (L. Ye et al., 2018; Zhu et al., 2018). A case study reported a similar observation in neonate humans, where a newborn suffering from AMI recovered cardiac function to physiological perimeters (Haubner et al., 2016). Comparable to the pig heart, CMs become post-mitotic rapidly and CM turnover rate is less than 1% per year in young adults (Bergmann et al., 2009; Bergmann et al., 2015). Nonetheless, there are many reparative processes beyond CM proliferation that are age-dependent and impact regenerative capacity and post-infarct healing; these include angiogenesis, fibrosis, and inflammation (Hendee et al., 2021; Ma et al., 2015; Scavello et al., 2021; Yabluchanskiy et al., 2014; Y. Yang et al., 2008). These are possible confounders and need to be addressed prior to clinical application.

Animal models provide the optimal means for translationality, as they bridge the gap between *in vitro* studies and *in vivo* application. This is particularly true for the porcine ischemia/ reperfusion model. Porcine coronary anatomy is very similar to that of men; this allows for patient like heart catheterization, clinical PCI protocols, and antegrade injection of agents into the coronary artery (Bähr et al., 2021; Sahni et al., 2008). Prior studies have demonstrated that antegrade delivery of agents is efficient in targeting specific myocardial regions in pigs (Bozoglu et al., 2022; Hinkel et al., 2013; Hinkel et

al., 2020). However, preclinical studies on large animals also come with relevant downfalls. Ethical implications need to be considered regarding any study performed on animals. Additionally, large animal experiments are high maintenance regarding manpower and costs, such as nutrition, housing, and pharmacotherapy. Taken together with fluctuating availability of swine, this limits sample size and may impact reliability and generalizability of investigative results.

A viable alternative are murine ischemia/ reperfusion models. They are associated with less maintenance and larger sample sizes, which promotes reproducibility and reliability of investigative results. However, patient like heart catheterization and PCI cannot be performed; mice are too small for instrumentation and there are significant differences in murine and human coronary anatomy (Kumar et al., 2005). Therefore, agents must be delivered in a clinically irrelevant manner, such as intramyocardial injection following thoracotomy (Bassat et al., 2017; K. Wei et al., 2015). This reduces the translational potential of the murine model.

Organs-on-chip (OOCs) are a relatively new method and a possible outlook for future cardiovascular research. They involve *in vitro* engineered 3D tissue growing in a microfluidic device, which can mimic a physiological *in vivo* environment to imitate one or more organ level functions (Kurokawa et al., 2017; Leung et al., 2022; Maoz et al., 2017; Nunes et al., 2013). There have previously been successes in OOCs containing endothelialized myocardium with preserved function and contractility, as well as co-cultured OOCs, which involve the autonomic nervous system and a functional myocardium (Maoz et al., 2017; Oiwa et al., 2016; Y. S. Zhang et al., 2016). This preservation of function within an *in vitro* cultured tissue is a major advancement from cell culture experiments; a cell culture based approach is consistent, scalable, robust and reproducible, but lacks translationality, as it cannot imitate physiological organ level function (Arango et al., 2013; Ronaldson-Bouchard & Vunjak-Novakovic, 2018)

9.3.2. Limitations of rhAgrin

Agrin is a physiological component of the ECM in neonate mice and contributes to the cardiac regenerative capacity by enhancing CM proliferation via Yap-mediated signaling. However, agrin expression is rapidly downregulated postpartum. (Bassat et al., 2017)

In adults, upregulated agrin expression has been linked to the progression of various malignant entities, such as oral-, rectal-, cholangio-, hepatocellular-, and non-small cellular lung carcinomas (Chakraborty et al., 2015; Chakraborty et al., 2020; L. Han et al., 2021; He et al., 2021; Rivera et al., 2018; Z. Q. Wang et al., 2021). This oncogenic potential has been attributed to agrin promoting angiogenesis, proliferation, migration, and invasion of tumorous cells via various signaling pathways, including LRP4-MuSK, Yap, Erk, FAK and WNT (Chakraborty et al., 2015; He et al., 2021; Rivera et al., 2018; Z. Q. Wang et al., 2021). This poses a potential adverse reaction upon rhAgrin treatment. Nonetheless, there are several factors notably reducing the likelihood of such adverse effects. First, agrin is only retained within the heart for up to three days and therefore its effect is transient in nature (Bassat et al., 2017). Second, agrin could not be detected in lung, spleen, or liver after antegrade injection in pigs; this makes a systemic impact upon antegrade, intracoronary injection highly unlikely (Baehr et al., 2020). Third, primary cardiac sarcomas are very rare in nature and to date, there is no known association with Yap- or Hippo-signaling (Hamidi et al., 2010).

Nonetheless, further investigations are inevitable to assess agrin's oncogenic potential prior to clinical application. Additionally, pharmacokinetics, dose range and toxicity need further evaluation; this is preferably conducted in long-term studies.

9.3.3. Advantages and Disadvantages of *In Vivo* Functional Data Collection

The collection of *in vivo* functional data is imperative for preclinical research, as it allows for the translation of isolated cellular events observed in cell culture to their interaction in a complex organ structure.

LVEF obtained during ventriculography was utilized to assess *in vivo* cardiac function. This proves to be a reliable and accurate method, which is comparable to LVEF data obtained from a pressure-volume loop catheter or a thermodilution based method (Patel et al., 2021). However, total intravenous anesthesia (TIVA) was required to collect *in vivo* functional data. Prior studies have demonstrated that a propofol-fentanyl anesthesia generates myocardial depression; propofol is a negative chronotrope and reduces cardiac output (Fairfield et al., 1991; Monk et al., 1987; Vermeyen et al., 1991; Vermeyen et al., 1987). TIVA therefore modulates cardiac performance and may

lessen validity of the results. Nonetheless, inter-group comparability is not impaired, as anesthesia set up was consistent in between groups.

A viable and less invasive alternative to assess LVEF is 3D echocardiography, in which 2D images are reconstructed into 3D volumes (Chan et al., 2021; Nadkarni et al., 2000). This method has already been applied in the swine and generated results comparable to data obtained from cardiac magnetic resonance (Santos-Gallego et al., 2019). This provides the opportunity of eliminating the need for TIVA by alternatively using mild sedation. Another advantage is the option to analyze LV sphericity via 3D echocardiography; LV sphericity has prognostic significance for the progression of ACR (Karuzas et al., 2019; Santos-Gallego et al., 2019).

9.3.4. Advantages and Disadvantages of Histological Analysis

There are many advantages to histological stainings. It is a cost efficient, standardized, and reproducible method, that allows for the analysis of large tissue sections and provides insights into the internal architecture of functional cell groups. Additionally, a variety of specific antigens can be targeted with immunofluorescent stains and signals can be precisely localised within the different components of the sample by utilizing co-staining protocols.

However, quantification of signal density can be subject to human error, as it can involve manual counting. To bypass this issue, automated counting via ImageJ software was applied to determine PECAM-1^{+} signal density in an objective manner. Furthermore, cell size and relative amount of interstitial fibrosis was analysed in a semi-automated manner using SMASH toolbox and ImageJ respectively. Nonetheless, this is a potential source of error that needs to be addressed.

Another issue to be addressed are the antibodies used in the Ki67 cTnI co-staining protocol. Both primary antibodies share the same origin (rabbit). This is problematic since it reduces specificity of the secondary antibody, as it can bind to either. However, both primary antibodies proved most specific towards their respective target during the establishment process of the staining protocol and no appropriate replacement for either could be identified. This is a relevant issue when conducting immunofluorescent studies on pigs, as the number of antibodies available that specifically target porcine antigens is very limited compared to mouse or rabbit. To circumvent this issue,

antibody incubation was performed in a successive manner. First, sections were incubated with the primary followed by the secondary Ki67 antibody. Therefore, any signal elucidated from the secondary Ki67 antibody is specific to the detection of Ki67. Afterwards, the cTnI protocol was initiated. Signals generated from the secondary cTnI antibody are therefore nonspecific for cTnI, as they can also detect the primary Ki67 antibody. These considerations were taken into account during the analysis and signal quantification process; signals were only identified as Ki67$^+$ CMs if the specific Ki67$^+$ signal was surrounded on all borders by cTnI$^+$ signals with no signal crossover in the separate channels. Therefore, validity of investigative results is not compromised. Nonetheless, the protocol should be optimised in future investigations.

Capillary density was assessed by analysing PECAM-1$^+$ signal density. PECAM-1 is a specific marker for endothelial cells and therefore colocalizes with blood vessels (Kobayashi et al., 2005; Winkler et al., 2018). However, it does not provide insight into the maturation or functionality of blood vessels present. Pericytes drive vessel maturation via angiopoietin-1 mediated signalling; their presence can be determined by NG2 immunofluorescent staining (Sundberg et al., 2002; Teichert et al., 2017; Ziegler et al., 2013). Future investigations should therefore apply a PECAM-1 NG2 co-staining protocol to determine blood vessel maturity and functionality.

10. Summary and Outlook

AMI and subsequent ACR progressing into CHF are a significant socioeconomic burden. Revascularisation strategies aim to impede ACR by reducing infarct size; yet they are unsuccessful in controlling CHF to date. Recent studies have demonstrated that the ECM protein agrin induces cardiac regeneration by enhancing CM proliferation in mice. However, the murine ischemia/ reperfusion model lacks translationality, as agrin was delivered in a clinically irrelevant manner.

This study contributes to a better understanding of agrin's cardio-regenerative potential in a porcine ischemia/ reperfusion model. *In vivo* functional data and histological analysis provided insight into agrin's pleiotropic mechanism of action, which involves promoting CM proliferation and angiogenesis and simultaneously controlling cell death, inflammation, fibrosis, and hypertrophy. Further, this study poses a single antegrade injection of rhAgrin into the coronary artery as a clinically feasible therapy option in preserving cardiac function, preventing ACR and impeding progression into CHF.

Now, future investigations are required to assess efficacy, safety, and pharmacokinetics of rhAgrin treatment prior to clinical application. Large animal studies with prolonged reperfusion periods can give further insights into long-term patient outcome. They also provide a platform to investigate pharmacokinetics and determine the appropriate doses required for rhAgrin to enfold its full effect. Further, new scientific technologies like OOCs can be utilized to assess adverse effects, such as toxicity and carcinogenesis.

11. Tables

12. Figures

13. Acknowledgments

First, I would like to express my sincere thank you to my mentor Prof. Christian Kupatt. Not only did he support me with profound experience and expertise, provided help and guidance in my pursuit of this project, but he also gave me an insight into the diversity, complexity, and fascination of medical preclinical research, which made me want to pursue a career as a clinical scientist. For that I will be forever grateful.

Second, I would like to thank Prof. Kupatt's working group, who helped, supported, and encouraged me continuously over the years. I would like to thank Dr. Andrea Bähr and Dr. Katharina Klett for providing me insight into the complex makings of large animal studies and for teaching me the basic and not so basic principles of histological analysis. Further, I would like to thank Dr. Tarik Bozoglu, Dr. Farah Abdel-Rhaman, Christina Kim and Anja Wolf for being loyal, supportive, and reliant co-workers. Dr. Tarik Bozoglu greatly supported me in establishing new protocols within the lab and made late nights a fun and enjoyable experience. It was an absolute pleasure working with all of you over the years.

Third, I would like to thank Prof. Eldad Tzahor and the Weizmann Institute of Science for making this project possible and for trusting me to be part of this international cooperation study. Further, I would like to extent my thank you to Dr. Kfir Baruch-Umansky who shared his knowledge of histological analysis with me.

Next, Prof. Karl-Ludwig Laugwitz granted me access to his laboratory and technical devices and for that, I would like to thank him. Further, I would like to say thank you for providing me with the opportunity of conducting research in his clinic.

Last, I would like to thank my parents, Dr. Thomas and Catharina Jurisch, and my best friend Narcisse Gross. Without your unwavering support, unconditional love, and encouragement, this would not have been possible and for that, I am forever grateful.

PUBLIKATIONEN

05.2022 Poch CM, Foo KS, de Angelis MT, Jennbacken K, Santamaria G, Bähr A, Wang Q-D, Reiter F, Hornaschewitz N, Zawada D, Bozoglu T, My I, Meier A, Dorn T, Hege S, Lethinen ML, Tsoi YL, Hovdal D, Hyllner J, Schwarz S, Sudhop S, Jurisch V, Sini M, Fellows MD, Cummings M, Clarke J, Baptista R, Eroglu E, Wolf E, Klymiuk N, Lu K, Tomasi R, Dendorfer A, Gaspari M, Parrotta E, Cuda G, Krane M, Sinnecker D, Hoppmann P, Kupatt C, Fritsche-Danielson R, Moretti A, Chien KR, Laugwitz K-L. **Migratory and anti-fibrotic programmes define the regenerative potential of human cardiac progenitors.** *Nature Cell Biology* 2022, PMID: 35550611

01.2022 Bozoglu T, Seungmin L, Ziegler T, Jurisch V, Maas S, Baehr A, Hinkel R, Hoenig A, Hariharan A, Inyeop Kim C, Decker S, Haider S, Koppara T, Oellinger R, Müller O, Frank D, Megens R, Nelson P, Weber C, Schnieke A, Sperandio M, Santamaria G, Rad R, Moretti A, Laugwitz KL, Soehnlein O, Ogris M, Kupatt C. **Endothelial Retargeting of AAV9 in vivo.** *Advanced Science* 2022, PMID: 35023328

06.2021 Hinkel R, Batkai S, Baehr A, Bozoglu T, Straub S, Borchert T, Viereck J, Howe A, Hornaschewitz N, Oberberger L, Jurisch V, Kozlik-Feldmann R, Freudenthal F, Ziegler T, Weber C, Sperandio M, Engelhardt S, Laugwitz KL, Moretti A, Klymiuk N, Thum T, Kupatt C. **AntimiR-132 attenuates myocardial hypertrophy in an animal model of percutaneous aortic constriction.** *Journal of the American College of Cardiology* 2021, PMID: 34112319

05.2020 Baehr A, Umansky K, Bassat E, Jurisch V, Klett K, Bozoglu T, Hornaschewitz N, Solyanik O, Kain D, Ferraro B, Cohen-Rabbi R, Krane M, Cyran C, Soehnlein O, Laugwitz KL, Hinkel R, Kupatt C, Tzahor E. **Agrin promotes coordinates therapeutic processes leading to improved cardiac repair in pigs.** *Circulation* 2020, PMID: 32508131

02.2020 Moretti A, Fonteyne L, Giesert F, Hoppmann P, Meier AB, Bozoglu T, Baehr A, Schneider CM, Sinnecker D, Klett K, Fröhlich T, Abdel Rahman F, Haufe T, Sun S, Jurisch V, Kessler B, Hinkel R, Dirschinger R, Martens E, Jilek C, Graf A, Krebs S, Santamaria G, Kurome M, Zakhartchenko V, Campbell B, Voelse K, Wolf A, Ziegler T, Reichert S, Lee S, Flenkenthaler F, Dorn T, Jeremias I, Blum H, Dendorfer A, Schnieke A, Krause s, Walter MC, Klymiuk N, Laugwitz KL, Wolf E, Wurst W, Kupatt C. **Somatic Gene Editing Ameliorates Skeletal and Cardiac Muscle Failure in Pig and Human Models of Duchenne Muscular Dystrophy.** *Nature Medicine* 2020, PMID: 31988462

12.2019 Ziegler T, Abdel Rahman F, Jurisch V, Kupatt C. **Artherosclerosis and the Capillary Network; Pathophysiology and Potential Therapeutic Strategies.** *Cells* 2020, PMID: 31878229

16. Bibliography

Agewall, S., Antunes, M. J., Bucciarelli-Ducci, C., Bueno, H., Caforio, A. L. P., Crea, F., . . . Widimsky, P. (2017). *ESC Pocket Guidelines - Therapie des akuten Herzinfarktes bei Patienten mit ST-Streckenhebung (STEMI)*. Bröm Bruckmeier Verlag GmbH.

Agostini, L., Martinon, F., Burns, K., McDermott, M. F., Hawkins, P. N., & Tschopp, J. (2004). NALP3 forms an IL-1beta-processing inflammasome with increased activity in Muckle-Wells autoinflammatory disorder. *Immunity, 20*(3), 319-325. doi:10.1016/s1074-7613(04)00046-9

Ali, M. H., Schlidt, S. A., Chandel, N. S., Hynes, K. L., Schumacker, P. T., & Gewertz, B. L. (1999). Endothelial permeability and IL-6 production during hypoxia: role of ROS in signal transduction. *Am J Physiol, 277*(5), L1057-1065. doi:10.1152/ajplung.1999.277.5.L1057

Arango, M.-T., Quintero-Ronderos, P., Castiblanco, J., & Montoya-Ortíz, G. (2013). Cell culture and cell analysis. In J.-M. Anaya, Y. Shoenfeld, A. Rojas-Villarraga, R. A. Levy, & R. Cervera (Eds.), *Autoimmunity: From Bench to Bedside*. Retrieved from https://www.ncbi.nlm.nih.gov/books/NBK459464/

Arunachalam, S. P., Arani, A., Baffour, F., Rysavy, J. A., Rossman, P. J., Glaser, K. J., . . . Araoz, P. A. (2018). Regional assessment of in vivo myocardial stiffness using 3D magnetic resonance elastography in a porcine model of myocardial infarction. *Magn Reson Med, 79*(1), 361-369. doi:10.1002/mrm.26695

Assmann, G., Cullen, P., Jossa, F., Lewis, B., & Mancini, M. (1999). Coronary heart disease: reducing the risk: the scientific background to primary and secondary prevention of coronary heart disease. A worldwide view. International Task force for the Prevention of Coronary Heart disease. *Arterioscler Thromb Vasc Biol, 19*(8), 1819-1824. doi:10.1161/01.atv.19.8.1819

Bachmann, J. M., Willis, B. L., Ayers, C. R., Khera, A., & Berry, J. D. (2012). Association between family history and coronary heart disease death across long-term follow-up in men: the Cooper Center Longitudinal Study. *Circulation, 125*(25), 3092-3098. doi:10.1161/circulationaha.111.065490

Badenhorst, D., Maseko, M., Tsotetsi, O. J., Naidoo, A., Brooksbank, R., Norton, G. R., & Woodiwiss, A. J. (2003). Cross-linking influences the impact of quantitative changes in myocardial collagen on cardiac stiffness and remodelling in hypertension in rats. *Cardiovasc Res, 57*(3), 632-641. doi:10.1016/s0008-6363(02)00733-2

Baehr, A., Umansky, K. B., Bassat, E., Jurisch, V., Klett, K., Bozoglu, T., . . . Tzahor, E. (2020). Agrin Promotes Coordinated Therapeutic Processes Leading to Improved Cardiac Repair in Pigs. *Circulation, 142*(9), 868-881. doi:10.1161/circulationaha.119.045116

Bähr, A., Hornaschewitz, N., & Kupatt, C. (2021). Myocardial Infarction in Pigs. *Methods Mol Biol, 2158*, 43-50. doi:10.1007/978-1-0716-0668-1_4

Barandon, L., Couffinhal, T., Ezan, J., Dufourcq, P., Costet, P., Alzieu, P., . . . Duplàa, C. (2003). Reduction of infarct size and prevention of cardiac rupture in transgenic mice overexpressing FrzA. *Circulation, 108*(18), 2282-2289. doi:10.1161/01.Cir.0000093186.22847.4c

Barth, W., Deten, A., Bauer, M., Reinohs, M., Leicht, M., & Zimmer, H. G. (2000). Differential remodeling of the left and right heart after norepinephrine treatment in rats: studies on cytokines and collagen. *J Mol Cell Cardiol, 32*(2), 273-284. doi:10.1006/jmcc.1999.1075

Bassat, E., Mutlak, Y. E., Genzelinakh, A., Shadrin, I. Y., Baruch Umansky, K., Yifa, O., . . . Tzahor, E. (2017). The extracellular matrix protein agrin promotes heart regeneration in mice. *Nature, 547*(7662), 179-184. doi:10.1038/nature22978

Basu, S., Binder, R. J., Suto, R., Anderson, K. M., & Srivastava, P. K. (2000). Necrotic but not apoptotic cell death releases heat shock proteins, which deliver a partial maturation signal to dendritic cells and activate the NF-kappa B pathway. *Int Immunol, 12*(11), 1539-1546. doi:10.1093/intimm/12.11.1539

Bauer, T. M., & Murphy, E. (2020). Role of Mitochondrial Calcium and the Permeability Transition Pore in Regulating Cell Death. *Circ Res, 126*(2), 280-293. doi:10.1161/circresaha.119.316306

Baumann, C. L., Aspalter, I. M., Sharif, O., Pichlmair, A., Blüml, S., Grebien, F., . . . Superti-Furga, G. (2010). CD14 is a coreceptor of Toll-like receptors 7 and 9. *J Exp Med, 207*(12), 2689-2701. doi:10.1084/jem.20101111

Bechthold, A., Boeing, H., Schwedhelm, C., Hoffmann, G., Knüppel, S., Iqbal, K., . . . Schwingshackl, L. (2019). Food groups and risk of coronary heart disease, stroke and heart failure: A systematic review and dose-response meta-analysis of prospective studies. *Crit Rev Food Sci Nutr, 59*(7), 1071-1090. doi:10.1080/10408398.2017.1392288

Behar, S., Reicher-Reiss, H., Abinader, E., Agmon, J., Barzilai, J., Friedman, Y., . . . et al. (1992). Long-term prognosis after acute myocardial infarction in patients with left ventricular hypertrophy on the electrocardiogram. SPRINT Study Group. *Am J Cardiol, 69*(12), 985-990. doi:10.1016/0002-9149(92)90851-o

Berg, K. E., Ljungcrantz, I., Andersson, L., Bryngelsson, C., Hedblad, B., Fredrikson, G. N., . . . Björkbacka, H. (2012). Elevated CD14++CD16- monocytes predict cardiovascular events. *Circ Cardiovasc Genet, 5*(1), 122-131. doi:10.1161/circgenetics.111.960385

Bergmann, O., Bhardwaj, R. D., Bernard, S., Zdunek, S., Barnabé-Heider, F., Walsh, S., . . . Frisén, J. (2009). Evidence for cardiomyocyte renewal in humans. *Science, 324*(5923), 98-102. doi:10.1126/science.1164680

Bergmann, O., Zdunek, S., Felker, A., Salehpour, M., Alkass, K., Bernard, S., . . . Frisén, J. (2015). Dynamics of Cell Generation and Turnover in the Human Heart. *Cell, 161*(7), 1566-1575. doi:10.1016/j.cell.2015.05.026

Blake, D. J., Weir, A., Newey, S. E., & Davies, K. E. (2002). Function and genetics of dystrophin and dystrophin-related proteins in muscle. *Physiol Rev, 82*(2), 291-329. doi:10.1152/physrev.00028.2001

Bond, J. M., Herman, B., & Lemasters, J. J. (1991). Protection by acidotic pH against anoxia/reoxygenation injury to rat neonatal cardiac myocytes. *Biochem Biophys Res Commun, 179*(2), 798-803. doi:10.1016/0006-291x(91)91887-i

Bowe, M. A., Deyst, K. A., Leszyk, J. D., & Fallon, J. R. (1994). Identification and purification of an agrin receptor from Torpedo postsynaptic membranes: a heteromeric complex related to the dystroglycans. *Neuron, 12*(5), 1173-1180. doi:10.1016/0896-6273(94)90324-7

Bozkurt, B., Coats, A. J., Tsutsui, H., Abdelhamid, M., Adamopoulos, S., Albert, N., . . . Zieroth, S. (2021). Universal Definition and Classification of Heart Failure: A Report of the Heart Failure Society of America, Heart Failure Association of the European Society of Cardiology, Japanese

Heart Failure Society and Writing Committee of the Universal Definition of Heart Failure. *J Card Fail*. doi:10.1016/j.cardfail.2021.01.022

Bozoglu, T., Lee, S., Ziegler, T., Jurisch, V., Maas, S., Baehr, A., . . . Kupatt, C. (2022). Endothelial Retargeting of AAV9 In Vivo. *Adv Sci (Weinh), 9*(7), e2103867. doi:10.1002/advs.202103867

Bujak, M., Dobaczewski, M., Chatila, K., Mendoza, L. H., Li, N., Reddy, A., & Frangogiannis, N. G. (2008). Interleukin-1 receptor type I signaling critically regulates infarct healing and cardiac remodeling. *Am J Pathol, 173*(1), 57-67. doi:10.2353/ajpath.2008.070974

Bujak, M., Ren, G., Kweon, H. J., Dobaczewski, M., Reddy, A., Taffet, G., . . . Frangogiannis, N. G. (2007). Essential role of Smad3 in infarct healing and in the pathogenesis of cardiac remodeling. *Circulation, 116*(19), 2127-2138. doi:10.1161/circulationaha.107.704197

Burden, S. J., Yumoto, N., & Zhang, W. (2013). The role of MuSK in synapse formation and neuromuscular disease. *Cold Spring Harb Perspect Biol, 5*(5), a009167. doi:10.1101/cshperspect.a009167

Bürger, A., Benicke, M., Deten, A., & Zimmer, H. G. (2001). Catecholamines stimulate interleukin-6 synthesis in rat cardiac fibroblasts. *Am J Physiol Heart Circ Physiol, 281*(1), H14-21. doi:10.1152/ajpheart.2001.281.1.H14

Burgess, R. W., Dickman, D. K., Nunez, L., Glass, D. J., & Sanes, J. R. (2002). Mapping sites responsible for interactions of agrin with neurons. *J Neurochem, 83*(2), 271-284. doi:10.1046/j.1471-4159.2002.01102.x

Campbell, D. J., Somaratne, J. B., Jenkins, A. J., Prior, D. L., Yii, M., Kenny, J. F., . . . Black, M. J. (2013). Reduced microvascular density in non-ischemic myocardium of patients with recent non-ST-segment-elevation myocardial infarction. *Int J Cardiol, 167*(3), 1027-1037. doi:10.1016/j.ijcard.2012.03.075

Carnethon, M. R., Pu, J., Howard, G., Albert, M. A., Anderson, C. A. M., Bertoni, A. G., . . . Yancy, C. W. (2017). Cardiovascular Health in African Americans: A Scientific Statement From the American Heart Association. *Circulation, 136*(21), e393-e423. doi:10.1161/cir.0000000000000534

Cavero-Redondo, I., Peleteiro, B., Álvarez-Bueno, C., Rodriguez-Artalejo, F., & Martínez-Vizcaíno, V. (2017). Glycated haemoglobin A1c as a risk factor of cardiovascular outcomes and all-cause mortality in diabetic and non-diabetic populations: a systematic review and meta-analysis. *BMJ Open, 7*(7), e015949. doi:10.1136/bmjopen-2017-015949

Chakraborty, S., Lakshmanan, M., Swa, H. L., Chen, J., Zhang, X., Ong, Y. S., . . . Hong, W. (2015). An oncogenic role of Agrin in regulating focal adhesion integrity in hepatocellular carcinoma. *Nat Commun, 6*, 6184. doi:10.1038/ncomms7184

Chakraborty, S., Njah, K., & Hong, W. (2020). Agrin Mediates Angiogenesis in the Tumor Microenvironment. *Trends Cancer, 6*(2), 81-85. doi:10.1016/j.trecan.2019.12.002

Chakraborty, S., Njah, K., Pobbati, A. V., Lim, Y. B., Raju, A., Lakshmanan, M., . . . Hong, W. (2017). Agrin as a Mechanotransduction Signal Regulating YAP through the Hippo Pathway. *Cell Rep, 18*(10), 2464-2479. doi:10.1016/j.celrep.2017.02.041

Chakraborty, S., Sampath, D., Yu Lin, M. O., Bilton, M., Huang, C. K., Nai, M. H., . . . Hong, W. (2021). Agrin-Matrix Metalloproteinase-12 axis confers a mechanically competent microenvironment in skin wound healing. *Nat Commun, 12*(1), 6349. doi:10.1038/s41467-021-26717-7

Chan, W. X., Zheng, Y., Wiputra, H., Leo, H. L., & Yap, C. H. (2021). Full cardiac cycle asynchronous temporal compounding of 3D echocardiography images. *Med Image Anal, 74*, 102229. doi:10.1016/j.media.2021.102229

Chazotte, B. (2011). Labeling membrane glycoproteins or glycolipids with fluorescent wheat germ agglutinin. *Cold Spring Harb Protoc, 2011*(5), pdb.prot5623. doi:10.1101/pdb.prot5623

Chekeni, F. B., Elliott, M. R., Sandilos, J. K., Walk, S. F., Kinchen, J. M., Lazarowski, E. R., . . . Ravichandran, K. S. (2010). Pannexin 1 channels mediate 'find-me' signal release and membrane permeability during apoptosis. *Nature, 467*(7317), 863-867. doi:10.1038/nature09413

Chen, K., Chen, J., Li, D., Zhang, X., & Mehta, J. L. (2004). Angiotensin II Regulation of Collagen Type I Expression in Cardiac Fibroblasts. *Hypertension, 44*(5), 655-661. doi:doi:10.1161/01.HYP.0000144400.49062.6b

Chen, T., Li, W., Wang, Y., Xu, B., & Guo, J. (2012). Smoking status on outcomes after percutaneous coronary intervention. *Clin Cardiol, 35*(9), 570-574. doi:10.1002/clc.22004

Chen, W., Syldath, U., Bellmann, K., Burkart, V., & Kolb, H. (1999). Human 60-kDa heat-shock protein: a danger signal to the innate immune system. *J Immunol, 162*(6), 3212-3219. Retrieved from https://www.jimmunol.org/content/jimmunol/162/6/3212.full.pdf

Chen, Y., Corriden, R., Inoue, Y., Yip, L., Hashiguchi, N., Zinkernagel, A., . . . Junger, W. G. (2006). ATP release guides neutrophil chemotaxis via P2Y2 and A3 receptors. *Science, 314*(5806), 1792-1795. doi:10.1126/science.1132559

Ciz, M., Denev, P., Kratchanova, M., Vasicek, O., Ambrozova, G., & Lojek, A. (2012). Flavonoids inhibit the respiratory burst of neutrophils in mammals. *Oxid Med Cell Longev, 2012*, 181295. doi:10.1155/2012/181295

Cleutjens, J. P., Kandala, J. C., Guarda, E., Guntaka, R. V., & Weber, K. T. (1995). Regulation of collagen degradation in the rat myocardium after infarction. *J Mol Cell Cardiol, 27*(6), 1281-1292. doi:10.1016/s0022-2828(05)82390-9

Cleutjens, J. P., Verluyten, M. J., Smiths, J. F., & Daemen, M. J. (1995). Collagen remodeling after myocardial infarction in the rat heart. *Am J Pathol, 147*(2), 325-338.

Cohn, J. N., Ferrari, R., & Sharpe, N. (2000). Cardiac remodeling--concepts and clinical implications: a consensus paper from an international forum on cardiac remodeling. Behalf of an International Forum on Cardiac Remodeling. *J Am Coll Cardiol, 35*(3), 569-582. doi:10.1016/s0735-1097(99)00630-0

Collet, J.-P., Thiele, H., Barbato, E., Barthélémy, O., Bauersachs, J., Bhatt, D. L., . . . Group, E. S. D. (2020). 2020 ESC Guidelines for the management of acute coronary syndromes in patients presenting without persistent ST-segment elevation: The Task Force for the management of acute coronary syndromes in patients presenting without persistent ST-segment elevation of the European Society of Cardiology (ESC). *European Heart Journal, 42*(14), 1289-1367. doi:10.1093/eurheartj/ehaa575

Cong, B. H., Zhu, X. Y., & Ni, X. (2017). The roles of microRNA-22 in myocardial infarction. *Sheng Li Xue Bao, 69*(5), 571-578.

Crespo-Leiro, M. G., Anker, S. D., Maggioni, A. P., Coats, A. J., Filippatos, G., Ruschitzka, F., . . . Mebazaa, A. (2016). European Society of Cardiology Heart Failure Long-Term Registry (ESC-HF-LT): 1-year follow-up outcomes and differences across regions. *Eur J Heart Fail, 18*(6), 613-625. doi:10.1002/ejhf.566

Crick, S. J., Sheppard, M. N., Ho, S. Y., Gebstein, L., & Anderson, R. H. (1998). Anatomy of the pig heart: comparisons with normal human cardiac structure. *J Anat, 193 (Pt 1)*(Pt 1), 105-119. doi:10.1046/j.1469-7580.1998.19310105.x

Crowley, L. C., Marfell, B. J., & Waterhouse, N. J. (2016). Detection of DNA Fragmentation in Apoptotic Cells by TUNEL. *Cold Spring Harb Protoc, 2016*(10). doi:10.1101/pdb.prot087221

D'Uva, G., Aharonov, A., Lauriola, M., Kain, D., Yahalom-Ronen, Y., Carvalho, S., . . . Tzahor, E. (2015). ERBB2 triggers mammalian heart regeneration by promoting cardiomyocyte dedifferentiation and proliferation. *Nat Cell Biol, 17*(5), 627-638. doi:10.1038/ncb3149

Davoodi, H., Hashemi, S. R., & Seow, H. F. (2012). Increased NFk-B activity in HCT116 colorectal cancer cell line harboring TLR4 Asp299Gly variant. *Iran J Allergy Asthma Immunol, 11*(2), 121-132. Retrieved from https://ijaai.tums.ac.ir/index.php/ijaai/article/download/337/337

Denning, N. L., Aziz, M., Gurien, S. D., & Wang, P. (2019). DAMPs and NETs in Sepsis. *Front Immunol, 10*, 2536. doi:10.3389/fimmu.2019.02536

Desmoulière, A., Geinoz, A., Gabbiani, F., & Gabbiani, G. (1993). Transforming growth factor-beta 1 induces alpha-smooth muscle actin expression in granulation tissue myofibroblasts and in quiescent and growing cultured fibroblasts. *J Cell Biol, 122*(1), 103-111. doi:10.1083/jcb.122.1.103

Deten, A., Volz, H. C., Briest, W., & Zimmer, H. G. (2002). Cardiac cytokine expression is upregulated in the acute phase after myocardial infarction. Experimental studies in rats. *Cardiovasc Res, 55*(2), 329-340. doi:10.1016/s0008-6363(02)00413-3

Dobaczewski, M., Bujak, M., Li, N., Gonzalez-Quesada, C., Mendoza, L. H., Wang, X. F., & Frangogiannis, N. G. (2010). Smad3 signaling critically regulates fibroblast phenotype and function in healing myocardial infarction. *Circ Res, 107*(3), 418-428. doi:10.1161/circresaha.109.216101

Dobaczewski, M., Xia, Y., Bujak, M., Gonzalez-Quesada, C., & Frangogiannis, N. G. (2010). CCR5 signaling suppresses inflammation and reduces adverse remodeling of the infarcted heart, mediating recruitment of regulatory T cells. *Am J Pathol, 176*(5), 2177-2187. doi:10.2353/ajpath.2010.090759

Doughty, R. N., Rodgers, A., Sharpe, N., & MacMahon, S. (1997). Effects of beta-blocker therapy on mortality in patients with heart failure. A systematic overview of randomized controlled trials. *Eur Heart J, 18*(4), 560-565. doi:10.1093/oxfordjournals.eurheartj.a015297

Drozd, M., Relton, S. D., Walker, A. M. N., Slater, T. A., Gierula, J., Paton, M. F., . . . Cubbon, R. M. (2021). Association of heart failure and its comorbidities with loss of life expectancy. *Heart, 107*(17), 1417-1421. doi:10.1136/heartjnl-2020-317833

Ducharme, A., Frantz, S., Aikawa, M., Rabkin, E., Lindsey, M., Rohde, L. E., . . . Lee, R. T. (2000). Targeted deletion of matrix metalloproteinase-9 attenuates left ventricular enlargement and collagen accumulation after experimental myocardial infarction. *J Clin Invest, 106*(1), 55-62. doi:10.1172/jci8768

Elliott, M. R., Chekeni, F. B., Trampont, P. C., Lazarowski, E. R., Kadl, A., Walk, S. F., . . . Ravichandran, K. S. (2009). Nucleotides released by apoptotic cells act as a find-me signal to promote phagocytic clearance. *Nature, 461*(7261), 282-286. doi:10.1038/nature08296

Eltzschig, H. K., Eckle, T., Mager, A., Küper, N., Karcher, C., Weissmüller, T., . . . Colgan, S. P. (2006). ATP release from activated neutrophils occurs via connexin 43 and modulates adenosine-dependent endothelial cell function. *Circ Res, 99*(10), 1100-1108. doi:10.1161/01.Res.0000250174.31269.70

Eltzschig, H. K., Ibla, J. C., Furuta, G. T., Leonard, M. O., Jacobson, K. A., Enjyoji, K., . . . Colgan, S. P. (2003). Coordinated adenine nucleotide phosphohydrolysis and nucleoside signaling in posthypoxic endothelium: role of ectonucleotidases and adenosine A2B receptors. *J Exp Med, 198*(5), 783-796. doi:10.1084/jem.20030891

Ervasti, J. M., & Campbell, K. P. (1993). A role for the dystrophin-glycoprotein complex as a transmembrane linker between laminin and actin. *J Cell Biol, 122*(4), 809-823. doi:10.1083/jcb.122.4.809

Eulalio, A., Mano, M., Dal Ferro, M., Zentilin, L., Sinagra, G., Zacchigna, S., & Giacca, M. (2012). Functional screening identifies miRNAs inducing cardiac regeneration. *Nature, 492*(7429), 376-381. doi:10.1038/nature11739

Fairfield, J. E., Dritsas, A., & Beale, R. J. (1991). Haemodynamic effects of propofol: induction with 2.5 mg kg-1. *Br J Anaesth, 67*(5), 618-620. doi:10.1093/bja/67.5.618

Fan, D., Takawale, A., Shen, M., Wang, W., Wang, X., Basu, R., . . . Kassiri, Z. (2015). Cardiomyocyte A Disintegrin And Metalloproteinase 17 (ADAM17) Is Essential in Post-Myocardial Infarction Repair by Regulating Angiogenesis. *Circ Heart Fail, 8*(5), 970-979. doi:10.1161/circheartfailure.114.002029

Fealey, M. E., Horn, B., Coffman, C., Miller, R., Lin, A. Y., Thompson, A. R., . . . Thomas, D. D. (2018). Dynamics of Dystrophin's Actin-Binding Domain. *Biophys J, 115*(3), 445-454. doi:10.1016/j.bpj.2018.05.039

Feldberg, W., & Wei, E. (1986). Analysis of cardiovascular effects of morphine in the cat. *Neuroscience, 17*(2), 495-506. doi:10.1016/0306-4522(86)90262-9

Flather, M. D., Yusuf, S., Køber, L., Pfeffer, M., Hall, A., Murray, G., . . . Braunwald, E. (2000). Long-term ACE-inhibitor therapy in patients with heart failure or left-ventricular dysfunction: a systematic overview of data from individual patients. ACE-Inhibitor Myocardial Infarction Collaborative Group. *Lancet, 355*(9215), 1575-1581. doi:10.1016/s0140-6736(00)02212-1

Frangogiannis, N. G. (2014). The inflammatory response in myocardial injury, repair, and remodelling. *Nat Rev Cardiol, 11*(5), 255-265. doi:10.1038/nrcardio.2014.28

Frangogiannis, N. G., Mendoza, L. H., Lindsey, M. L., Ballantyne, C. M., Michael, L. H., Smith, C. W., & Entman, M. L. (2000). IL-10 is induced in the reperfused myocardium and may modulate the reaction to injury. *J Immunol, 165*(5), 2798-2808. doi:10.4049/jimmunol.165.5.2798

Frank, A., Bonney, M., Bonney, S., Weitzel, L., Koeppen, M., & Eckle, T. (2012). Myocardial ischemia reperfusion injury: from basic science to clinical bedside. *Semin Cardiothorac Vasc Anesth, 16*(3), 123-132. doi:10.1177/1089253211436350

Freemantle, N., Cleland, J., Young, P., Mason, J., & Harrison, J. (1999). beta Blockade after myocardial infarction: systematic review and meta regression analysis. *Bmj, 318*(7200), 1730-1737. doi:10.1136/bmj.318.7200.1730

Gabisonia, K., Prosdocimo, G., Aquaro, G. D., Carlucci, L., Zentilin, L., Secco, I., . . . Giacca, M. (2019). MicroRNA therapy stimulates uncontrolled cardiac repair after myocardial infarction in pigs. *Nature, 569*(7756), 418-422. doi:10.1038/s41586-019-1191-6

Gao, X. M., Ming, Z., Su, Y., Fang, L., Kiriazis, H., Xu, Q., . . . Du, X. J. (2010). Infarct size and post-infarct inflammation determine the risk of cardiac rupture in mice. *Int J Cardiol, 143*(1), 20-28. doi:10.1016/j.ijcard.2009.01.019

Gao, X. M., Tsai, A., Al-Sharea, A., Su, Y., Moore, S., Han, L. P., . . . Du, X. J. (2017). Inhibition of the Renin-Angiotensin System Post Myocardial Infarction Prevents Inflammation-Associated Acute Cardiac Rupture. *Cardiovasc Drugs Ther, 31*(2), 145-156. doi:10.1007/s10557-017-6717-2

Gao, X. M., Xu, Q., Kiriazis, H., Dart, A. M., & Du, X. J. (2005). Mouse model of post-infarct ventricular rupture: time course, strain- and gender-dependency, tensile strength, and histopathology. *Cardiovasc Res, 65*(2), 469-477. doi:10.1016/j.cardiores.2004.10.014

Gee, S. H., Montanaro, F., Lindenbaum, M. H., & Carbonetto, S. (1994). Dystroglycan-alpha, a dystrophin-associated glycoprotein, is a functional agrin receptor. *Cell, 77*(5), 675-686. doi:10.1016/0092-8674(94)90052-3

Gerber, B. L., Rochitte, C. E., Melin, J. A., McVeigh, E. R., Bluemke, D. A., Wu, K. C., . . . Lima, J. A. (2000). Microvascular obstruction and left ventricular remodeling early after acute myocardial infarction. *Circulation, 101*(23), 2734-2741. doi:10.1161/01.cir.101.23.2734

Glass, D. J., Bowen, D. C., Stitt, T. N., Radziejewski, C., Bruno, J., Ryan, T. E., . . . Yancopoulos, G. D. (1996). Agrin Acts via a MuSK Receptor Complex. *Cell, 85*(4), 513-523. doi:10.1016/S0092-8674(00)81252-0

González-Santamaría, J., Villalba, M., Busnadiego, O., López-Olañeta, M. M., Sandoval, P., Snabel, J., . . . Rodríguez-Pascual, F. (2015). Matrix cross-linking lysyl oxidases are induced in response to myocardial infarction and promote cardiac dysfunction. *Cardiovascular Research, 109*(1), 67-78. doi:10.1093/cvr/cvv214

Gordon, H. P., Katz, M. G., Fargnoli, A. S., Gillespie, V. L., Hajjar, R. J., & Bridges, C. R. (2018). Scar Size and Other Parameters for Tracking Left Ventricular Dysfunction after Induction of Myocardial Infarcts in Sheep (Ovisaries). *Comp Med, 68*(3), 215-220. doi:10.30802/aalas-cm-17-000040

Grasl-Kraupp, B., Ruttkay-Nedecky, B., Koudelka, H., Bukowska, K., Bursch, W., & Schulte-Hermann, R. (1995). In situ detection of fragmented DNA (TUNEL assay) fails to discriminate among apoptosis, necrosis, and autolytic cell death: a cautionary note. *Hepatology, 21*(5), 1465-1468. doi:10.1002/hep.1840210534

Gray, M. O., Long, C. S., Kalinyak, J. E., Li, H. T., & Karliner, J. S. (1998). Angiotensin II stimulates cardiac myocyte hypertrophy via paracrine release of TGF-beta 1 and endothelin-1 from fibroblasts. *Cardiovasc Res, 40*(2), 352-363. doi:10.1016/s0008-6363(98)00121-7

Groenewegen, A., Rutten, F. H., Mosterd, A., & Hoes, A. W. (2020). Epidemiology of heart failure. *European Journal of Heart Failure, 22*(8), 1342-1356. doi:https://doi.org/10.1002/ejhf.1858

Hamidi, M., Moody, J. S., Weigel, T. L., & Kozak, K. R. (2010). Primary cardiac sarcoma. *Ann Thorac Surg, 90*(1), 176-181. doi:10.1016/j.athoracsur.2010.03.065

Hammoud, L., Lu, X., Lei, M., & Feng, Q. (2011). Deficiency in TIMP-3 increases cardiac rupture and mortality post-myocardial infarction via EGFR signaling: beneficial effects of cetuximab. *Basic Res Cardiol, 106*(3), 459-471. doi:10.1007/s00395-010-0147-7

Han, F., Chen, Q., Su, J., Zheng, A., Chen, K., Sun, S., . . . Zhang, L. (2019). MicroRNA-124 regulates cardiomyocyte apoptosis and myocardial infarction through targeting Dhcr24. *J Mol Cell Cardiol, 132*, 178-188. doi:10.1016/j.yjmcc.2019.05.007

Han, L., Shi, H., Ma, S., Luo, Y., Sun, W., Li, S., . . . Gong, Y. (2021). Agrin Promotes Non-Small Cell Lung Cancer Progression and Stimulates Regulatory T Cells via Increasing IL-6 Secretion Through PI3K/AKT Pathway. *Front Oncol, 11*, 804418. doi:10.3389/fonc.2021.804418

Hao, P. P., Chen, Y. G., Wang, X. L., & Zhang, Y. (2010). Efficacy and safety of drug-eluting stents in patients with acute ST-segment-elevation myocardial infarction: a meta-analysis of randomized controlled trials. *Tex Heart Inst J, 37*(5), 516-524. Retrieved from https://www.ncbi.nlm.nih.gov/pmc/articles/PMC2953216/pdf/20101000s00003p516.pdf

Haubner, B. J., Schneider, J., Schweigmann, U., Schuetz, T., Dichtl, W., Velik-Salchner, C., . . . Penninger, J. M. (2016). Functional Recovery of a Human Neonatal Heart After Severe Myocardial Infarction. *Circ Res, 118*(2), 216-221. doi:10.1161/circresaha.115.307017

He, M., Cheng, C., Tu, J., Ji, S. S., Lou, D., & Bai, B. (2021). Agrin expression is correlated with tumor development and poor prognosis in cholangiocarcinoma. *J Int Med Res, 49*(5), 3000605211009722. doi:10.1177/03000605211009722

Heallen, T., Zhang, M., Wang, J., Bonilla-Claudio, M., Klysik, E., Johnson, R. L., & Martin, J. F. (2011). Hippo pathway inhibits Wnt signaling to restrain cardiomyocyte proliferation and heart size. *Science, 332*(6028), 458-461. doi:10.1126/science.1199010

Hendee, K., Hunyenyiwa, T., Matus, K., Toledo, M., Mammoto, A., & Mammoto, T. (2021). Twist1 signaling in age-dependent decline in angiogenesis and lung regeneration. *Aging (Albany NY), 13*(6), 7781-7799. doi:10.18632/aging.202875

Herold, G. (2021). Koronare Herzerkrankungen (KHK). In *Innere Medizin* (pp. 237-248). Köln: Dr. med. Gerd Herold.

Hinkel, R., Penzkofer, D., Zühlke, S., Fischer, A., Husada, W., Xu, Q. F., . . . Dimmeler, S. (2013). Inhibition of microRNA-92a protects against ischemia/reperfusion injury in a large-animal model. *Circulation, 128*(10), 1066-1075. doi:10.1161/circulationaha.113.001904

Hinkel, R., Ramanujam, D., Kaczmarek, V., Howe, A., Klett, K., Beck, C., . . . Engelhardt, S. (2020). AntimiR-21 Prevents Myocardial Dysfunction in a Pig Model of Ischemia/Reperfusion Injury. *J Am Coll Cardiol, 75*(15), 1788-1800. doi:10.1016/j.jacc.2020.02.041

Hochman, J. S., & Bulkley, B. H. (1982). Expansion of acute myocardial infarction: an experimental study. *Circulation, 65*(7), 1446-1450. doi:10.1161/01.cir.65.7.1446

Hollander, M. R., de Waard, G. A., Konijnenberg, L. S., Meijer-van Putten, R. M., van den Brom, C. E., Paauw, N., . . . Van Royen, N. (2016). Dissecting the Effects of Ischemia and Reperfusion on the Coronary Microcirculation in a Rat Model of Acute Myocardial Infarction. *PLoS One, 11*(7), e0157233. doi:10.1371/journal.pone.0157233

Hopf, C., & Hoch, W. (1996). Agrin binding to alpha-dystroglycan. Domains of agrin necessary to induce acetylcholine receptor clustering are overlapping but not identical to the alpha-dystroglycan-binding region. *J Biol Chem, 271*(9), 5231-5236. doi:10.1074/jbc.271.9.5231

Horckmans, M., Ring, L., Duchene, J., Santovito, D., Schloss, M. J., Drechsler, M., . . . Steffens, S. (2017). Neutrophils orchestrate post-myocardial infarction healing by polarizing macrophages towards a reparative phenotype. *Eur Heart J, 38*(3), 187-197. doi:10.1093/eurheartj/ehw002

Huang, J., Wu, S., Barrera, J., Matthews, K., & Pan, D. (2005). The Hippo signaling pathway coordinately regulates cell proliferation and apoptosis by inactivating Yorkie, the Drosophila Homolog of YAP. *Cell, 122*(3), 421-434. doi:10.1016/j.cell.2005.06.007

Huang, Z.-Q., Xu, W., Wu, J.-L., Lu, X., & Chen, X.-M. (2019). MicroRNA-374a protects against myocardial ischemia-reperfusion injury in mice by targeting the MAPK6 pathway. *Life Sciences, 232*, 116619. doi:https://doi.org/10.1016/j.lfs.2019.116619

Hutchins, G. M., & Bulkley, B. H. (1978). Infarct expansion versus extension: two different complications of acute myocardial infarction. *Am J Cardiol, 41*(7), 1127-1132. doi:10.1016/0002-9149(78)90869-x

Huynh, M. L., Fadok, V. A., & Henson, P. M. (2002). Phosphatidylserine-dependent ingestion of apoptotic cells promotes TGF-beta1 secretion and the resolution of inflammation. *J Clin Invest, 109*(1), 41-50. doi:10.1172/jci11638

Ibanez, B., James, S., Agewall, S., Antunes, M. J., Bucciarelli-Ducci, C., Bueno, H., . . . Group, E. S. D. (2017). 2017 ESC Guidelines for the management of acute myocardial infarction in patients presenting with ST-segment elevation: The Task Force for the management of acute myocardial infarction in patients presenting with ST-segment elevation of the European Society of Cardiology (ESC). *European Heart Journal, 39*(2), 119-177. doi:10.1093/eurheartj/ehx393

Ibanez, B., Macaya, C., Sánchez-Brunete, V., Pizarro, G., Fernández-Friera, L., Mateos, A., . . . Fuster, V. (2013). Effect of early metoprolol on infarct size in ST-segment-elevation myocardial infarction patients undergoing primary percutaneous coronary intervention: the Effect of Metoprolol in Cardioprotection During an Acute Myocardial Infarction (METOCARD-CNIC) trial. *Circulation, 128*(14), 1495-1503. doi:10.1161/circulationaha.113.003653

Ibraghimov-Beskrovnaya, O., Ervasti, J. M., Leveille, C. J., Slaughter, C. A., Sernett, S. W., & Campbell, K. P. (1992). Primary structure of dystrophin-associated glycoproteins linking dystrophin to the extracellular matrix. *Nature, 355*(6362), 696-702. doi:10.1038/355696a0

Iyer, S. S., Pulskens, W. P., Sadler, J. J., Butter, L. M., Teske, G. J., Ulland, T. K., . . . Sutterwala, F. S. (2009). Necrotic cells trigger a sterile inflammatory response through the Nlrp3 inflammasome. *Proc Natl Acad Sci U S A, 106*(48), 20388-20393. doi:10.1073/pnas.0908698106

James, S. L., Abate, D., Abate, K. H., Abay, S. M., Abbafati, C., Abbasi, N., . . . Murray, C. J. L. (2018). Global, regional, and national incidence, prevalence, and years lived with disability for 354 diseases and injuries for 195 countries and territories, 1990–2017: a systematic analysis for the Global Burden of Disease Study 2017. *The Lancet, 392*(10159), 1789-1858. doi:10.1016/S0140-6736(18)32279-7

James, T. N. (1998). The variable morphological coexistence of apoptosis and necrosis in human myocardial infarction: significance for understanding its pathogenesis, clinical course, diagnosis and prognosis. *Coron Artery Dis, 9*(5), 291-307. doi:10.1097/00019501-199809050-00007

Jennings, R. B., Ganote, C. E., & Reimer, K. A. (1975). Ischemic tissue injury. *Am J Pathol, 81*(1), 179-198. Retrieved from https://www.ncbi.nlm.nih.gov/pmc/articles/PMC2032306/pdf/amjpathol00455-0191.pdf

Jennings, R. B., Murry, C. E., Steenbergen, C., Jr., & Reimer, K. A. (1990). Development of cell injury in sustained acute ischemia. *Circulation, 82*(3 Suppl), Ii2-12.

Jetten, N., Verbruggen, S., Gijbels, M. J., Post, M. J., De Winther, M. P., & Donners, M. M. (2014). Anti-inflammatory M2, but not pro-inflammatory M1 macrophages promote angiogenesis in vivo. *Angiogenesis, 17*(1), 109-118. doi:10.1007/s10456-013-9381-6

Jia, D., Chen, S., Bai, P., Luo, C., Liu, J., Sun, A., & Ge, J. (2022). Cardiac Resident Macrophage-Derived Legumain Improves Cardiac Repair by Promoting Clearance and Degradation of Apoptotic Cardiomyocytes After Myocardial Infarction. *Circulation, 145*(20), 1542-1556. doi:10.1161/circulationaha.121.057549

Juenger, J., Schellberg, D., Kraemer, S., Haunstetter, A., Zugck, C., Herzog, W., & Haass, M. (2002). Health related quality of life in patients with congestive heart failure: comparison with other chronic diseases and relation to functional variables. *Heart, 87*(3), 235-241. doi:10.1136/heart.87.3.235

Jung, D., Yang, B., Meyer, J., Chamberlain, J. S., & Campbell, K. P. (1995). Identification and characterization of the dystrophin anchoring site on beta-dystroglycan. *J Biol Chem, 270*(45), 27305-27310. doi:10.1074/jbc.270.45.27305

Jung, M., Ma, Y., Iyer, R. P., DeLeon-Pennell, K. Y., Yabluchanskiy, A., Garrett, M. R., & Lindsey, M. L. (2017). IL-10 improves cardiac remodeling after myocardial infarction by stimulating M2 macrophage polarization and fibroblast activation. *Basic Res Cardiol, 112*(3), 33. doi:10.1007/s00395-017-0622-5

Junqueira, L. C., Bignolas, G., & Brentani, R. R. (1979). Picrosirius staining plus polarization microscopy, a specific method for collagen detection in tissue sections. *Histochem J, 11*(4), 447-455. doi:10.1007/bf01002772

Kamon, D., Sugawara, Y., Soeda, T., Okamura, A., Nakada, Y., Hashimoto, Y., . . . Saito, Y. (2021). Predominant subtype of heart failure after acute myocardial infarction is heart failure with non-reduced ejection fraction. *ESC Heart Fail, 8*(1), 317-325. doi:10.1002/ehf2.13070

Karuzas, A., Rumbinaite, E., Verikas, D., Ptasinskas, T., Muckiene, G., Kazakauskaite, E., . . . Zaliaduonyte-Peksiene, D. (2019). Accuracy of three-dimensional systolic dyssynchrony and sphericity indexes for identifying early left ventricular remodeling after acute myocardial infarction. *Anatol J Cardiol, 22*(1), 13-20. doi:10.14744/AnatolJCardiol.2019.02844

Khan, M. A., Hashim, M. J., Mustafa, H., Baniyas, M. Y., Al Suwaidi, S., AlKatheeri, R., . . . Lootah, S. (2020). Global Epidemiology of Ischemic Heart Disease: Results from the Global Burden of Disease Study. *Cureus, 12*(7), e9349. doi:10.7759/cureus.9349

Kim, N., Stiegler, A. L., Cameron, T. O., Hallock, P. T., Gomez, A. M., Huang, J. H., . . . Burden, S. J. (2008). Lrp4 is a receptor for Agrin and forms a complex with MuSK. *Cell, 135*(2), 334-342. doi:10.1016/j.cell.2008.10.002

Kivelä, R., Hemanthakumar, K. A., Vaparanta, K., Robciuc, M., Izumiya, Y., Kidoya, H., . . . Alitalo, K. (2019). Endothelial Cells Regulate Physiological Cardiomyocyte Growth via VEGFR2-Mediated Paracrine Signaling. *Circulation, 139*(22), 2570-2584. doi:10.1161/circulationaha.118.036099

Knuuti, J., Wijns, W., Saraste, A., Capodanno, D., Barbato, E., Funck-Brentano, C., . . . Group, E. S. D. (2019). 2019 ESC Guidelines for the diagnosis and management of chronic coronary syndromes: The Task Force for the diagnosis and management of chronic coronary syndromes of the European Society of Cardiology (ESC). *European Heart Journal, 41*(3), 407-477. doi:10.1093/eurheartj/ehz425

Kobayashi, M., Inoue, K., Warabi, E., Minami, T., & Kodama, T. (2005). A simple method of isolating mouse aortic endothelial cells. *J Atheroscler Thromb, 12*(3), 138-142. doi:10.5551/jat.12.138

Kromhout, D., Menotti, A., Bloemberg, B., Aravanis, C., Blackburn, H., Buzina, R., . . . et al. (1995). Dietary saturated and trans fatty acids and cholesterol and 25-year mortality from coronary heart disease: the Seven Countries Study. *Prev Med, 24*(3), 308-315. doi:10.1006/pmed.1995.1049

Kuida, K., Lippke, J. A., Ku, G., Harding, M. W., Livingston, D. J., Su, M. S., & Flavell, R. A. (1995). Altered cytokine export and apoptosis in mice deficient in interleukin-1 beta converting enzyme. *Science, 267*(5206), 2000-2003. doi:10.1126/science.7535475

Kumar, D., Hacker, T. A., Buck, J., Whitesell, L. F., Kaji, E. H., Douglas, P. S., & Kamp, T. J. (2005). Distinct mouse coronary anatomy and myocardial infarction consequent to ligation. *Coron Artery Dis, 16*(1), 41-44. doi:10.1097/00019501-200502000-00008

Kupatt, C., Horstkotte, J., Vlastos, G. A., Pfosser, A., Lebherz, C., Semisch, M., . . . Hatzopoulos, A. K. (2005). Embryonic endothelial progenitor cells expressing a broad range of proangiogenic and remodeling factors enhance vascularization and tissue recovery in acute and chronic ischemia. *Faseb j, 19*(11), 1576-1578. doi:10.1096/fj.04-3282fje

Kurokawa, Y. K., Yin, R. T., Shang, M. R., Shirure, V. S., Moya, M. L., & George, S. C. (2017). Human Induced Pluripotent Stem Cell-Derived Endothelial Cells for Three-Dimensional Microphysiological Systems. *Tissue Eng Part C Methods, 23*(8), 474-484. doi:10.1089/ten.TEC.2017.0133

Le May, M. R., Wells, G. A., So, D. Y., Glover, C. A., Froeschl, M., Maloney, J., . . . Labinaz, M. (2012). Reduction in mortality as a result of direct transport from the field to a receiving center for primary percutaneous coronary intervention. *J Am Coll Cardiol, 60*(14), 1223-1230. doi:10.1016/j.jacc.2012.07.008

Leivonen, S. K., Lazaridis, K., Decock, J., Chantry, A., Edwards, D. R., & Kähäri, V. M. (2013). TGF-β-elicited induction of tissue inhibitor of metalloproteinases (TIMP)-3 expression in fibroblasts involves complex interplay between Smad3, p38α, and ERK1/2. *PLoS One, 8*(2), e57474. doi:10.1371/journal.pone.0057474

Lelovas, P. P., Kostomitsopoulos, N. G., & Xanthos, T. T. (2014). A comparative anatomic and physiologic overview of the porcine heart. *J Am Assoc Lab Anim Sci, 53*(5), 432-438.

Lertkiatmongkol, P., Liao, D., Mei, H., Hu, Y., & Newman, P. J. (2016). Endothelial functions of platelet/endothelial cell adhesion molecule-1 (CD31). *Curr Opin Hematol, 23*(3), 253-259. doi:10.1097/moh.0000000000000239

Leung, C. M., de Haan, P., Ronaldson-Bouchard, K., Kim, G.-A., Ko, J., Rho, H. S., . . . Toh, Y.-C. (2022). A guide to the organ-on-a-chip. *Nature Reviews Methods Primers, 2*(1), 33. doi:10.1038/s43586-022-00118-6

Levraut, J., Iwase, H., Shao, Z. H., Vanden Hoek, T. L., & Schumacker, P. T. (2003). Cell death during ischemia: relationship to mitochondrial depolarization and ROS generation. *Am J Physiol Heart Circ Physiol, 284*(2), H549-558. doi:10.1152/ajpheart.00708.2002

Lewis, E. F., Moye, L. A., Rouleau, J. L., Sacks, F. M., Arnold, J. M., Warnica, J. W., . . . Pfeffer, M. A. (2003). Predictors of late development of heart failure in stable survivors of myocardial infarction: the CARE study. *J Am Coll Cardiol, 42*(8), 1446-1453. doi:10.1016/s0735-1097(03)01057-x

Li, M., Carpio, D. F., Zheng, Y., Bruzzo, P., Singh, V., Ouaaz, F., . . . Beg, A. A. (2001). An essential role of the NF-kappa B/Toll-like receptor pathway in induction of inflammatory and tissue-repair gene expression by necrotic cells. *J Immunol, 166*(12), 7128-7135. doi:10.4049/jimmunol.166.12.7128

Li, S., Wang, Y., Jiang, D., Ni, D., Kutyreff, C. J., Barnhart, T. E., . . . Cai, W. (2020). Spatiotemporal Distribution of Agrin after Intrathecal Injection and Its Protective Role in Cerebral Ischemia/Reperfusion Injury. *Adv Sci (Weinh), 7*(4), 1902600. doi:10.1002/advs.201902600

Li, Y., Hu, S., Ma, G., Yao, Y., Yan, G., Chen, J., . . . Zhang, Z. (2013). Acute myocardial infarction induced functional cardiomyocytes to re-enter the cell cycle. *Am J Transl Res, 5*(3), 327-335.

Lin, H. C., Lee, H. S., Chiueh, T. S., Lin, Y. C., Lin, H. A., Lin, Y. C., . . . Meng, E. (2015). Histopathological assessment of inflammation and expression of inflammatory markers in patients with ketamine-induced cystitis. *Mol Med Rep, 11*(4), 2421-2428. doi:10.3892/mmr.2014.3110

Lindpaintner, K., Lu, W., Neidermajer, N., Schieffer, B., Just, H., Ganten, D., & Drexler, H. (1993). Selective activation of cardiac angiotensinogen gene expression in post-infarction ventricular remodeling in the rat. *J Mol Cell Cardiol, 25*(2), 133-143. doi:10.1006/jmcc.1993.1017

Lindsey, M. L., Gannon, J., Aikawa, M., Schoen, F. J., Rabkin, E., Lopresti-Morrow, L., . . . Lee, R. T. (2002). Selective matrix metalloproteinase inhibition reduces left ventricular remodeling but does not inhibit angiogenesis after myocardial infarction. *Circulation, 105*(6), 753-758. doi:10.1161/hc0602.103674

Liu, D., Guo, M., Zhou, P., Xiao, J., & Ji, X. (2019). TSLP promote M2 macrophages polarization and cardiac healing after myocardial infarction. *Biochem Biophys Res Commun, 516*(2), 437-444. doi:10.1016/j.bbrc.2019.06.041

Liu, S., Chen, J., Shi, J., Zhou, W., Wang, L., Fang, W., . . . Liu, S. (2020). M1-like macrophage-derived exosomes suppress angiogenesis and exacerbate cardiac dysfunction in a myocardial infarction microenvironment. *Basic Res Cardiol, 115*(2), 22. doi:10.1007/s00395-020-0781-7

Lu, M., Qin, Q., Yao, J., Sun, L., & Qin, X. (2019). Induction of LOX by TGF-β1/Smad/AP-1 signaling aggravates rat myocardial fibrosis and heart failure. *IUBMB Life, 71*(11), 1729-1739. doi:10.1002/iub.2112

Lu, W., Wang, Q., Sun, X., He, H., Wang, Q., Wu, Y., . . . Li, C. (2019). Qishen Granule Improved Cardiac Remodeling via Balancing M1 and M2 Macrophages. *Front Pharmacol, 10*, 1399. doi:10.3389/fphar.2019.01399

Ma, Y., Chiao, Y. A., Clark, R., Flynn, E. R., Yabluchanskiy, A., Ghasemi, O., . . . Jin, Y. F. (2015). Deriving a cardiac ageing signature to reveal MMP-9-dependent inflammatory signalling in senescence. *Cardiovasc Res, 106*(3), 421-431. doi:10.1093/cvr/cvv128

Ma, Y., Halade, G. V., Zhang, J., Ramirez, T. A., Levin, D., Voorhees, A., . . . Lindsey, M. L. (2013). Matrix metalloproteinase-28 deletion exacerbates cardiac dysfunction and rupture after myocardial infarction in mice by inhibiting M2 macrophage activation. *Circ Res, 112*(4), 675-688. doi:10.1161/circresaha.111.300502

Ma, Y., Yuan, J., Hu, J., Gao, W., Zou, Y., & Ge, J. (2019). ACE inhibitor suppresses cardiac remodeling after myocardial infarction by regulating dendritic cells and AT(2) receptor-mediated mechanism in mice. *Biomed Pharmacother, 114*, 108660. doi:10.1016/j.biopha.2019.108660

Manfroi, W. C., Peukert, C., Berti, C. B., Noer, C., Gutierres Dde, A., & Silva, F. T. (2002). Acute myocardial infarction: the first manifestation of ischemic heart disease and relation to risk factors. *Arq Bras Cardiol, 78*(4), 392-395. doi:10.1590/s0066-782x2002000400006

Maoz, B. M., Herland, A., Henry, O. Y. F., Leineweber, W. D., Yadid, M., Doyle, J., . . . Ingber, D. E. (2017). Organs-on-Chips with combined multi-electrode array and transepithelial electrical resistance measurement capabilities. *Lab on a Chip, 17*(13), 2294-2302. doi:10.1039/C7LC00412E

Mariathasan, S., Weiss, D. S., Newton, K., McBride, J., O'Rourke, K., Roose-Girma, M., . . . Dixit, V. M. (2006). Cryopyrin activates the inflammasome in response to toxins and ATP. *Nature, 440*(7081), 228-232. doi:10.1038/nature04515

Mascarenhas, J. B., Rüegg, M. A., Winzen, U., Halfter, W., Engel, J., & Stetefeld, J. (2003). Mapping of the laminin-binding site of the N-terminal agrin domain (NtA). *Embo j, 22*(3), 529-536. doi:10.1093/emboj/cdg041

McDonagh, T. A., Metra, M., Adamo, M., Gardner, R. S., Baumbach, A., Böhm, M., . . . Kathrine Skibelund, A. (2021). 2021 ESC Guidelines for the diagnosis and treatment of acute and chronic heart failure. *Eur Heart J, 42*(36), 3599-3726. doi:10.1093/eurheartj/ehab368

McKay, R. G., Pfeffer, M. A., Pasternak, R. C., Markis, J. E., Come, P. C., Nakao, S., . . . Grossman, W. (1986). Left ventricular remodeling after myocardial infarction: a corollary to infarct expansion. *Circulation, 74*(4), 693-702. doi:doi:10.1161/01.CIR.74.4.693

Mehran, R. J., Ricci, M. A., Graham, A. M., Carter, K., & Symes, J. F. (1991). Porcine model for vascular graft studies. *J Invest Surg, 4*(1), 37-44. doi:10.3109/08941939109140760

Mendis, S., Thygesen, K., Kuulasmaa, K., Giampaoli, S., Mähönen, M., Ngu Blackett, K., . . . infarction, W. g. o. b. o. t. p. e. o. t. W. c. f. r. o. W. d. o. m. (2010). World Health Organization definition of myocardial infarction: 2008–09 revision. *International Journal of Epidemiology, 40*(1), 139-146. doi:10.1093/ije/dyq165

Meng, F., Xie, B., & Martin, J. F. (2021). Targeting the Hippo pathway in heart repair. *Cardiovasc Res*. doi:10.1093/cvr/cvab291

Miller, I., Min, M., Yang, C., Tian, C., Gookin, S., Carter, D., & Spencer, S. L. (2018). Ki67 is a Graded Rather than a Binary Marker of Proliferation versus Quiescence. *Cell Rep, 24*(5), 1105-1112.e1105. doi:10.1016/j.celrep.2018.06.110

Mizuta, R., Araki, S., Furukawa, M., Furukawa, Y., Ebara, S., Shiokawa, D., . . . Kitamura, D. (2013). DNase γ is the effector endonuclease for internucleosomal DNA fragmentation in necrosis. *PLoS One, 8*(12), e80223. doi:10.1371/journal.pone.0080223

Monk, C. R., Coates, D. P., Prys-Roberts, C., Turtle, M. J., & Spelina, K. (1987). Haemodynamic effects of a prolonged infusion of propofol as a supplement to nitrous oxide anaesthesia. Studies in association with peripheral arterial surgery. *Br J Anaesth, 59*(8), 954-960. doi:10.1093/bja/59.8.954

Mons, U., Müezzinler, A., Gellert, C., Schöttker, B., Abnet, C. C., Bobak, M., . . . Brenner, H. (2015). Impact of smoking and smoking cessation on cardiovascular events and mortality among older adults: meta-analysis of individual participant data from prospective cohort studies of the CHANCES consortium. *Bmj, 350*, h1551. doi:10.1136/bmj.h1551

Moreo, A., Ambrosio, G., De Chiara, B., Pu, M., Tran, T., Mauri, F., & Raman, S. V. (2009). Influence of myocardial fibrosis on left ventricular diastolic function: noninvasive assessment by cardiac magnetic resonance and echo. *Circ Cardiovasc Imaging, 2*(6), 437-443. doi:10.1161/circimaging.108.838367

Morikawa, Y., Heallen, T., Leach, J., Xiao, Y., & Martin, J. F. (2017). Dystrophin-glycoprotein complex sequesters Yap to inhibit cardiomyocyte proliferation. *Nature, 547*(7662), 227-231. doi:10.1038/nature22979

Nadkarni, S. K., Boughner, D. R., Drangova, M., & Fenster, A. (2000). Three-dimensional echocardiography: assessment of inter- and intra-operator variability and accuracy in the measurement of left ventricular cavity volume and myocardial mass. *Phys Med Biol, 45*(5), 1255-1273. doi:10.1088/0031-9155/45/5/313

Nakagawa, M., Karim, M. R., Izawa, T., Kuwamura, M., & Yamate, J. (2021). Immunophenotypical Characterization of M1/M2 Macrophages and Lymphocytes in Cisplatin-Induced Rat Progressive Renal Fibrosis. *Cells, 10*(2). doi:10.3390/cells10020257

Neaton, J. D., & Wentworth, D. (1992). Serum cholesterol, blood pressure, cigarette smoking, and death from coronary heart disease. Overall findings and differences by age for 316,099 white men. Multiple Risk Factor Intervention Trial Research Group. *Arch Intern Med, 152*(1), 56-64. Retrieved from https://jamanetwork.com/journals/jamainternalmedicine/article-abstract/615878

Nelissen-Vrancken, H. J. M. G., Debets, J. J. M., Snoeckx, L. H. E. H., Daemen, M. J. A. P., & Smits, J. F. M. (1996). Time-Related Normalization of Maximal Coronary Flow in Isolated Perfused Hearts of Rats With Myocardial Infarction. *Circulation, 93*(2), 349-355. doi:doi:10.1161/01.CIR.93.2.349

Nian, M., Lee, P., Khaper, N., & Liu, P. (2004). Inflammatory cytokines and postmyocardial infarction remodeling. *Circ Res, 94*(12), 1543-1553. doi:10.1161/01.RES.0000130526.20854.fa

Nielsen, M. C., Andersen, M. N., & Møller, H. J. (2020). Monocyte isolation techniques significantly impact the phenotype of both isolated monocytes and derived macrophages in vitro. *Immunology, 159*(1), 63-74. doi:10.1111/imm.13125

Niles, A. L., Cali, J. J., & Lazar, D. F. (2021). A live-cell assay for the real-time assessment of extracellular ATP levels. *Anal Biochem, 628*, 114286. doi:10.1016/j.ab.2021.114286

Njah, K., Chakraborty, S., Qiu, B., Arumugam, S., Raju, A., Pobbati, A. V., . . . Hong, W. (2019). A Role of Agrin in Maintaining the Stability of Vascular Endothelial Growth Factor Receptor-2 during Tumor Angiogenesis. *Cell Rep, 28*(4), 949-965.e947. doi:10.1016/j.celrep.2019.06.036

Norton, G. R., Tsotetsi, J., Trifunovic, B., Hartford, C., Candy, G. P., & Woodiwiss, A. J. (1997). Myocardial stiffness is attributed to alterations in cross-linked collagen rather than total collagen or phenotypes in spontaneously hypertensive rats. *Circulation, 96*(6), 1991-1998. doi:10.1161/01.cir.96.6.1991

Nunes, S. S., Miklas, J. W., Liu, J., Aschar-Sobbi, R., Xiao, Y., Zhang, B., . . . Radisic, M. (2013). Biowire: a platform for maturation of human pluripotent stem cell–derived cardiomyocytes. *Nature Methods, 10*(8), 781-787. doi:10.1038/nmeth.2524

Ogawa, S., Gerlach, H., Esposito, C., Pasagian-Macaulay, A., Brett, J., & Stern, D. (1990). Hypoxia modulates the barrier and coagulant function of cultured bovine endothelium. Increased monolayer permeability and induction of procoagulant properties. *J Clin Invest, 85*(4), 1090-1098. doi:10.1172/jci114540

Ohashi, K., Burkart, V., Flohé, S., & Kolb, H. (2000). Cutting edge: heat shock protein 60 is a putative endogenous ligand of the toll-like receptor-4 complex. *J Immunol, 164*(2), 558-561. doi:10.4049/jimmunol.164.2.558

Oiwa, K., Shimba, K., Numata, T., Takeuchi, A., Kotani, K., & Jimbo, Y. (2016). A device for co-culturing autonomic neurons and cardiomyocytes using micro-fabrication techniques. *Integrative Biology, 8*(3), 341-348. doi:10.1039/C5IB00273G

Olimulder, M. A., Kraaier, K., Galjee, M. A., Scholten, M. F., van Es, J., Wagenaar, L. J., . . . von Birgelen, C. (2012). Infarct tissue characteristics of patients with versus without early revascularization for acute myocardial infarction: a contrast-enhancement cardiovascular magnetic resonance imaging study. *Heart Vessels, 27*(3), 250-257. doi:10.1007/s00380-011-0150-4

Olivetti, G., Capasso, J. M., Sonnenblick, E. H., & Anversa, P. (1990). Side-to-side slippage of myocytes participates in ventricular wall remodeling acutely after myocardial infarction in rats. *Circ Res, 67*(1), 23-34. doi:10.1161/01.res.67.1.23

Osterloh, A., Geisinger, F., Piédavent, M., Fleischer, B., Brattig, N., & Breloer, M. (2009). Heat shock protein 60 (HSP60) stimulates neutrophil effector functions. *J Leukoc Biol, 86*(2), 423-434. doi:10.1189/jlb.0109011

Otero-García, O., Cid-Álvarez, A. B., Juskova, M., Álvarez-Álvarez, B., Tasende-Rey, P., Gude-Sampedro, F., . . . González-Juanatey, J. R. (2021). Prognostic impact of left ventricular ejection fraction recovery in patients with ST-segment elevation myocardial infarction undergoing primary percutaneous coronary intervention: analysis of an 11-year all-comers registry. *Eur Heart J Acute Cardiovasc Care, 10*(8), 898-908. doi:10.1093/ehjacc/zuab058

Paoletti, E., Cassottana, P., Amidone, M., Gherzi, M., Rolla, D., & Cannella, G. (2007). ACE inhibitors and persistent left ventricular hypertrophy after renal transplantation: a randomized clinical trial. *Am J Kidney Dis, 50*(1), 133-142. doi:10.1053/j.ajkd.2007.04.013

Patel, N., Abdou, H., Edwards, J., Elansary, N. N., Poe, K., Richmond, M. J., . . . Morrison, J. J. (2021). Measuring Cardiac Output in a Swine Model. *J Vis Exp*(171). doi:10.3791/62333

Pencina, M. J., Navar, A. M., Wojdyla, D., Sanchez, R. J., Khan, I., Elassal, J., . . . Sniderman, A. D. (2019). Quantifying Importance of Major Risk Factors for Coronary Heart Disease. *Circulation, 139*(13), 1603-1611. doi:10.1161/circulationaha.117.031855

Peng, H. B., Ali, A. A., Daggett, D. F., Rauvala, H., Hassell, J. R., & Smalheiser, N. R. (1998). The relationship between perlecan and dystroglycan and its implication in the formation of the neuromuscular junction. *Cell Adhes Commun, 5*(6), 475-489. doi:10.3109/15419069809005605

Peterson, J. T., Hallak, H., Johnson, L., Li, H., O'Brien, P. M., Sliskovic, D. R., . . . Spinale, F. G. (2001). Matrix metalloproteinase inhibition attenuates left ventricular remodeling and dysfunction in a rat model of progressive heart failure. *Circulation, 103*(18), 2303-2309. doi:10.1161/01.cir.103.18.2303

Pfeffer, J. M., Pfeffer, M. A., Fletcher, P. J., & Braunwald, E. (1991). Progressive ventricular remodeling in rat with myocardial infarction. *Am J Physiol, 260*(5 Pt 2), H1406-1414. doi:10.1152/ajpheart.1991.260.5.H1406

Pfeffer, M. A., Braunwald, E., Moyé, L. A., Basta, L., Brown, E. J., Jr., Cuddy, T. E., . . . et al. (1992). Effect of captopril on mortality and morbidity in patients with left ventricular dysfunction after myocardial infarction. Results of the survival and ventricular enlargement trial. The SAVE Investigators. *N Engl J Med, 327*(10), 669-677. doi:10.1056/nejm199209033271001

Piccoli, M. T., Gupta, S. K., Viereck, J., Foinquinos, A., Samolovac, S., Kramer, F. L., . . . Thum, T. (2017). Inhibition of the Cardiac Fibroblast-Enriched lncRNA Meg3 Prevents Cardiac Fibrosis and Diastolic Dysfunction. *Circ Res, 121*(5), 575-583. doi:10.1161/circresaha.117.310624

Raats, C. J., Bakker, M. A., Hoch, W., Tamboer, W. P., Groffen, A. J., van den Heuvel, L. P., . . . van den Born, J. (1998). Differential expression of agrin in renal basement membranes as revealed by domain-specific antibodies. *J Biol Chem, 273*(28), 17832-17838. doi:10.1074/jbc.273.28.17832

Riccardi, A., Danova, M., Wilson, G., Ucci, G., Dörmer, P., Mazzini, G., . . . Ascari, E. (1988). Cell kinetics in human malignancies studied with in vivo administration of bromodeoxyuridine and flow cytometry. *Cancer Res, 48*(21), 6238-6245. Retrieved from https://cancerres.aacrjournals.org/content/canres/48/21/6238.full.pdf

Ripplinger, C. M., Lou, Q., Li, W., Hadley, J., & Efimov, I. R. (2009). Panoramic imaging reveals basic mechanisms of induction and termination of ventricular tachycardia in rabbit heart with chronic infarction: implications for low-voltage cardioversion. *Heart Rhythm, 6*(1), 87-97. doi:10.1016/j.hrthm.2008.09.019

Rivera, C., Zandonadi, F. S., Sánchez-Romero, C., Soares, C. D., Granato, D. C., González-Arriagada, W. A., & Paes Leme, A. F. (2018). Agrin has a pathological role in the progression of oral cancer. *Br J Cancer, 118*(12), 1628-1638. doi:10.1038/s41416-018-0135-5

Roberds, S. L., Anderson, R. D., Ibraghimov-Beskrovnaya, O., & Campbell, K. P. (1993). Primary structure and muscle-specific expression of the 50-kDa dystrophin-associated glycoprotein (adhalin). *J Biol Chem, 268*(32), 23739-23742.

Roberts, R., Husain, A., Ambos, H. D., Oliver, G. C., Cox, J. R., Jr., & Sobel, B. E. (1975). Relation between infarct size and ventricular arrhythmia. *Br Heart J, 37*(11), 1169-1175. doi:10.1136/hrt.37.11.1169

Rogers, D., Campbell, R., Catha, G., Patterson, K., & Puccio, D. (2017). Classes of Heart Failure. Retrieved from https://www.heart.org/en/health-topics/heart-failure/what-is-heart-failure/classes-of-heart-failure

Rohde, L. E., Ducharme, A., Arroyo, L. H., Aikawa, M., Sukhova, G. H., Lopez-Anaya, A., . . . Lee, R. T. (1999). Matrix metalloproteinase inhibition attenuates early left ventricular enlargement after experimental myocardial infarction in mice. *Circulation, 99*(23), 3063-3070. doi:10.1161/01.cir.99.23.3063

Romanic, A. M., Harrison, S. M., Bao, W., Burns-Kurtis, C. L., Pickering, S., Gu, J., . . . Yue, T. L. (2002). Myocardial protection from ischemia/reperfusion injury by targeted deletion of matrix metalloproteinase-9. *Cardiovasc Res, 54*(3), 549-558. doi:10.1016/s0008-6363(02)00254-7

Ronaldson-Bouchard, K., & Vunjak-Novakovic, G. (2018). Organs-on-a-Chip: A Fast Track for Engineered Human Tissues in Drug Development. *Cell Stem Cell, 22*(3), 310-324. doi:10.1016/j.stem.2018.02.011

Rubin, S. A., Fishbein, M. C., & Swan, H. J. (1983). Compensatory hypertrophy in the heart after myocardial infarction in the rat. *J Am Coll Cardiol, 1*(6), 1435-1441. doi:10.1016/s0735-1097(83)80046-1

Sabaté, M., Räber, L., Heg, D., Brugaletta, S., Kelbaek, H., Cequier, A., . . . Windecker, S. (2014). Comparison of newer-generation drug-eluting with bare-metal stents in patients with acute ST-segment elevation myocardial infarction: a pooled analysis of the EXAMINATION (clinical Evaluation of the Xience-V stent in Acute Myocardial INfArcTION) and COMFORTABLE-AMI (Comparison of Biolimus Eluted From an Erodible Stent Coating With Bare Metal Stents in Acute ST-Elevation Myocardial Infarction) trials. *JACC Cardiovasc Interv, 7*(1), 55-63. doi:10.1016/j.jcin.2013.07.012

Sahni, D., Kaur, G. D., Jit, H., & Jit, I. (2008). Anatomy & distribution of coronary arteries in pig in comparison with man. *Indian J Med Res, 127*(6), 564-570.

Sanchis-Gomar, F., Perez-Quilis, C., Leischik, R., & Lucia, A. (2016). Epidemiology of coronary heart disease and acute coronary syndrome. *Ann Transl Med, 4*(13), 256. doi:10.21037/atm.2016.06.33

Santos-Gallego, C. G., Requena-Ibanez, J. A., San Antonio, R., Garcia-Ropero, A., Ishikawa, K., Watanabe, S., . . . Badimon, J. J. (2021). Empagliflozin Ameliorates Diastolic Dysfunction and Left Ventricular Fibrosis/Stiffness in Nondiabetic Heart Failure: A Multimodality Study. *JACC Cardiovasc Imaging, 14*(2), 393-407. doi:10.1016/j.jcmg.2020.07.042

Santos-Gallego, C. G., Requena-Ibanez, J. A., San Antonio, R., Ishikawa, K., Watanabe, S., Picatoste, B., . . . Badimon, J. J. (2019). Empagliflozin Ameliorates Adverse Left Ventricular Remodeling in Nondiabetic Heart Failure by Enhancing Myocardial Energetics. *J Am Coll Cardiol, 73*(15), 1931-1944. doi:10.1016/j.jacc.2019.01.056

Scaffidi, P., Misteli, T., & Bianchi, M. E. (2002). Release of chromatin protein HMGB1 by necrotic cells triggers inflammation. *Nature, 418*(6894), 191-195. doi:10.1038/nature00858

Scavello, F., Zeni, F., Milano, G., Macrì, F., Castiglione, S., Zuccolo, E., . . . Raucci, A. (2021). Soluble Receptor for Advanced Glycation End-products regulates age-associated Cardiac Fibrosis. *Int J Biol Sci, 17*(10), 2399-2416. doi:10.7150/ijbs.56379

Schipke, J., Brandenberger, C., Rajces, A., Manninger, M., Alogna, A., Post, H., & Mühlfeld, C. (2017). Assessment of cardiac fibrosis: a morphometric method comparison for collagen quantification. *J Appl Physiol (1985), 122*(4), 1019-1030. doi:10.1152/japplphysiol.00987.2016

Schultz Jel, J., Witt, S. A., Glascock, B. J., Nieman, M. L., Reiser, P. J., Nix, S. L., . . . Doetschman, T. (2002). TGF-beta1 mediates the hypertrophic cardiomyocyte growth induced by angiotensin II. *J Clin Invest, 109*(6), 787-796. doi:10.1172/jci14190

Scotton, P., Bleckmann, D., Stebler, M., Sciandra, F., Brancaccio, A., Meier, T., . . . Ruegg, M. A. (2006). Activation of muscle-specific receptor tyrosine kinase and binding to dystroglycan are regulated by alternative mRNA splicing of agrin. *J Biol Chem, 281*(48), 36835-36845. doi:10.1074/jbc.M607887200

Sharif Nia, H., Sivarajan-Froelicher, E., Haghdoost, A. A., Moosazadeh, M., Huak-Chan, Y., Farsavian, A. A., . . . Goudarzian, A. H. (2018). The estimate of average age at the onset of acute myocardial infarction in Iran: A systematic review and meta-analysis study. *ARYA Atheroscler, 14*(5), 225-232. doi:10.22122/arya.v14i5.1739

Siwik, D. A., Chang, D. L., & Colucci, W. S. (2000). Interleukin-1beta and tumor necrosis factor-alpha decrease collagen synthesis and increase matrix metalloproteinase activity in cardiac fibroblasts in vitro. *Circ Res, 86*(12), 1259-1265. doi:10.1161/01.res.86.12.1259

Sulo, G., Igland, J., Vollset, S. E., Nygård, O., Ebbing, M., Sulo, E., . . . Tell, G. S. (2016). Heart Failure Complicating Acute Myocardial Infarction; Burden and Timing of Occurrence: A Nation-wide Analysis Including 86 771 Patients From the Cardiovascular Disease in Norway (CVDNOR) Project. *J Am Heart Assoc, 5*(1). doi:10.1161/jaha.115.002667

Sun, J., Shen, H., Shao, L., Teng, X., Chen, Y., Liu, X., . . . Shen, Z. (2020). HIF-1α overexpression in mesenchymal stem cell-derived exosomes mediates cardioprotection in myocardial infarction by enhanced angiogenesis. *Stem Cell Res Ther, 11*(1), 373. doi:10.1186/s13287-020-01881-7

Sun, Y., Zhang, J. Q., Zhang, J., & Lamparter, S. (2000). Cardiac remodeling by fibrous tissue after infarction in rats. *J Lab Clin Med, 135*(4), 316-323. doi:10.1067/mlc.2000.105971

Sunada, Y., Bernier, S. M., Kozak, C. A., Yamada, Y., & Campbell, K. P. (1994). Deficiency of merosin in dystrophic dy mice and genetic linkage of laminin M chain gene to dy locus. *J Biol Chem, 269*(19), 13729-13732.

Sundberg, C., Kowanetz, M., Brown, L. F., Detmar, M., & Dvorak, H. F. (2002). Stable expression of angiopoietin-1 and other markers by cultured pericytes: phenotypic similarities to a subpopulation of cells in maturing vessels during later stages of angiogenesis in vivo. *Lab Invest, 82*(4), 387-401. doi:10.1038/labinvest.3780433

Sundström, J., Evans, J. C., Benjamin, E. J., Levy, D., Larson, M. G., Sawyer, D. B., . . . Vasan, R. S. (2004). Relations of Plasma Matrix Metalloproteinase-9 to Clinical Cardiovascular Risk Factors and Echocardiographic Left Ventricular Measures. *Circulation, 109*(23), 2850-2856. doi:doi:10.1161/01.CIR.0000129318.79570.84

Sutterwala, F. S., Ogura, Y., Szczepanik, M., Lara-Tejero, M., Lichtenberger, G. S., Grant, E. P., . . . Flavell, R. A. (2006). Critical role for NALP3/CIAS1/Cryopyrin in innate and adaptive immunity through its regulation of caspase-1. *Immunity, 24*(3), 317-327. doi:10.1016/j.immuni.2006.02.004

Talman, V., & Ruskoaho, H. (2016). Cardiac fibrosis in myocardial infarction-from repair and remodeling to regeneration. *Cell Tissue Res, 365*(3), 563-581. doi:10.1007/s00441-016-2431-9

Teichert, M., Milde, L., Holm, A., Stanicek, L., Gengenbacher, N., Savant, S., . . . Augustin, H. G. (2017). Pericyte-expressed Tie2 controls angiogenesis and vessel maturation. *Nat Commun, 8*, 16106. doi:10.1038/ncomms16106

The Acute Infarction Ramipril Efficacy Study, I. (1993). Effect of ramipril on mortality and morbidity of survivors of acute myocardial infarction with clinical evidence of heart failure. *The Lancet, 342*(8875), 821-828. doi:10.1016/0140-6736(93)92693-N

Thygesen, K., Alpert, J. S., Jaffe, A. S., Chaitman, B. R., Bax, J. J., Morrow, D. A., & White, H. D. (2018). Fourth Universal Definition of Myocardial Infarction (2018). *Circulation, 138*(20), e618-e651. doi:doi:10.1161/CIR.0000000000000617

Timmers, L., Sluijter, J. P. G., Keulen, J. K. v., Hoefer, I. E., Nederhoff, M. G. J., Goumans, M.-J., . . . Kleijn, D. P. V. d. (2008). Toll-Like Receptor 4 Mediates Maladaptive Left Ventricular Remodeling and Impairs Cardiac Function After Myocardial Infarction. *Circulation Research, 102*(2), 257-264. doi:doi:10.1161/CIRCRESAHA.107.158220

Timmers, L., Sluijter, J. P. G., Verlaan, C. W. J., Steendijk, P., Cramer, M. J., Emons, M., . . . Kleijn, D. P. V. d. (2007). Cyclooxygenase-2 Inhibition Increases Mortality, Enhances Left Ventricular Remodeling, and Impairs Systolic Function After Myocardial Infarction in the Pig. *Circulation, 115*(3), 326-332. doi:doi:10.1161/CIRCULATIONAHA.106.647230

Torabi, A., Cleland, J. G., Rigby, A. S., & Sherwi, N. (2014). Development and course of heart failure after a myocardial infarction in younger and older people. *J Geriatr Cardiol, 11*(1), 1-12. doi:10.3969/j.issn.1671-5411.2014.01.002

Townsend, N., Wilson, L., Bhatnagar, P., Wickramasinghe, K., Rayner, M., & Nichols, M. (2016). Cardiovascular disease in Europe: epidemiological update 2016. *European Heart Journal, 37*(42), 3232-3245. doi:10.1093/eurheartj/ehw334

Triastuti, E., Nugroho, A. B., Zi, M., Prehar, S., Kohar, Y. S., Bui, T. A., . . . Oceandy, D. (2019). Pharmacological inhibition of Hippo pathway, with the novel kinase inhibitor XMU-MP-1, protects the heart against adverse effects during pressure overload. *Br J Pharmacol, 176*(20), 3956-3971. doi:10.1111/bph.14795

Tripathi, H., Al-Darraji, A., Abo-Aly, M., Peng, H., Shokri, E., Chelvarajan, L., . . . Abdel-Latif, A. (2020). Autotaxin inhibition reduces cardiac inflammation and mitigates adverse cardiac remodeling after myocardial infarction. *J Mol Cell Cardiol, 149*, 95-114. doi:10.1016/j.yjmcc.2020.09.011

Tschabrunn, C. M., Roujol, S., Nezafat, R., Faulkner-Jones, B., Buxton, A. E., Josephson, M. E., & Anter, E. (2016). A swine model of infarct-related reentrant ventricular tachycardia: Electroanatomic, magnetic resonance, and histopathological characterization. *Heart Rhythm, 13*(1), 262-273. doi:10.1016/j.hrthm.2015.07.030

Tsim, K. W., Ruegg, M. A., Escher, G., Kröger, S., & McMahan, U. J. (1992). cDNA that encodes active agrin. *Neuron, 8*(4), 677-689. doi:10.1016/0896-6273(92)90089-v

Urbich, M., Globe, G., Pantiri, K., Heisen, M., Bennison, C., Wirtz, H. S., & Di Tanna, G. L. (2020). A Systematic Review of Medical Costs Associated with Heart Failure in the USA (2014-2020). *Pharmacoeconomics, 38*(11), 1219-1236. doi:10.1007/s40273-020-00952-0

Van de Werf, F., Bax, J., Betriu, A., Blomstrom-Lundqvist, C., Crea, F., Falk, V., . . . Weis, M. (2008). Management of acute myocardial infarction in patients presenting with persistent ST-segment elevation: the Task Force on the Management of ST-Segment Elevation Acute Myocardial Infarction of the European Society of Cardiology. *Eur Heart J, 29*(23), 2909-2945. doi:10.1093/eurheartj/ehn416

Vermeyen, K. M., De Hert, S. G., Erpels, F. A., & Adriaensen, H. F. (1991). Myocardial metabolism during anaesthesia with propofol--low dose fentanyl for coronary artery bypass surgery. *Br J Anaesth, 66*(4), 504-508. doi:10.1093/bja/66.4.504

Vermeyen, K. M., Erpels, F. A., Janssen, L. A., Beeckman, C. P., & Hanegreefs, G. H. (1987). Propofol-fentanyl anaesthesia for coronary bypass surgery in patients with good left ventricular function. *Br J Anaesth, 59*(9), 1115-1120. doi:10.1093/bja/59.9.1115

Verrecchia, F., Chu, M. L., & Mauviel, A. (2001). Identification of novel TGF-beta /Smad gene targets in dermal fibroblasts using a combined cDNA microarray/promoter transactivation approach. *J Biol Chem, 276*(20), 17058-17062. doi:10.1074/jbc.M100754200

Virani, S. S., Alonso, A., Aparicio, H. J., Benjamin, E. J., Bittencourt, M. S., Callaway, C. W., . . . Tsao, C. W. (2021). Heart Disease and Stroke Statistics—2021 Update. *Circulation, 143*(8), e254-e743. doi:doi:10.1161/CIR.0000000000000950

Volgman, A. S., Palaniappan, L. S., Aggarwal, N. T., Gupta, M., Khandelwal, A., Krishnan, A. V., . . . Watson, K. E. (2018). Atherosclerotic Cardiovascular Disease in South Asians in the United States: Epidemiology, Risk Factors, and Treatments: A Scientific Statement From the American Heart Association. *Circulation, 138*(1), e1-e34. doi:10.1161/cir.0000000000000580

von Gise, A., Lin, Z., Schlegelmilch, K., Honor, L. B., Pan, G. M., Buck, J. N., . . . Pu, W. T. (2012). YAP1, the nuclear target of Hippo signaling, stimulates heart growth through cardiomyocyte proliferation but not hypertrophy. *Proc Natl Acad Sci U S A, 109*(7), 2394-2399. doi:10.1073/pnas.1116136109

Wallentin, L., Becker, R. C., Budaj, A., Cannon, C. P., Emanuelsson, H., Held, C., . . . Thorsén, M. (2009). Ticagrelor versus clopidogrel in patients with acute coronary syndromes. *N Engl J Med, 361*(11), 1045-1057. doi:10.1056/NEJMoa0904327

Wang, X., Guo, Z., Ding, Z., & Mehta, J. L. (2018). Inflammation, Autophagy, and Apoptosis After Myocardial Infarction. *J Am Heart Assoc, 7*(9). doi:10.1161/jaha.117.008024

Wang, Z. Q., Sun, X. L., Wang, Y. L., & Miao, Y. L. (2021). Agrin promotes the proliferation, invasion and migration of rectal cancer cells via the WNT signaling pathway to contribute to rectal cancer progression. *J Recept Signal Transduct Res, 41*(4), 363-370. doi:10.1080/10799893.2020.1811325

Waring, C. D., Vicinanza, C., Papalamprou, A., Smith, A. J., Purushothaman, S., Goldspink, D. F., . . . Ellison, G. M. (2014). The adult heart responds to increased workload with physiologic hypertrophy, cardiac stem cell activation, and new myocyte formation. *Eur Heart J, 35*(39), 2722-2731. doi:10.1093/eurheartj/ehs338

Weber, C., Müller, C., Podszuweit, A., Montino, C., Vollmer, J., & Forsbach, A. (2012). Toll-like receptor (TLR) 3 immune modulation by unformulated small interfering RNA or DNA and the role of CD14 (in TLR-mediated effects). *Immunology, 136*(1), 64-77. doi:10.1111/j.1365-2567.2012.03559.x

Wei, H., Fang, L., Song, J., & Chatterjee, S. (2005). Statin-inhibited endothelial permeability could be associated with its effect on PECAM-1 in endothelial cells. *FEBS Lett, 579*(5), 1272-1278. doi:10.1016/j.febslet.2005.01.020

Wei, K., Serpooshan, V., Hurtado, C., Diez-Cuñado, M., Zhao, M., Maruyama, S., . . . Ruiz-Lozano, P. (2015). Epicardial FSTL1 reconstitution regenerates the adult mammalian heart. *Nature, 525*(7570), 479-485. doi:10.1038/nature15372

Weisman, H. F., Bush, D. E., Mannisi, J. A., Weisfeldt, M. L., & Healy, B. (1988). Cellular mechanisms of myocardial infarct expansion. *Circulation, 78*(1), 186-201. doi:doi:10.1161/01.CIR.78.1.186

Westman, P. C., Lipinski, M. J., Luger, D., Waksman, R., Bonow, R. O., Wu, E., & Epstein, S. E. (2016). Inflammation as a Driver of Adverse Left Ventricular Remodeling After Acute Myocardial Infarction. *J Am Coll Cardiol, 67*(17), 2050-2060. doi:10.1016/j.jacc.2016.01.073

Whyte, M. K., Meagher, L. C., MacDermot, J., & Haslett, C. (1993). Impairment of function in aging neutrophils is associated with apoptosis. *J Immunol, 150*(11), 5124-5134.

Wijesundera, K. K., Izawa, T., Murakami, H., Tennakoon, A. H., Golbar, H. M., Kato-Ichikawa, C., . . . Yamate, J. (2014). M1- and M2-macrophage polarization in thioacetamide (TAA)-induced rat liver lesions; a possible analysis for hepato-pathology. *Histol Histopathol, 29*(4), 497-511. doi:10.14670/hh-29.10.497

Winkler, F., Herz, K., Rieck, S., Kimura, K., Hu, T., Röll, W., . . . Wenzel, D. (2018). PECAM/eGFP transgenic mice for monitoring of angiogenesis in health and disease. *Sci Rep, 8*(1), 17582. doi:10.1038/s41598-018-36039-2

Witkowski, A., Ruzyłło, W., Górecka, B., Chmielak, Z., Jodkowski, J., Dabrowski, M., . . . et al. (1994). Reversal of ischaemic systolic and diastolic left ventricular dysfunction by successful coronary angioplasty in patients with non-Q wave anterior myocardial infarction. *Eur Heart J, 15*(8), 1106-1112. doi:10.1093/oxfordjournals.eurheartj.a060635

Wiviott, S. D., Braunwald, E., McCabe, C. H., Montalescot, G., Ruzyllo, W., Gottlieb, S., . . . Antman, E. M. (2007). Prasugrel versus clopidogrel in patients with acute coronary syndromes. *N Engl J Med, 357*(20), 2001-2015. doi:10.1056/NEJMoa0706482

World Health Organization. (2021). Cardiovascular diseases (CVDs). Retrieved from https://www.who.int/en/news-room/fact-sheets/detail/cardiovascular-diseases-(cvds)

Xin, M., Kim, Y., Sutherland, L. B., Murakami, M., Qi, X., McAnally, J., . . . Olson, E. N. (2013). Hippo pathway effector Yap promotes cardiac regeneration. *Proc Natl Acad Sci U S A, 110*(34), 13839-13844. doi:10.1073/pnas.1313192110

Yabluchanskiy, A., Ma, Y., Chiao, Y. A., Lopez, E. F., Voorhees, A. P., Toba, H., . . . Jin, Y. F. (2014). Cardiac aging is initiated by matrix metalloproteinase-9-mediated endothelial dysfunction. *Am J Physiol Heart Circ Physiol, 306*(10), H1398-1407. doi:10.1152/ajpheart.00090.2014

Yahalom-Ronen, Y., Rajchman, D., Sarig, R., Geiger, B., & Tzahor, E. (2015). Reduced matrix rigidity promotes neonatal cardiomyocyte dedifferentiation, proliferation and clonal expansion. *Elife, 4*. doi:10.7554/eLife.07455

Yang, B., Ibraghimov-Beskrovnaya, O., Moomaw, C. R., Slaughter, C. A., & Campbell, K. P. (1994). Heterogeneity of the 59-kDa dystrophin-associated protein revealed by cDNA cloning and expression. *J Biol Chem, 269*(8), 6040-6044.

Yang, Q., Zhang, Z., Gregg, E. W., Flanders, W. D., Merritt, R., & Hu, F. B. (2014). Added sugar intake and cardiovascular diseases mortality among US adults. *JAMA Intern Med, 174*(4), 516-524. doi:10.1001/jamainternmed.2013.13563

Yang, Y., Ma, Y., Han, W., Li, J., Xiang, Y., Liu, F., . . . Gao, X. M. (2008). Age-related differences in postinfarct left ventricular rupture and remodeling. *Am J Physiol Heart Circ Physiol, 294*(4), H1815-1822. doi:10.1152/ajpheart.00831.2007

Yarbrough, W. M., Mukherjee, R., Escobar, G. P., Mingoia, J. T., Sample, J. A., Hendrick, J. W., . . . Spinale, F. G. (2003). Selective Targeting and Timing of Matrix Metalloproteinase Inhibition in Post-Myocardial Infarction Remodeling. *Circulation, 108*(14), 1753-1759. doi:doi:10.1161/01.CIR.0000091087.78630.79

Ye, L., D'Agostino, G., Loo, S. J., Wang, C. X., Su, L. P., Tan, S. H., . . . Cook, S. A. (2018). Early Regenerative Capacity in the Porcine Heart. *Circulation, 138*(24), 2798-2808. doi:10.1161/circulationaha.117.031542

Ye, Q., Zhang, J., & Ma, L. (2020). Predictors of all-cause 1-year mortality in myocardial infarction patients. *Medicine (Baltimore), 99*(29), e21288. doi:10.1097/md.0000000000021288

Yu, M., Wang, H., Ding, A., Golenbock, D. T., Latz, E., Czura, C. J., . . . Yang, H. (2006). HMGB1 signals through toll-like receptor (TLR) 4 and TLR2. *Shock, 26*(2), 174-179. doi:10.1097/01.shk.0000225404.51320.82

Yuan, W., & Varga, J. (2001). Transforming growth factor-beta repression of matrix metalloproteinase-1 in dermal fibroblasts involves Smad3. *J Biol Chem, 276*(42), 38502-38510. doi:10.1074/jbc.M107081200

Yuan, X., Deng, Y., Guo, X., Shang, J., Zhu, D., & Liu, H. (2014). Atorvastatin attenuates myocardial remodeling induced by chronic intermittent hypoxia in rats: partly involvement of TLR-4/MYD88 pathway. *Biochem Biophys Res Commun, 446*(1), 292-297. doi:10.1016/j.bbrc.2014.02.091

Yumoto, N., Kim, N., & Burden, S. J. (2012). Lrp4 is a retrograde signal for presynaptic differentiation at neuromuscular synapses. *Nature, 489*(7416), 438-442. doi:10.1038/nature11348

Yusuf, S., Hawken, S., Ounpuu, S., Dans, T., Avezum, A., Lanas, F., . . . Lisheng, L. (2004). Effect of potentially modifiable risk factors associated with myocardial infarction in 52 countries (the INTERHEART study): case-control study. *Lancet, 364*(9438), 937-952. doi:10.1016/s0140-6736(04)17018-9

Yusuf, S., Ramsdale, D., Peto, R., Furse, L., Bennett, D., Bray, C., & Sleight, P. (1980). Early intravenous atenolol treatment in suspected acute myocardial infarction. Preliminary report of a randomised trial. *Lancet, 2*(8189), 273-276. doi:10.1016/s0140-6736(80)90231-7

Zannad, F., Ferreira, J. P., Pocock, S. J., Anker, S. D., Butler, J., Filippatos, G., . . . Packer, M. (2020). SGLT2 inhibitors in patients with heart failure with reduced ejection fraction: a meta-analysis of the EMPEROR-Reduced and DAPA-HF trials. *Lancet, 396*(10254), 819-829. doi:10.1016/s0140-6736(20)31824-9

Zhang, Q., Cao, Y., Liu, Y., Huang, W., Ren, J., Wang, P., . . . Sun, H. (2021). Shear stress inhibits cardiac microvascular endothelial cells apoptosis to protect against myocardial ischemia reperfusion injury via YAP/miR-206/PDCD4 signaling pathway. *Biochem Pharmacol, 186*, 114466. doi:10.1016/j.bcp.2021.114466

Zhang, Q., Raoof, M., Chen, Y., Sumi, Y., Sursal, T., Junger, W., . . . Hauser, C. J. (2010). Circulating mitochondrial DAMPs cause inflammatory responses to injury. *Nature, 464*(7285), 104-107. doi:10.1038/nature08780

Zhang, Y. S., Arneri, A., Bersini, S., Shin, S. R., Zhu, K., Goli-Malekabadi, Z., . . . Khademhosseini, A. (2016). Bioprinting 3D microfibrous scaffolds for engineering endothelialized myocardium and heart-on-a-chip. *Biomaterials, 110*, 45-59. doi:10.1016/j.biomaterials.2016.09.003

Zhong, Z., Hou, J., Zhang, Q., Zhong, W., Li, B., Li, C., . . . Zhao, P. (2019). Assessment of the LDL-C/HDL-C ratio as a predictor of one year clinical outcomes in patients with acute coronary syndromes after percutaneous coronary intervention and drug-eluting stent implantation. *Lipids Health Dis, 18*(1), 40. doi:10.1186/s12944-019-0979-6

Zhu, W., Zhang, E., Zhao, M., Chong, Z., Fan, C., Tang, Y., . . . Zhang, J. (2018). Regenerative Potential of Neonatal Porcine Hearts. *Circulation, 138*(24), 2809-2816. doi:10.1161/circulationaha.118.034886

Ziegler, T., Horstkotte, J., Schwab, C., Pfetsch, V., Weinmann, K., Dietzel, S., . . . Kupatt, C. (2013). Angiopoietin 2 mediates microvascular and hemodynamic alterations in sepsis. *J Clin Invest, 123*(8), 3436-3445. doi:10.1172/jci66549

Zile, M. R., Gaasch, W. H., Carroll, J. D., Feldman, M. D., Aurigemma, G. P., Schaer, G. L., . . . Liebson, P. R. (2001). Heart Failure With a Normal Ejection Fraction. *Circulation, 104*(7), 779-782. doi:doi:10.1161/hc3201.094226